The Dissertation Committee for Xianmao Lu Certifies that this is the approved version of the following dissertation:

Synthesis and Characterization of Group IV Semiconductor Nanocrystals and Nanowires

Committee:

Keith P. Johnston, Supervisor

Brian A. Korgel, Co-Supervisor

John G. Ekerdt

Yueh-Lin Loo

Peter J. Rossky

Synthesis and Characterization of Group IV Semiconductor Nanocrystals and Nanowires

by

Xianmao Lu, B.E.; M.E.

Dissertation

Presented to the Faculty of the Graduate School of

The University of Texas at Austin

in Partial Fulfillment

of the Requirements

for the Degree of

Doctor of Philosophy

The University of Texas at Austin

December 2005

Dedication

To my family and loved ones.

Acknowledgements

I would like to express my deep gratitude to all of the people who have assisted during the course of my dissertation. A special thanks to my advisor Dr. Keith Johnston for the guidance and support to the completion of the thesis, and my co-supervisor Dr. Brian Korgel for the directions in the field of nanomaterials. I would also like to thank Dr. John Ekerdt, Dr. Yueh-Lin Loo, and Dr. Peter Rossky for their valuable comments and suggestions as members of my committee.

I would like to give a very special thanks to all the current and past members of Dr. Johnston's group: Kirk Ziegler, Parag Shah, Xiaoxia Chen, Griffin Smith, Jasper Dickson, John Keagy, Michal Matteucci, Mehul Patel, Gaurav Gupta, Todd Crisp, Josh Engstrom and Dr. Korgel's group: Lindsay Pell, Tobias Hanrath, Aaron Saunders, Ali Ghezelbash, Cindy Stowell, Hsing-Yu Tuan, Dayne Fanfair, Fred Mikulec, and Doh Lee for their assistance, suggestions, and insightful discussions, and many other who are also deserving of thanks for help.

Finally I want to thank my parents and family for their encouragement, love, patience and support.

Synthesis and Characterization of Group IV Semiconductor Nanocrystals and Nanowires

Publication No._____

Xianmao Lu, Ph.D.

The University of Texas at Austin, 2005

Supervisors: Keith P. Johnston and Brian A. Korgel

Group IV semiconductor nanostructures, such as Si and Ge nanocrystals and nanowires, have been challenging to synthesize in solution, primarily due to their strong covalent bonding and the resulting need for high temperatures for crystallization. Here, we present solution-based synthetic approaches for solvents including supercritical fluids and coordinating liquid solvents at elevated temperatures.

Si nanowires were successfully synthesized in supercritical fluid alkanes and octanol by thermolysis of an organosilane precursor with gold nanocrystals as growth seeds on a Si substrate. With a flow reactor designed for rapid heatup and constant concentrations of Si precursor, straight Si nanowires were grown with minimal contamination of Si particulates. By decomposing organogermane precursors in a supercritical organic solvent or

supercritical CO_2 (sc-CO_2) in the presence of a hydrocarbon capping ligand, Ge nanocrystals with tunable diameters ranging from 2-70 nm were synthesized. The nanocrystals exhibited high crystallinity and 3-4 nm Ge nanoparticles showed blue-shifted UV-visible and photoluminescence spectra. Compared with similar reactions in supercritical organic fluid, the synthesis in sc-CO_2 produced much less organic contamination.

A new synthetic approach was developed to produce Ge nanocrystals and nanowires in a coordinating liquid solvent at atmospheric pressure. A carbon-free and highly reactive Ge precursor, germanium diiodide (GeI_2), was employed to synthesize Ge nanocrystals with controllable sizes ranging from 3-10nm and moderate polydispersity. High chemical yield of Ge nanocrystals was achieved due to the high reactivity of the Ge precursor, the moderate reaction temperature, and a reduction in organic by-product contaminants. When seeded with bismuth (Bi) nanocrystals, highly crystalline Ge nanowires were also synthesized by decomposing GeI_2 in solution. The synthesis was enabled by the combination of the low decomposition temperature of GeI_2, high solubility of GeI_2 in the solvent and low eutectic point of Ge and Bi. This is the first example of group IV semiconductor nanowires synthesized in a liquid solvent at atmospheric pressure.

Table of Contents

List of Tables

List of Figures

Chapter 1: Introduction

1.1 BACKGROUND ON NANOSTRUCTURES

Nanoscience is a growing research area with sweeping implications for new technologies. In the past few decades, nanotechnology has become one of the most intensively studied fields driven by the excitement of understanding new science and by the potential applications and economic impact. At the nanometer length-scale, material dimensions lead to quantum confinement effects that give rise to unique electrical, optical, magnetic, chemical, thermal, and mechanical properties, which can be utilized to enhance a variety of technologies including electronic, sensing, coating, environmental, chemical processing, and medical applications. [1-3]

A highly active research field in nanotechnology has been the synthesis of new nanostructures, especially semiconductor nanostructures, including nanoparticles, nanowires, nanotubes, etc. Compared to group II-VI semiconductor nanocrystals, which have well-developed synthetic methods, much less attention has been paid to the group IV semiconductors, i.e. silicon and germanium. These materials are indirect band gap semiconductors and usually crystallize in a diamond cubic lattice. Whereas group II-VI

semiconductor nanocrystals may be synthesized readily from organic precursors, this approach is more challenging for Si and Ge. As a result of the network covalent bonds for Si and Ge, crystallization often requires high temperatures. Given that group IV materials are of great interest in the semiconductor industry, it would be desirable to develop novel synthetic techniques to achieve greater control over nanocrystal morphology and optical properties, and to achieve high chemical yields.

1.2 SIZE-DEPENDENT PROPERTIES

Semiconductor crystals exhibit a broad spectrum of strong size-dependent properties for particle sizes below the Bohr radius of their bulk exciton. The size-dependence of the nanocrystal electronic energy level has attracted special interest. It allows one to tailor the materials optical and electronic properties by controlling particle size, and many potential new applications such as nanocrystal bio-tags,[4] quantum dot lasers,[5] polymer-based nanocrystal solar cells,[6] and single electron transistors[7] have been suggested.

The concept of quantum confinement describes the effects of reduced dimensions on the electronic properties of nanostructures. If the size of the nanoparticle becomes similar to the wavelength of the charge carriers in the

valence and conduction band, the particle can be described as a potential well where waves are reflected at the potential barrier and spatially confined. As a result, the electronic structure of the crystal is altered from continuous bands to discrete levels and the continuous optical transitions between the electronic bands become discrete and size-dependent as well. The basic idea behind quantum confinement can be visualized as a classical particle in a box problem. For a free particle with an effective mass of m^* confined in a crystal with a one dimension barrier at a distance of L, the movement of the particle can be described with the Schröedinger equation:

$$\frac{\partial^2 \Psi(x)}{\partial x^2} = -\frac{2m^* E}{(h/2\pi)^2}\Psi(x) \qquad (1.1)$$

where $\Psi(x)$ is the wavefunction and E is the energy of the particle. This equation can be solved by using the boundary conditions that $\Psi(x) = 0$ at x = 0 and $x = L$:

$$E_n = \frac{\hbar^2 k_n^2}{2m^*} = \frac{n^2 \hbar^2 \pi^2}{2m^* L^2} \qquad \text{for n = 1, 2, 3 …} \qquad (1.2)$$

where k_n is the allowed wave factors and $k_n = n\pi / L$.

When this simplified solution is extended to a semiconductor nanocrystal with a size close to the Bohr radius a_B, the resulting expression for the energy shift from the ground state of the corresponding bulk materials is:

$$\Delta E_n = \frac{n^2 \hbar^2 \pi^2}{2m^* a^2} \qquad (1.3)$$

where a is the size of the nanocrystal, m^* is the reduced effective exciton mass which is defined by $1/m^* = 1/m_e^* + 1/m_h^*$. m_e^* and m_h^* are the effective mass of electron and hole of the material, respectively. The Bohr radius of a semiconductor can be obtained from the dielectric constant ε and the reduced exciton mass m^*: $a_B = \varepsilon \hbar^2 / m^* e^2$.

Thus, the band gap of the material can be engineered to a desired level by changing the size of the nanocrystals:

$$E_{g,\text{nanocrystal}} = E_{g,\text{bulk}} + \Delta E = E_{g,\text{bulk}} + \frac{\hbar^2 \pi^2}{2m^* a^2} \qquad (1.4)$$

The band gap energy increases with a decrease in the size of the nanocrystals. Since the optical transition is directly related to the band gap, it is possible to tune the absorption and photoluminescence wavelength of the nanocrystals just by manipulating their size. Extensive studies have been

done for the size dependent optical properties of semiconductor nanostructures experimentally and theoretically.[8-11]

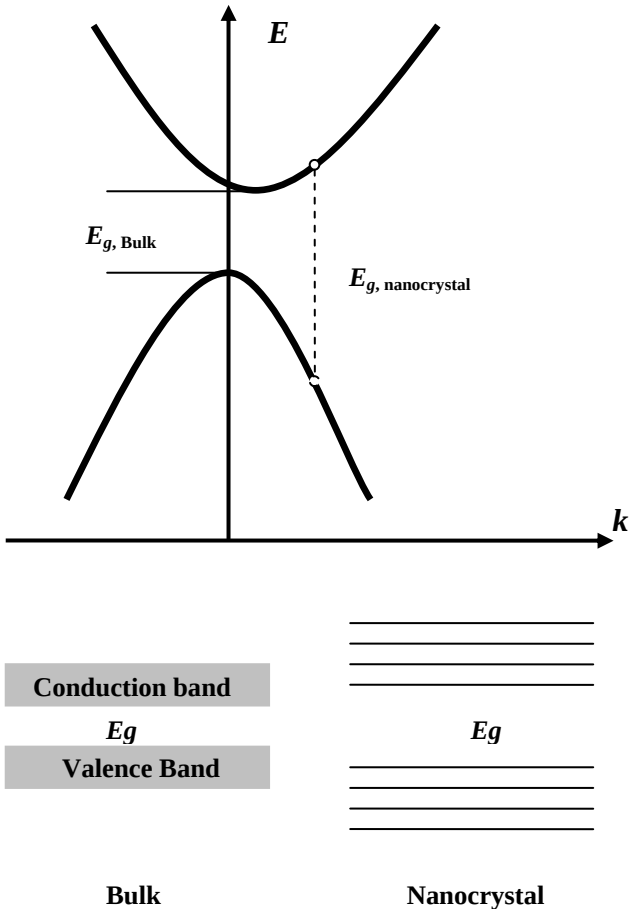

Figure 1.1 Illustration of a semiconductor band structure showing shift of energy band gap.

1.3 SUPERCRITICAL FLUID

In the last five years, interest in the synthesis of nanocrystals in supercritical fluids has grown considerably. A supercritical fluid (SCF) is a substance heated and pressurized above its critical temperature and pressure. The temperature-pressure phase diagram in Figure 1.2 shows a single phase fluid when the vapor coexistence curve disappears beyond the critical point. SCFs exhibit the combined characteristics of both gas and liquid solvents to provide a medium with densities characteristic of liquids, and gas-like viscosities and diffusivities. Thus, mass transfer rates approach those in gases, while solvation properties resemble those of conventional liquid solvents. SCFs offer several processing advantages over conventional solvents, which has led to its increased use in materials chemistry and more specifically, nanostructure synthesis.[12-18]

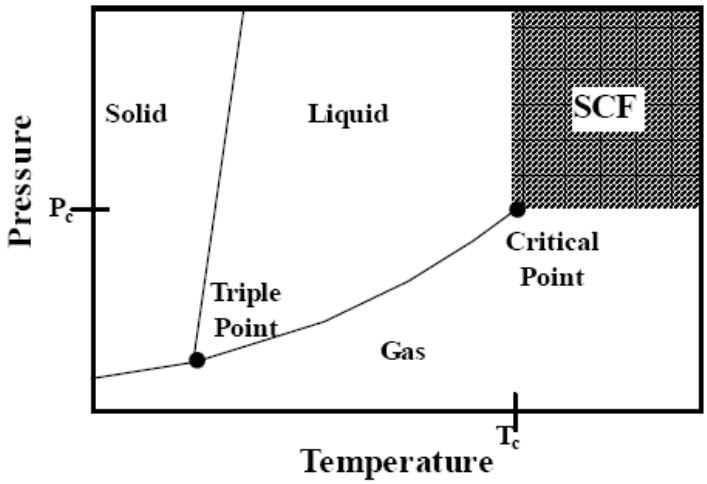

Figure 1.2 Schematic pressure-temperature phase diagram showing the triple point, the critical point and the supercritical point and the supercritical region.

When nanocrystals are synthesized in SCFs, the SCF must stabilize the capping ligands on the particles to control the growth. This stabilization of ligands, needed to control nanocrystal size and morphology, is not available in gas phase reactions. SCF density can be altered through modest changes in pressure and temperature. The solvent density strongly influences the interactions between surfactant tails and solvent molecules that are directly responsible for steric stabilization, making SCF solvation characteristics highly tunable. The effect of solvent density on colloid steric stabilization in SCF has been characterized by lattice-fluid theory,[19,20] Monte Carlo

simulation[21], light scattering[22] and neutron scattering[23]. A tunable SCF solvent may be utilized to provide reversible stabilization and destabilization of colloidal dispersions, which could improve many aspects of nanocrystal processing, such as size-selective separations, synthesis and self-assembly.

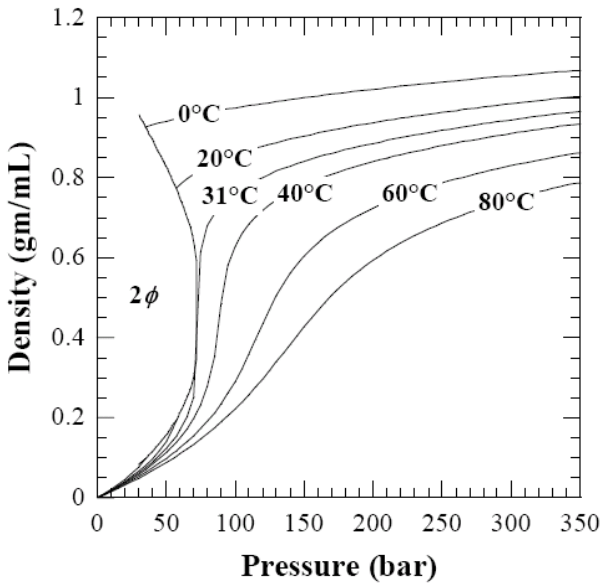

Figure 1.3 Density-pressure phase diagram of CO_2. The critical temperature and pressure of CO_2 are 31°C and 71 bar respectively.

Compared to the organic supercritical fluids used to make nanocrystals, carbon dioxide (CO_2) has a variety of attractive features. CO_2

is non-flammable, essentially non-toxic and environmentally benign, and it has low critical temperature and pressure (31ºC and 71 bar, Figure 1.3). Since CO_2 is more chemically stable than organic solvents, less organic contaminants would be produced when making Ge nanoparticles in supercritical CO_2 (sc-CO_2) than in supercritical hydrocarbon fluids due to the degradation of the solvent itself at high temperature. The prevention of the formation of impurities from the solvent is very important since it is difficult to separate the organic byproducts from Ge nanoparticles capped with a layer of organic ligands. Besides these advantages, there are, however, significant challenges in using sc-CO_2 to synthesize Ge nanoparticles. CO_2 has a low polarizability per volume resulting in far weaker van der Waals forces than in the case of hydrocarbon solvents, which makes it more like a fluorocarbon. Thus it is important to find a suitable surfactant to stabilize the colloidal dispersions of Ge nanoparticles in CO_2. Surfactants with fluorinated tails, such as fluoroacrylates, alkanes and ethers, have proven to be highly effective for silver nanoparticles.[13]

1.4 SEMICONDUCTOR NANOWIRE SYNTHESIS

Various synthetic pathways have been investigated in recent years to synthesize group IV[14,16,18,24], II-VI[25] and III-V[26,27] semiconductor nanowires.

Depending on different growth mechanisms, strategies that have successfully grown high respect ratio nanowires include vapor-liquid-solid (VLS)[28-31], solution-liquid-solid (SLS)[32,33], supercritical fluid-liquid-solid (SFLS)[14,15,17], laser catalytic growth[34], and template-directed growth[35-37], etc. Among all of the various synthetic methods for group IV semiconductor nanowires, e.g. Si and Ge, VLS-based growth mechanism has been the most widely used.

The VLS process was first discovered by Wagner and Ellis[38] in a study of whisker growth 40 years ago. In their work, liquid gold droplets on a substrate surface were employed as the growth seeds to grow silicon nanowires. The gas phase Si precursor was introduced into the reaction chamber and decomposed to form Si. According to the binary phase diagram of Si and Au, these two elements form an alloy at 363±3°C when the concentration of Si in Au reaches to a certain point[39]. With continuous feeding of Si into Au:Si liquid alloy droplets to achieve saturation, Si crystallized from the droplets and grew into one-dimensional nanowires with diameter of ~ 100 nm which typically mirrored the size of liquid droplets (Figure 1.4). An adaptation of this chemical vapor deposition (CVD) based method was taken by Morales and Lieber[34] in 1998 to produce 1 to 30 nm Si and Ge nanowires through laser ablation of targets containing the corresponding elements and metal catalyst.

Although the CVD-based approaches have been successfully utilized to make a variety of semiconductor nanowires, the solution-based syntheses are more desirable for scale up. It is possible to achieve much higher throughput of free-floating nanowires and in-situ passivation with an organic monolayer to prevent oxidation of the nanowires and to facilitate fabrication of devices. A first solution-base synthesis of Ge nanowires was reported by Heath and LeGoues[40] in 1993 by reduction of $GeCl_4$ and phenyl-$GeCl_3$ with sodium in hexane heated to 275°C at a pressure of 10 MPa. This approach produced nanowires, although the yield and the crystallinity were low. In 2000, Holmes et al.[14] proposed a supercritical fluid method (SFLS) to make 2.5 nm Si nanowires by decomposing diphenylsilane in hexane in a high pressure reaction cell heated well above the critical point of the solvent.

To date, most solution syntheses of group IV semiconductor (Si and Ge) nanowires have only been achieved in high temperature and high pressure solvents based on the SFLS mechanism. While the SLS approach has been successfully employed to grow group II-VI[25] and group III-V[26,27] nanowires in conventional solvents, it has been difficult to identify appropriate Si or Ge precursors with high boiling points that readily decompose in organic solvents at atmospheric pressure to sustain the growth of the nanowire crystal.

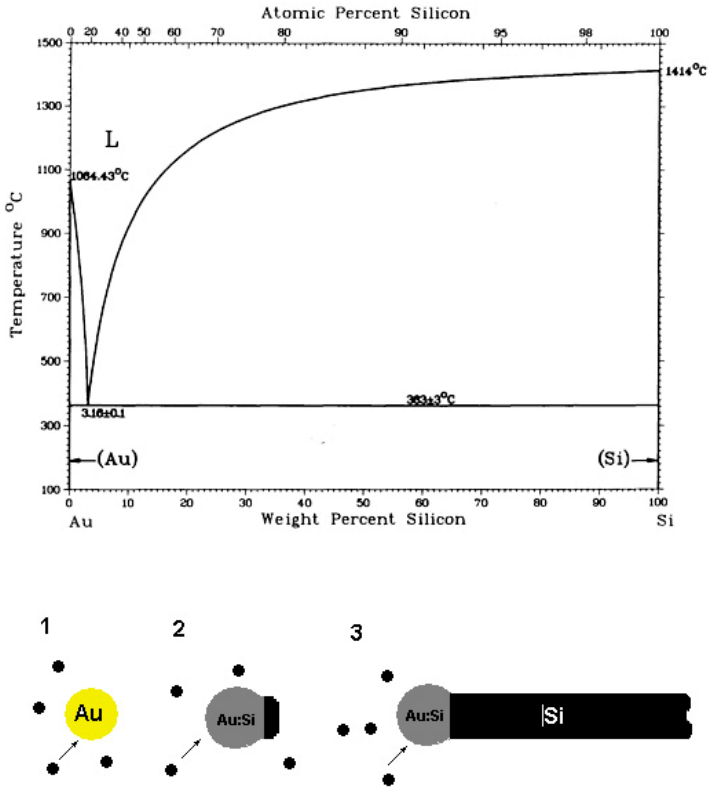

Figure 1.4 Phase diagram of Au:Si and representative VLS growth mechanism of Si nanowires.

1.5 COLLOIDAL NANOCRYSTAL SYNTHESIS

A variety of semiconductors, including group II-VI[41-45], group III-V[44,46], and group IV-VI[47,48], and metal colloidal nanoparticles[49-51] have been successfully synthesized by reaction in solution by arrested growth methods.

Colloidal nanocrystal growth involves the precipitation of a solid phase from solution to form particles and surface passivation of the nanoparticles with a protection layer. The precipitation process consists of a nucleation step followed by particle growth. Generally, the solution phase synthesis of nanoparticles starts with rapid addition of a precursor into a reaction vessel containing coordinating solvent. The solution is supersaturated and unstable in energy due to reaction of the precursor to an insoluble form. To release the supersaturation, solute molecules combine and form nuclei and precipitate out of solution. The driving force for nucleation is determined by the overall free energy change, ΔG, which is the sum of the free energy due to the formation of a new phase of given volume and the free energy due to the new surface area created. By assuming that solid phase nucleates as spheres with radius r, it may be shown that the free energy for a single nucleus, $\Delta G(r)$ can be derived as following:

$$\Delta G(r) = -\frac{4}{V}\pi r^3 k_b T \ln(S) + 4\pi r^2 \gamma \qquad (1.5)$$

where V is the molecular volume of the precipitated nucleus, k_b is the Boltzman constant, S is the saturation ratio, and γ is the solid/liquid interfacial

free energy per unit surface area. Figure 1.5 illustrates the free energy as a function of the particle size.

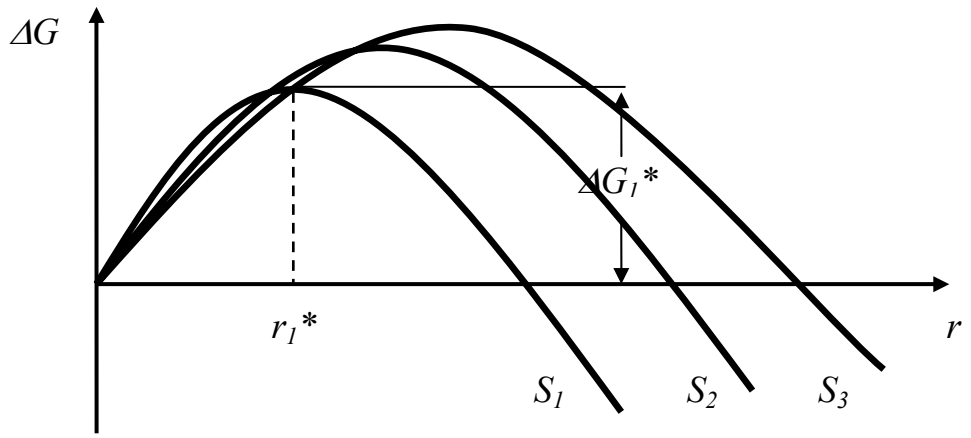

Figure 1.5 Free energy as a function of the radius of the nuclei at given supersaturation ratios. $S_1 > S_2 > S_3$.

For the case of $S>1$, a critical radius, r^*, can be obtained by setting $\mathrm{d}\Delta G(r)/\mathrm{d}r = 0$. ΔG reaches a maximum of ΔG^* (eq. 1.6) at a critical

radius r^* and this free energy is the activation energy for nucleation where

$$r^* = \frac{2V\gamma}{3k_bT\ln(S)} \qquad (1.6)$$

For a given saturation ratio S, all nuclei with size greater than r^* will grow and all nuclei with radius less than r^* will dissolve to lower their free energy.

When the concentration of the solute drops below the critical level, nucleation stops and the particles grow through addition, until the concentration of the precipitated molecules reaches equilibrium. If a continuous supply of precursor is provided to sustain the growth, but the concentration is kept under a level so as to prevent formation of more nuclei, nearly monodisperse particles can be obtained. At this growth stage, particles with smaller radius grow faster since their free energy driving force is larger than larger particles, when the size of the particles is above the critical radius r^* (Figure 1.5). This situation leads to focusing of the particle size. If the precursor is depleted at the growth stage, however, defocusing in particle size will occur. In this case, the saturation ratio S decreases and the corresponding critical radius r^* increases. Particles smaller than the new critical radius will dissolve and particles bigger than the critical radius will grow, resulting in broader size distribution. During actual experiment, the

particles can also grow through aggregation, where two or more particles and/or nuclei combine and form larger particles. This type of growth can further broaden the size distribution of the particles.

To prevent the particles from aggregation, the nanoparticles need to be protected with a stabilizer to form a passivation layer during growth. This stabilizer usually is one or multiple organic species which physically or chemically absorbs to the nanocrystal surface. The particle size can also be tailored by the selection of stabilizers and the ratio of stabilizer to precursor. Stronger stabilizers or stabilizers with larger molecular weight provide a greater barrier and slower growth rate, resulting in smaller particles. A high capping ligand to precursor ratio favors the formation of smaller nuclei and thus smaller nanocrystals.

1.6 DISSERTATION OVERVIEW

The objective of this research is to synthesize group IV semiconductor nanostructures, including Si nanowires, Ge nanoparticles and Ge nanowires, in solution phase, either in SCFs or in conventional solvents, and to explore the morphology and optical properties of the nanocrystals.

Chapter 2 represents the synthesis of Si nanowires on a substrate in a SCF. Gold nanoparticles with an average diameter of 7 nm were utilized as growth seeds to synthesize Si nanowires. The Si precursor, diphenylsilane, was decomposed in supercritical hexane at 400-500°C and 3000 psia. Both batch reactor and flow reactor were employed to grow Si nanowires and the morphologies of the wires obtained in both cases were compared. Kinetic analysis indicates that the nanowire morphology was influenced by the reaction temperature, reactor type and Si precursor concentration.

Synthesis of Ge nanocrystals in SCFs was described in Chapter 3. Two Ge precursors, diphenylgermane (DPG) and tetraethylgermane (TEG), were explored in supercritical organic solvents, including hexane and octanol, to make 2-70nm Ge nanoparticles. The nanocrystals were passivated with octanol which controls the growth of the particles. High resolution transmission electron microscopy (HRTEM), FTIR spectroscopy and X-ray diffraction (XRD) were utilized to investigate the morphology, surface chemistry and crystallinity of the nanoparticles, respectively. By changing the concentration of the precursor solution, Ge nanocrystals with different sizes can be obtained. The UV-visible absorption and photoluminescence spectra of the 3-4 nm nanocrystals exhibit blue shift from the bulk Ge, indicating that quantum confinement take effect for the optical properties of

those nanocrystals. The purification of the Ge nanoparticles synthesized with SCF approach, however, was challenging due to the degradation of the organic solvent at high temperature and high pressure and the formation of by-products with high molecular weight.

To reduce the formation of organic contaminants, an inorganic solvent, supercritical CO_2 was used to make Ge nanoparticles by decomposing DPG or TEG at 500°C and 4000 psia with octanol as the capping ligand, as discussed in Chapter 4. The synthesis in sc-CO_2 produced much less organic contamination compared with similar reactions in organic supercritical fluids. Ge nanoparticles with average diameter of 10 and 5 nm were observed for DPG and TEG in sc-CO_2, respectively. Without CO_2, the gas phase reaction did not produce nanocrystals, indicating that CO_2 provides sufficient solvation of the capping ligands to achieve steric stabilization.

A new synthetic approach to make Ge nanocrystals is described in Chapter 5. The utilization of a highly reactive Ge precursor, GeI_2, enables high yields (up to ~70%) of Ge nanocrystals when reduced with $LiAlH_4$ in a high boiling point solvent, tri-n-octylphosphine (TOP), at 300°C. The nanoparticles exhibited high crystallinity and the average size can be manipulated by varying the concentration of GeI_2. The nanoparticles were

passivated with TOP, as revealed by FTIR spectroscopy. Ge nanoparticles were also synthesized with tri-n-butylphosphine (TBP) and the broader size distribution of the particles compared to those made in TOP indicates that the stabilizer with longer tails provided a larger barrier and better control over size. The advantages of this method to make Ge nanocrystals include the high reactivity of GeI_2, high GeI_2 solubility in alkyl phosphines and the relatively mild reaction temperature, which led to higher chemical yield and facile recovery of the nanoparticles, due to limited byproduct formation and solvent degradation. Chapter 6 extends this synthetic approach to Ge nanowires. By using GeI_2 as the Ge precursor and a low melting point growth seed, bismuth nanoparticles, Ge nanowires of high chemical yield were synthesized in a TOP. This is the first example of group IV nanowires synthesized in a conventional solvent at atmospheric pressure.

1.7 REFERENCES

(1) Alivisatos, A. P. *Science* **1996**, *271*, 933-937.

(2) Klimov, V. I.; Editor *Semiconductor and Metal nanocrystals: Synthesis and Electronic and Optical Properties.*; Marcel Dekker, Inc.: New York, 2004; Vol. 87.

(3) Klabunde, K. J.; Editor *Nanoscale Materials in Chemistry*; John Wiley & Sons, Inc.: New York, 2001.

(4) Bruchez, M.; Moronne, M.; Gin, P.; Weiss, S.; Alivisatos, A. P. *Science* **1998**, *281*, 2013-2016.

(5) Klimov, V. I.; Mikhailovsky, A. A.; Xu, S.; Malko, A.; Hollingsworth, J. A.; Leatherdale, C. A.; Eisler, H. J.; Bawendi, M. G. *Science* **2000**, *290*, 314-317.

(6) Huynh, W. U.; Dittmer, J. J.; Alivisatos, A. P. *Science* **2002**, *295*, 2425-2427.

(7) Sato, T.; Ahmed, H.; Brown, D.; Johnson, B. F. G. *J. Appl. Phys.* **1997**, *82*, 696-701.

(8) Murray, C. B.; Kagan, C. R.; Bawendi, M. G. *Annu. Rev. Mater. Sci.* **2000**, *30*, 545-610.

(9) Alivisatos, A. P. *J. Phys. Chem.* **1996**, *100*, 13226-13239.

(10) Norris, D. J.; Sacra, A.; Murray, C. B.; Bawendi, M. G. *Phys. Rev. Lett.* **1994**, *72*, 2612-2615.

(11) Yoffe, A. D. *Adv. Phys.* **2001**, *50*, 1-208.

(12) Holmes, J. D.; Ziegler, K. J.; Doty, R. C.; Pell, L. E.; Johnston, K. P.; Korgel, B. A. *J. Am. Chem. Soc.* **2001**, *123*, 3743-3748.

(13) Shah, P. S.; Holmes, J. D.; Doty, R. C.; Johnston, K. P.; Korgel, B. A. *J. Am. Chem. Soc.* **2000**, *122*, 4245-4246.

(14) Holmes, J. D.; Johnston, K. P.; Doty, R. C.; Korgel, B. A. *Science* **2000**, *287*, 1471.

(15) Lu, X.; Hanrath, T.; Johnston, K. P.; Korgel, B. A. *Nano Lett.* **2003**, *3*, 93.

(16) Hanrath, T.; Korgel, B. A. *J. Am. Chem. Soc.* **2002**, *124*, 1424.

(17) Hanrath, T.; Korgel, B. A. *Adv. Mater.* **2003**, *15*, 437.

(18) Tuan, H. Y.; Lee, D. C.; Hanrath, T.; Korgel, B. A. *Nano Lett.* **2005**, *5*, 681.

(19) Meredith, J. C.; Johnston, K. P. *Macromolecules* **1998**, *31*, 5518-5528.

(20) Peck, D. G.; Johnston, K. P. *Macromolecules* **1993**, *26*, 1537-1545.

(21) Meredith, J. C.; Johnston, K. P. *Langmuir* **1999**, *15*, 8037-8044.

(22) ONeill, M. L.; Yates, M. Z.; Harrison, K. L.; Johnston, K. P.; Canelas, D. A.; Betts, D. E.; DeSimone, J. M.; Wilkinson, S. P. *Macromolecules* **1997**, *30*, 5050-5059.

(23) Lee, C. T.; Johnston, K. P.; Dai, H. J.; Cochran, H. D.; Melnichenko, Y. B.; Wignall, G. D. *J. Phys. Chem. B* **2001**, *105*, 3540-3548.

(24) Wang, D.; Tu, R.; Zhang, L.; Dai, H. *Angew. Chem.-Int. Edit.* **2005**, *44*, 2925.

(25) Yu, H.; Li, J. B.; Loomis, R. A.; Gibbons, P. C.; Wang, L. W.; Buhro, W. E. *J. Am. Chem. Soc.* **2003**, *125*, 16168.

(26) Yu, H.; Buhro, W. E. *Adv. Mater.* **2003**, *15*, 416.

(27) Yu, H.; Li, J. B.; Loomis, R. A.; Wang, L. W.; Buhro, W. E. *Nat. Mater.* **2003**, *2*, 517.

(28) Zaitseva, N.; Harper, J.; Gerion, D.; Saw, C. *Appl. Phys. Lett.* **2005**, *86*, 053105.

(29) Wu, Y.; Yang, P. *J. Am. Chem. Soc.* **2001**, *123*, 3165.

(30) Pan, L.; Lew, K.-K.; Redwing, J. M.; Dickey, E. C. *Nano Lett.* **2005**, *5*, 1081.

(31) Dailey, J. W.; Taraci, J.; Clement, T.; Smith, D. J.; Drucker, J.; Picraux, S. T. *J. Appl. Phys.* **2004**, *96*, 7556.

(32) Trentler, T. J.; Hickman, K. M.; Goel, S. C.; Viano, A. M.; Gibbons, P. C.; Buhro, W. E. *Science* **1995**, *270*, 1791-1794.

(33) Fanfair, D. D.; Korgel, B. A. *Crystal Growth & Design* **2005**, *5*, 1971.

(34) Morales, A. M.; Lieber, C. M. *Science* **1998**, *279*, 208.

(35) Zach, M. P.; Ng, K. H.; Penner, R. M. *Science* **2000**, *290*, 2120-2123.

(36) Ragan, R.; Chen, Y.; Ohlberg, D. A. A.; Medeiros-Ribeiro, G.; Williams, R. S. *J. Crystal Growth* **2003**, *251*, 657-661.

(37) Yun, M. H.; Myung, N. V.; Vasquez, R. P.; Lee, C. S.; Menke, E.; Penner, R. M. *Nano Lett.* **2004**, *4*, 419-422.

(38) Wagner, R. S.; Ellis, W. C. *App. Phys. Lett.* **1964**, *4*, 89.

(39) Okamoto, H.; Massalski, T. B. *J. Metals* **1984**, *36*, 57.

(40) Heath, J. R.; LeGoues, F. K. *Chem. Phys. Lett.* **1993**, *208*, 263.

(41) Murray, C. B.; Norris, D. J.; Bawendi, M. G. *J. Am. Chem. Soc.* **1993**, *115*, 8706-8715.

(42) Peng, Z. A.; Peng, X. G. *J. Am. Chem. Soc.* **2001**, *123*, 183-184.

(43) Talapin, D. V.; Rogach, A. L.; Mekis, I.; Haubold, S.; Kornowski, A.; Haase, M.; Weller, H. *Colloids Surf., A* **2002**, *202*, 145-154.

(44) Hines, M. A.; Guyot-Sionnest, P. *J. Phys. Chem. B* **1998**, *102*, 3655-3657.

(45) Shim, M.; Guyot-Sionnest, P. *J. Am. Chem. Soc.* **2001**, *123*, 11651-11654.

(46) Peng, X. G.; Wickham, J.; Alivisatos, A. P. *J. Am. Chem. Soc.* **1998**, *120*, 5343-5344.

(47) Steckel, J. S.; Coe-Sullivan, S.; Bulovic, V.; Bawendi, M. G. *Adv. Mater.* **2003**, *15*, 1862-1866.

(48) Wehrenberg, B. L.; Wang, C. J.; Guyot-Sionnest, P. *J. Phys. Chem. B* **2002**, *106*, 10634-10640.

(49) Sun, S. H.; Anders, S.; Thomson, T.; Baglin, J. E. E.; Toney, M. F.; Hamann, H. F.; Murray, C. B.; Terris, B. D. *J. Phys. Chem. B* **2003**, *107*, 5419-5425.

(50) Sun, S. H.; Murray, C. B.; Weller, D.; Folks, L.; Moser, A. *Science* **2000**, *287*, 1989-1992.

(51) Shevchenko, E. V.; Talapin, D. V.; Rogach, A. L.; Kornowski, A.; Haase, M.; Weller, H. *J. Am. Chem. Soc.* **2002**, *124*, 11480-11485.

Chapter 2: Growth of Single Crystal Silicon Nanowires in Supercritical Solution from Gold Particles on a Silicon Substrate*

Molecularly tethered gold (Au) nanocrystals with average diameter of 7 nm were used to grow single crystal silicon (Si) nanowires on a substrate through a supercritical fluid-liquid-solid (sc-FLS) mechanism. Si wires were obtained by degrading diphenylsilane (DPS) in cyclohexane heated and pressurized well above its critical point and the Si:Au eutectic temperature (363ºC). The nanowire diameter reflects the gold nanocrystal diameter, ranging from 5 to 30 nm, with lengths of several micrometers. Both batch and flow reactors were used. The flow reactor minimized the undesirable deposition of Si particulates formed in the bulk solution. SEM images of Si nanowires grown at a series of temperatures, reactor residence times, and Si precursor concentrations reveal that the wire growth kinetics influence nanowire morphology significantly and can be controlled effectively using a SCF flow reactor. A kinetic analysis of the process explains the dependence of the nanowire morphology on the reaction conditions qualitatively.

---

* Portions of this chapter have been previously published as Lu, Xianmao; Hanrath, Tobias; Johnston, Keith P.; and Korgel, Brian A.; *Nano Lett.*, **2003**, 3, 93-99.

2.1 INTRODUCTION

In the last few years, synthetic methods that do not rely on conventional lithographic techniques have been developed to form silicon nanowires micrometers in length with diameters below 10 nm.[1-6] These methods rely on metal particles to induce nanowire growth above the semiconductor:metal solution eutectic temperature and can be used to grow large quantities efficiently in either the gas or solution phase. Nanowires grown using these methods are receiving attention for application in technologies ranging from integrated circuit interconnects to functional electronic and optical devices. For example, nanowires have served as self-assembling building blocks in devices that include field effect transistors, photodetectors and biochemical sensors, light-emitting diodes and complementary logic devices.[2,7-9]

The fundamental process of metal particle directed semiconductor wire growth was developed over 30 years ago. The first experiments involved the chemical vapor deposition (CVD) of Si whiskers ~100 nm in diameter in the presence of ~100 nm diameter liquid gold droplets. In this process, a Si precursor decomposes at a hot surface to Si, which preferentially dissolves in the gold droplet. As more Si degrades, the gold droplets become saturated and expel Si in the form of crystalline whiskers. This process is known as

vapor-liquid-solid (VLS) growth.[10] A few years ago, much smaller 6 to 20 nm diameter Si nanowires were synthesized using nanoscale metal droplets formed in the gas-phase by laser ablation.[2] Ge, GaN and GaAs nanowires were also formed using these methods.[6,11-16] Alternatively, a solution-liquid-solid (SLS) method was used to synthesize 10 to 150 nm Group III-V semiconductors at temperatures from 164 to 203ºC.[17] The SLS technique cannot be applied to Group IV elements as eutectic temperatures for the alloys with most metals are above the boiling point and even the critical temperature of most solvents.

To synthesize Si nanowires less than 10 nm in diameter with a narrow size distribution, we introduced a new fluid-liquid-solid (FLS) method.[1] In the FLS method, a precursor such as diphenylsilane thermally degrades in a supercritical fluid at 450 to 500^{o}C, rather than a gas (VLS method) or liquid (SLS method).[10,17] Using 2.5 nm alkanethiol coated gold nanocrystals with low polydispersity, Si nanowires with diameters between 4 and 5 nm have been synthesized via the FLS method.[1] Lieber and co-workers later reported diameter control of Si[4] and GaP[18] nanowires by combining CVD with size-selected Au particles ranging from 3 to 20 nm attached to a surface. However, supercritical fluids such as hexane and cyclohexane disperse high concentrations of sterically-stabilized nanocrystals, and precursor

concentrations can range from 0.1 to 1.0 mol/L, in contrast with typical values of 4.0×10^{-3} mol/L in CVD. High concentrations of dissolved organometallic precursors have been used in chemical fluid deposition of metal films from supercritical fluid CO_2 solutions[19]. In the FLS method, the combination of high concentrations, and diffusion coefficients that approach gas phase values, affords fast growth rates and efficient nanowire production. The ability to manipulate the precursor concentration, the metal seed concentration and size, and the solvent strength of the supercritical fluid via pressure and temperature[20] provides flexibility in controlling the nanowire composition and morphology. In the development of certain nanoscale devices, the ability to deposit nanowires on a surface is an important step. Herein, we describe the growth of Si nanowires by the FLS method from gold seed crystals tethered to a silicon surface.

Sterically-stabilized gold nanocrystals were covalently attached to a Si substrate functionalized with 3-mercaptopropyl-trimethoxysilane (MPTMS). Si nanowires were formed via a templated FLS process by decomposing a Si precursor, diphenylsilane, in supercritical cyclohexane (C_6H_{12}) (See Figure 2.1). A flow reactor utilized in the FLS technique for the first time provides greater control relative to a batch reactor over the nanowire morphology, and under a limited range of reaction conditions produces straight low-defect

nanowires. The flow reactor provides the kinetic tunability necessary to minimize undesirable Si particle deposition and to optimize the production of straight wires. For example, manipulating the temperature and precursor concentration alters the morphology from tortuous to straight wires.

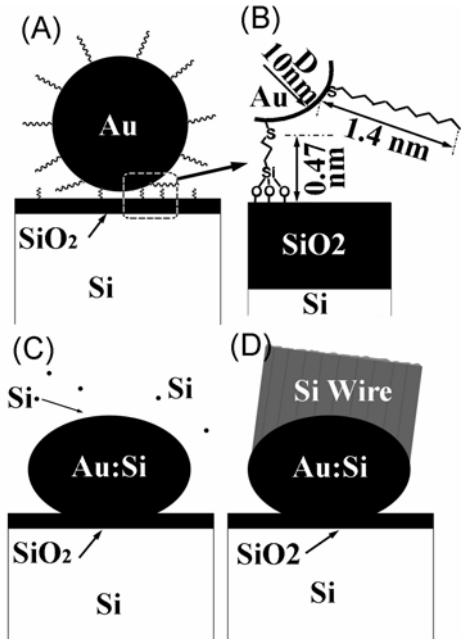

Figure 2.1 Schematic of Si nanowire synthesis from tethered sterically stabilized Au nanocrystals. (A) Au nanoparticles were adsorbed to an MPTMP-modified Si substrate. (B) Enlarged view of the selected region in (A). (C) DPS degrades to Si atoms that dissolve into the nanocrystals to form Au:Si alloy droplets on the Si substrate. (D) Si nanowires crystallize from the Au nanocrystal seeds upon saturation of the particle.

2.2 EXPERIMENTAL SECTION

2.2.1 Si substrate preparation

A Si wafer (<100>, with thermal oxide 10 nm, Wafer World, Inc.) was cut into 5 × 20 mm samples that were degreased with distilled deionized water (D-H_2O) and acetone in an ultrasonic bath. These small Si substrates were immersed in a HCl:methanol (w:w=1:1) solution and then 98% H_2SO_4 each for 30 minutes. After rinsing with D-H_2O and drying with N_2, the substrates were immersed for one hour in a dilute aqueous solution of 1:1:40 (v:v:v) MPTMS (Gelest, Inc.):D-H_2O:isopropyl alcohol to functionalize the surface. The MPTMS-treated Si substrate was transferred to a colloidal dispersion of alkanethiol-coated Au nanocrystals in chloroform. The Au nanocrystals were synthesized according to the procedures[21] described in the literature.[22,23] After incubating for 2 to 10 hours at room temperature, the substrate was rinsed with and stored in D-H_2O for later use.

2.2.2 Nanowire synthesis

Diphenylsilane (DPS, Gelest) was stored in an inert atmosphere under N_2. Feedstock solutions of DPS in anhydrous cyclohexane (Aldrich

Chemical Co.) were prepared in a N_2 glovebox with concentrations ranging from 0.1 to 0.9 M.

Batch reactions were carried out by loading an MPTMS and Au nanocrystal-treated Si substrate and 0.5 mL DPS feedstock solution into a 1 mL titanium grade-2 cell (0.5 cm I.D., 2.0 cm O.D. and 7.0 cm long with a titanium grade-2 LM6 HIP gland and plug, High Pressure Equipment, Inc) in a N_2 glovebox. A brass block (7X25X17 cm) designed to hold up to 6 reactors was used to heat the reactor. The block was thermostatted with a thermocouple (Omega, Inc.) and a temperature controller, and heated by four 300 watt 1/4" diameter by 4.5" long cartridge heaters (Omega). The block was heated to the desired reaction temperature prior to inserting the cell. The cell was inserted into the preheated block and reached the synthesis temperature within a few minutes with a calculated pressure[24] of 29.0 MPa. The reaction proceeded another 15 minutes at this temperature. A special cell filled with a thermocouple verified that significant temperature gradients do not occur during the reaction and that the cell interior rapidly reaches synthesis temperature. The reaction was quenched by rotating the brass block upside down with a cable and sliding the cell by gravity into an ice water bath. The cell contents cooled to less than 50ºC in two minutes. The entire device was shielded heavily with polycarbonate barricades.

The flow reactor was a 2 mL (0.5 cm I.D., 2.0 cm O.D. and 12.5 cm long) high-pressure titanium grade-2 cell with both ends connected to 1/16" O.D. and 0.03" I.D. stainless steel high-pressure tubing via titanium grade-2 LM-6 HIP reducers (High Pressure Equipment) (Figure 2.2). Cyclohexane and a modified Si substrate were loaded into the cell under an inert N_2 atmosphere in a glove box. Two stainless steel cylinders (1.7 cm I.D., 2.5 cm O.D. and 20 cm long) were equipped with stainless steel pistons and ethylene propylene O-rings. In the glove box, one of these cylinders was loaded with cyclohexane and the other with DPS:cyclohexane stock solution. The cylinders were removed from the glovebox and connected to the preheater tubing. The reaction cell was then removed from the glove box and connected via a three-way valve to the preheater tubing. The preheater tubing and the reaction cell were covered with heating tape and glass wool insulation and heated to 300°C to 350°C and 350°C to 500°C, respectively, in 3 to 5 minutes.

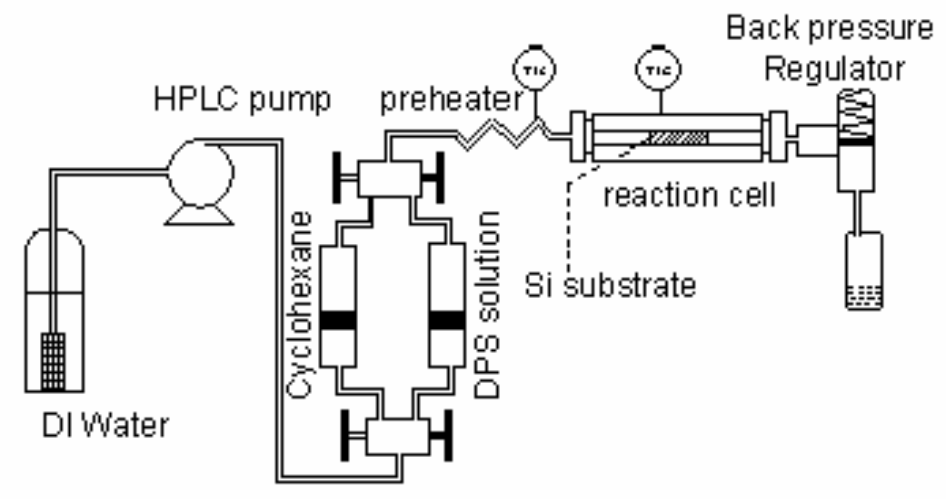

Figure 2.2 Schematic of the flow reactors used to synthesize Si nanowires.

The temperature was measured by thermocouples under the heating tape and controlled to within about 5°C in the preheater and 1°C in the reactor. The cylinder containing pure cyclohexane was pressurized by pumping DI-H_2O into the back of the piston using an HPLC (high pressure liquid chromatography) pump (Thermoquest) to inject oxygen-free cyclohexane through the preheater tubing and into the reaction cell until reaching the desired pressure. The valves to the first cylinder containing only solvent were closed and the DPS feed solution valves were opened. The HPLC pump controlled the DPS solution flow rates, which ranged from 0.5 to 3 mL/min. An SS-4R3A back-pressure regulator (Swagelok) connected after the reaction cell and a digital pressure gauge (Stratford) between the preheater tubing and the cell maintained the pressure at 24.1±1.4 MPa. The reaction proceeded for 5 minutes before switching the valves back to the solvent cylinder. Solvent was flushed through the cell at 3 mL/min to remove undesired reaction byproducts and particulates from the system.

2.2.3 Materials characterization

A LEO 1530 high resolution scanning electron microscope (HRSEM) was used with a 10 kV accelerating voltage to study the morphology of the nanowires on the Si substrate. X-ray photoelectron spectroscopy (XPS) was

performed using a Physical Electronics XPS 5700 equipped with monochromatic Al X-ray source (Al, K_α, 1.4866 keV). High resolution transmission electron microscopy (HRTEM) and selected area electron diffraction (SAED) were performed using a JEOL 2010F TEM operating at 200 kV. Images were obtained primarily with a GATAN digital photography system. To avoid structural damage to the nanowires that occurs with sonication or solvent redispersion, samples were prepared for HRTEM by scratching the surface of the silicon substrate with carbon coated 200 mesh Cu grids (Electron Microscope Sciences).

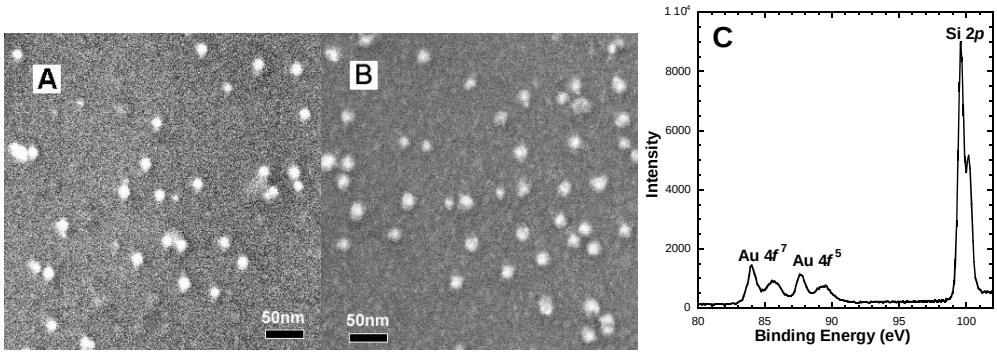

Figure 2.3 (A) HRSEM image and (C) XPS of a Si substrate after grafting Au nanocrystals to the surface. The average diameter of the gold particles are 12.95±3.69 nm. (B) HRSEM image of the the Si substrate with gold particles after being subjected to the reaction condition (T=500°C, P=24.1 MPa, flowing cyclohexane). The gold particles have an average diameter of 13.09±2.67 nm.

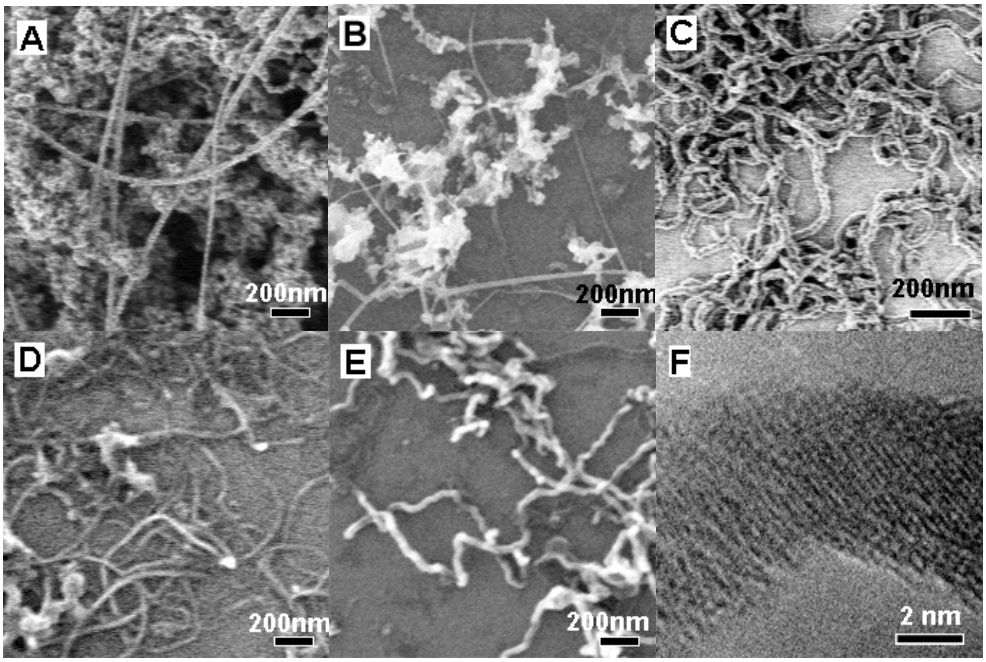

Figure 2.4 (A-E) HRSEM images of Si nanowires grown from Au nanocrystals on a Si substrate in the batch reactor and (F) HRTEM image for a wire from (E) showing a defect. (A), (B), and (C) are Si nanowires obtained at 500ºC with different concentrations of DPS: 0.9, 0.25 and 0.1 M respectively. (D) and (E) are Si nanowires synthesized with 0.25 M DPS at (B) 500ºC, (D) 450ºC and (E) 400ºC, respectively. (F) HRTEM image for a tortuous wire revealing good crystallinity and clear lattice fringes on the right of the joint, but lattice mismatched on the left.

2.3 RESULTS

For the experiments, Si substrates were functionalized with alkanethiol-coated Au nanocrystals with an average diameter of 6.7±2.6 nm as determined by TEM of the particles prior to deposition on the surface-modified Si substrates. The Au nanocrystal surface coverage was 2%. Figure 2.3A shows an HRSEM image of a nanocrystal-modified Si substrate with the associated XPS data (Figure 2.3C). Exposure of the substrate to the reaction conditions in the absence of nanowire formation as a control experiment (T=500ºC, P= 24.1 MPa, flowing cyclohexane) reveals no significant change in the Au nanocrystal size distribution (Figure 2.3B), indicating minimal particle aggregation . This observation is consistent with expectations that the siloxane monolayer is stable at least up to 815 K[25].

Although Si nanowires could be grown from the substrate under batch conditions, the nanowire quality was generally poor. Figure 2.4 shows HRSEM images of the Si nanowires grown in a batch reactor from Si substrates with 2% Au nanocrystal surface coverage. At 500ºC and [DPS]=0.9 M, straight Si wires several micrometers in length were observed (Figure 2.4A). However, the wires were heavily surrounded by Si particles.[26] Lowering the DPS concentration reduced Si particle formation considerably

([DPS]=0.25 M; Figure 2.4B); however, under these conditions, most of the wires were shorter than 1 μm. Further reduction in DPS concentration ([DPS]=0.1 M) decreased particulate formation even more, but under these growth conditions, the wires exhibit a tortuous morphology due to defects in the crystal lattice (Figure 2.4C and 2.4F). Reduced temperature continues to decrease Si particle formation (Figures 2.4D and 2.4E, [DPS]=0.25 M at 450ºC and 400ºC, respectively), but at the expense of exceedingly tortuous nanowire production. In summary, the batch reactions reveal that straight wires require high precursor concentrations and high temperatures. The homogeneous nucleation and growth of Si particles in the fluid phase under these conditions, and their subsequent deposition on the substrate, however, eliminates the suitability of the batch reactor for nanowire growth on a substrate.

A flow reactor provides the means to produce straight wires with minimal Si particulate formation, because it provides (1) fluid-phase reactant concentrations that vary less significantly with time and (2) a means to flush Si particulates formed in the fluid phase before depositing on the substrate. Si nanowires produced at 500^{o}C, [DPS]=0.25 M, and a feed rate of 0.5 mL/min were straight and contaminated with very few Si particles (Figure 2.5A). The inset in Figure 2.5A shows a gold particle at the end of a

nanowire, indicating that the Au seeds participate directly in wire growth. The average Si wire diameter measured by HRSEM, 16 ± 4 nm, resembles closely the Au particle size and size distribution prior to wire growth[27]. Nanowires as small as 5 nm and longer than 10 μm are present in the sample. Si particle formation increases at higher reactant flow rates. At 1.0 mL/min, particle formation becomes significant (Figure 2.5B), and at substantially higher flow rates (3 mL/min), nearly all the substrate ends up covered by Si particles (Figure 2.5C). As in the batch reactor, reduced temperature results in bent and/or curly wires. For example, Figure 2.5D shows curly wires formed at 0.5 mL/min at 450^{o}C. Comparing the observed Si nanowire morphology resulting from different reaction conditions, we found that high temperature and low flow rates produce straight wires with minimal particle formation.

HRTEM reveals the straight Si nanowires to be single crystals. Figure 2.6 shows a representative image of a 7.2 nm diameter wire with the atomic planes spaced by 0.31 nm corresponding to the (111) d-spacing of diamond cubic silicon. The single-crystal electron diffraction pattern recorded perpendicular to the long axis of the nanowires (Figure 2.6 inset) and the lattice-resolved TEM images of the crystalline Si corresponds to a <110> nanowire growth direction.

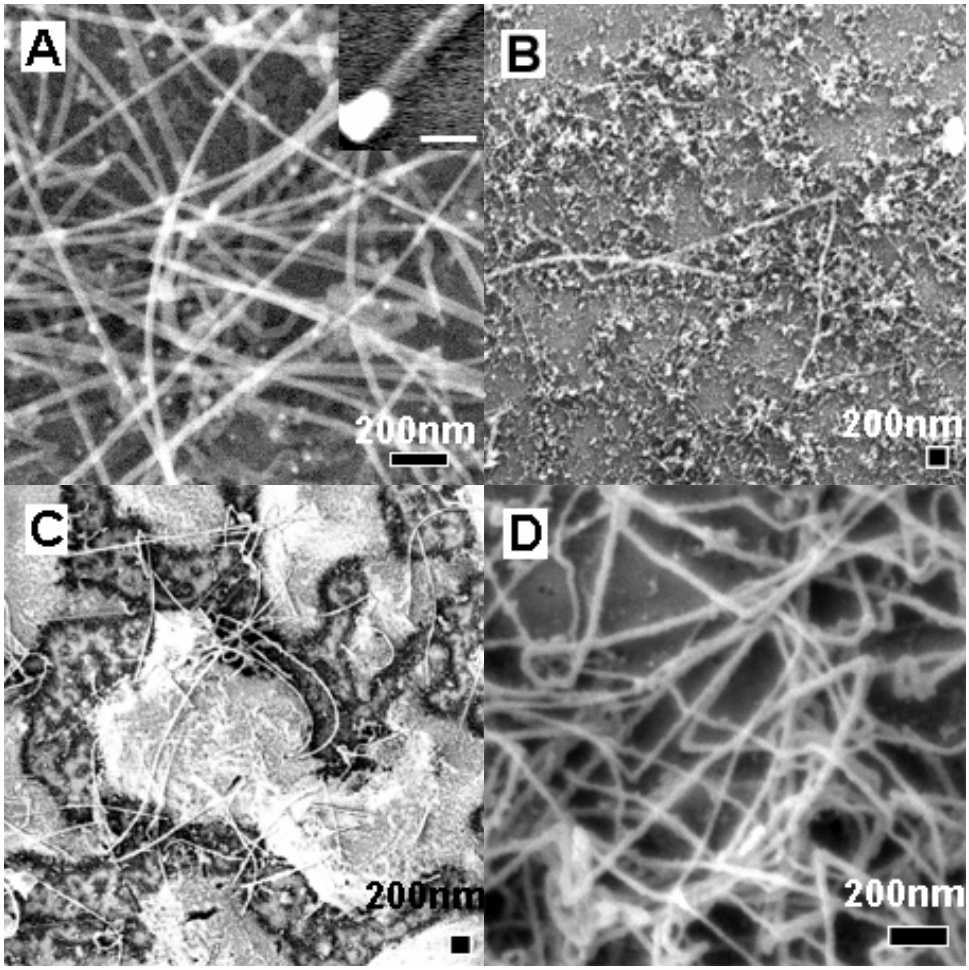

Figure 2.5 HRSEM images of Si nanowires synthesized in the flow reactor with [DPS]=0.25 M. The nanowires were grown at 500ºC with DPS feedstock flow rates of (A) 0.5 ml/min, (B) 1 ml/min and (C) 3 ml/min, respectively. (D) Nanowires grown at 450ºC with a feedstock flow rate of 0.5 ml/min. Scale bar for the inset of (A) is 50 nm.

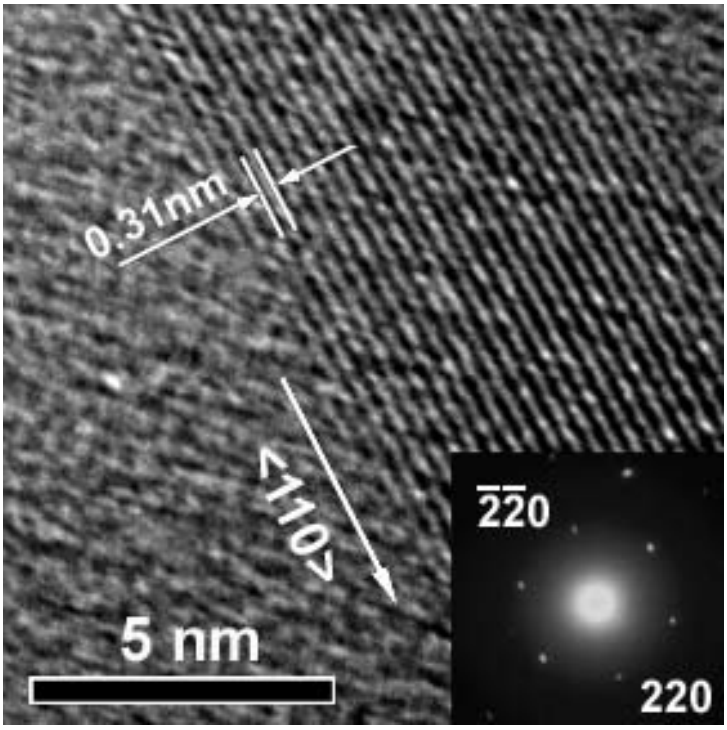

Figure 2.6 HRTEM image of the Si nanowires produced at 500ºC and 24.1 MPa in the flow reactor (0.5 ml/min). Inset: Electron diffraction pattern indexed for the <111> zone axis of Si indicates <110> growth direction.

2.4 DISCUSSION

The transition between straight and tortuous wires depends upon temperature in both the batch and flow reactors. High temperature favors straight wires. Sufficient Si atoms must arrive at the crystallization sites to drive the growth of a 1-D crystalline silicon nanowire. If the growth site is starved with respect to silicon atoms, or crystallization is slow, the likelihood of incorporating a contaminant into the growing crystal to produce a defect becomes significant. Both increased temperature and DPS concentration enhance the Si atom supply rate, which favor straight wires. However, very high DPS concentrations produce large amounts of homogeneously nucleated Si particles in addition to the heterogeneously nucleated nanowires. Presumably, there exists a critical precursor concentration above which the heterogenous nucleation pathway leading to nanowires is overwhelmed by homogeneous nucleation to form Si particles. By manipulating both the DPS concentration and the flow rate, the flow reactor enables the production of straight wires with minimal Si particulate formation on the substrate. At a DPS concentration of 0.25 M and 500ºC, the wires produced at a low flow rate of 0.5 mL/min in Figure 2.5A were straight and clean, whereas those produced in the batch reactor were shorter and surrounded by large quantities

of Si particles (Figure 2.4B). A kinetic analysis of the flow system explains qualitatively the ability to produce straight wires with minimal nanoparticles in the flow reactor.

We assume that the Si and DPS concentrations in the supercritical fluid phase of the reactor do not change with position. This assumption holds for the flow-through reactor as well as the batch reactor, since the reactor residence times far exceed the kinetic time scales for the occurring reactions. The high diffusion coefficients in the supercritical phase produce lower mass transfer resistances than in the liquid phase and further favors this assumption. The disappearance of DPS and the Si atoms in the reactor depend on the feed flow rate F, of DPS and the DPS concentration at the inlet and in the reactor, $c_{DPS,i}$ and c_{DPS}, respectively, as well as the free Si atom concentration c_{Si} in the reactor:

$$V\frac{dc_{DPS}}{dt} = F \cdot c_{DPS,i} - F \cdot c_{DPS} - V \cdot k_D \cdot c_{DPS} \qquad (2.1)$$

$$V\frac{dc_{Si}}{dt} = V \cdot k_D \cdot c_{DPS} - V \cdot k_W \cdot \phi_{Au} \cdot c_{Si} - V \cdot k_P \cdot c_{Si}^{\,2} - F \cdot c_{Si} \qquad (2.2)$$

In Equations (2.1) and (2.2), k_D, k_W and k_P are the kinetic rate constants for DPS decomposition to Si atoms, Si dissolution into Au particles to promote wire growth and Si aggregation into particles, respectively. ϕ_{Au} is

the surface coverage of Au nanocrystals on the Si substrate and V is the reaction cell volume. A key assumption in the rate equation (2.2) is that homogeneous reaction of Si atoms in solution is second order in c_{Si}, whereas Si wire growth occurs primarily as a first order process. Solution of equation (2.1) yields:

$$c_{DPS} = \frac{1}{1 + k_D \cdot \tau}(1 + k_D \cdot \tau \cdot e^{-(1/\tau + k_D)t}) c_{DPS,i} \qquad (2.3)$$

where τ is the residence time, V/F (between 4 minutes to 40 seconds in this system). According to the DPS decomposition kinetics,[28] k_D is on the order 10^3 min^{-1} making $k_D >> 1/\tau$ and the term $e^{-(1/\tau + k_D)t} \approx 0$ once the reaction begins, which simplifies Equation (2.3) to

$$c_{DPS} = \frac{1}{1 + k_D \cdot \tau} c_{DPS,i} \qquad (2.4)$$

Therefore, the DPS concentration in the reactor increases with flow rate F, leading to high atomic Si concentrations in the reactor. If n_W mol Si atoms react with Au nanocrystals to grow Si wires and n_P mol Si atoms aggregate to form Si particles:

$$\frac{dn_W}{dt} = k_W \cdot \phi_{Au} \cdot c_{Si} \cdot V \qquad (2.5)$$

$$\frac{dn_P}{dt} = k_P \cdot c_{Si}{}^2 \cdot V \tag{2.6}$$

The ratio of the Si atoms incorporated into Si wires to those forming particles from t to $t + dt$ is

$$\frac{dn_W}{dn_P} = \frac{k_W \cdot \phi_{Au}}{k_P \cdot c_{Si}} \tag{2.7}$$

Thus, the selectivity towards particles versus wires increases with c_{Si}. According to equation (2.4), an increase in flow rate raises the DPS concentration, and thus the concentration of Si atoms, leading to more Si particles, consistent with the observations in Figure 2.5.

Compared to the batch reactor, the flow reactor has several advantages. The most obvious advantage is the ability to flush out particulates from the fluid phase prior to deposition on the substrate. In addition, the ability to control the reactant concentration in the flow reactor provides the necessary means to maintain preferential wire growth over particle formation. Recall that wires grow with a tortuous morphology under conditions of very low DPS concentration. The growth sites become starved, which leads to a high probability of impurity adsorption at the growth interface leading to a defect in the crystal. Therefore, straight wires require a high growth temperature and a high DPS concentration. However, if the

reactant concentration is too high, particles form preferentially through homogeneous nucleation relative to formation of wires. The batch reactor simply does not provide the ability to access the concentration "window" for effective wire growth without contamination by a large number of undersired Si particles. In the batch reactor, the reactant concentration steadily decreases with time, and therefore, very high initial DPS concentrations are necessary, which leads to the formation of many particles. The flow reactor, on the other hand, enables the optimum DPS concentration to be maintained for wire growth without particle formation, as the reactant concentration can be maintained more or less time independent. Furthermore, after reaction, the flow cell can be flushed with pure solvent to further reduce physical deposition. Finally, the flow reactor provides more rapid heating of the feed, making it more isothermal than the batch reactor. In the batch reactor, the growing wires may become starved for Si at lower temperatures during heatup leading to lower selectivity to straight wires relative to curly wires and Si particles.

2.5 CONCLUSIONS

Single-crystal Si nanowires, 5 to 30 nm in diameter and several micrometers long, were synthesized in supercritical cyclohexane solution

from individual gold seed nanocrystals attached covalently to a Si substrate. The attachment prevents agglomeration of the gold seed particles, which is a necessary condition for the formation of nanometer-size silicon nanowires. A transition from tortuous to straight nanowire morphology occurs with an increase in temperature and DPS concentration. Temperatures greater than ~450^{o}C are needed to promote rapid crystallization of straight wires. Once these temperatures are reached, atomic Si concentrations (and thus DPS concentrations) must be sufficient to efficiently feed the growth sites to induce the formation of straight wires. Low DPS concentrations lead to the starvation of the growth sites resulting in defect formation and tortuous wire growth. In the batch reaction, the DPS concentration decreases rapidly as the reaction proceeds and the optimum window of DPS concentration for straight wires without particle contamination cannot be maintained. In the flow reactor, the DPS concentration can be controlled at the optimum DPS concentration favoring straight wire growth without leading to homogeneous particle production. Furthermore, it continually removes small Si clusters in the fluid phase.

The growth of Si nanowires from gold seed crystals on a Si substrate with the FLS method could provide an important method for the fabrication of nanoscale optical and electronic devices. The growth of nanowires in a flow

reactor in supercritical solution with high Si precursor concentrations and rapid diffusion rates is desirable for large-scale production. Furthermore, the ability to manipulate the precursor concentration, the seed particle concentration and size provides great flexibility in controlling the nanowire morphology.

2.6 REFERENCES AND NOTES

(1) Holmes, J. D.; Johnston, K. P.; Doty, R. C.; Korgel, B. A. *Science* **2000**, *287*, 1471.

(2) Morales, A. M.; Lieber, C. M. *Science* **1998**, *279*, 208.

(3) Cui, Y.; Lieber, C. M. *Science* **2001**, *291*, 851.

(4) Cui, Y.; Lauhon, L. J.; Gudiksen, M. S.; Wang, J.; Lieber, C. M. *Appl. Phys. Lett.* **2001**, *78*, 2214.

(5) Hanrath, T.; Korgel, B. A. *J. Am. Chem. Soc.* **2002**, *124*, 1424.

(6) Coleman, N. R.; Morris, M. A.; Spalding, T. R.; Holmes, J. D. *J. Am. Chem. Soc.* **2001**, *123*, 187.

(7) Duan, X.; Lieber, C. M. *Adv. Mater.* **2000**, *10*, 298.

(8) Derycke, V.; Martel, R.; Appenzeller, J. *Nano Letters* **2001**, *1*, 453.

(9) Odom, T. W.; Huang, J.-L.; Kim, P.; Lieber, C. M. *Nature* **1998**, *391*, 62.

(10) Wagner, R. S.; Ellis, W. C.; Jackson, K. A.; Arnold, S. M. *J. Appl. Phys.* **1964**, *35*, 2993.

(11) Heath, J. R.; LeGoues, F. K. *Chem. Phys. Lett.* **1993**, *208*, 263.

(12) Hu, J.; Odom, T. W.; Lieber, C. M. *Acc. Chem. Res.* **1999**, *32*, 435.

(13) Wu, Y.; Yang, P. *Chem. Mater.* **2000**, *12*, 605.

(14) Zhang, Y. F.; Tang, Y. H.; Wang, N.; Lee, C. S.; Bello, I.; Lee, S. T. *Phys. Rev. B* **2000**, *61*, 4518.

(15) Omi, H.; Ogino, T. *Appl. Phys. Lett.* **1997**, *71*, 2163.

(16) Shi, W.; Zhang, Y.; Lee, C. S.; Lee, S. T. *Adv. Mater.* **2001**, *13*, 591.

(17) Trentler, T. J.; Hickman, K. M.; Goel, S. C.; Viano, A. M.; Gibbons, P. C.; Buhro, W. E. *Science* **1995**, *270*, 1979.

(18) Gudiksen, M. S.; Lieber, C. M. *J. Am. Chem. Soc.* **2000**, *122*, 8801.

(19) Blackburn, J. M.; Long, D. P.; Cabanas, A.; Watkins, J. J. *Science* **2001**, *294*, 141.

(20) Shah, P. S.; Holmes, J. D.; Johnston, K. P.; Korgel, B. A. *J. Phys. Chem. B* **2002**, *106*, 2545.

(21) Dissovle 0.154 g $HAuCl_4$ in 15 ml D-H_2O and 1.114 g $(C_8H_{17})_4NBr$ in 10.2 ml $CHCl_3$. Combine the solutions obtained and stir for 1 hour. Collect the organic phase and add 100 ul dodecanethiol into it while stirring. Dissolve 0.197 g $NaBH_4$ in 12.5 ml D-H_2O and add the solution to the strring organic phase too. Stir for 8 hours. Collect the organic phase which is rich in gold nanocrystals.

(22) Korgel, B. A.; Fitzmaurice, D. *Phys. Rev. Lett.* **1998**, *80*, 3531.

(23) Brust, M.; Walker, M.; Bethell, D.; Schiffrin, D. J.; Whyman, R. *J. Che. Soc. Chem. Commun.* **1994**, *801*, 1994.

(24) Yaws, C. L. *Handbook of Thermodynamics Diagrams*; Gulf Publishing Company: Houston, Texas,1996.

(25) Kluth, G. J.; Sung, M. M.; Maboudian, R. *Langmuir* **1997**, *13*, 3775.

(26) Confirmed by EDS.

(27) Au particles imaged by TEM appear to be significantly smaller than when imaged by HRSEM due to the difference in resolution limits of the two instruments. By TEM, the diameter is 6.7±2.6 nm, whereas HRSEM shows that the nanocrystal diameter is 13.0±4 nm. The nanowire diameters determined by TEM match more precisely the nanocrystal

diameter determined by TEM, while the nanowire diameter determined by HRSEM matches the nanocrystal diameters measured by HRSEM.

(28) Coutant, R. W.; Levy, A. A *Kinetic Study of the Thermal Decomposition of Selected Cyclohexyl and Phenylsilanes;* 1969.

Chapter 3: Synthesis of Germanium Nanocrystals in High Temperature Supercritical Fluid Solvents*

Crystalline Ge nanocrystals were synthesized by arrested precipitation in supercritical hexane and octanol at 400~550^{o}C and 20.7 MPa in a continuous flow reactor. Two Ge precursors were explored, diphenylgermane (DPG) and tetraethylgermane (TEG), which undergo thermolysis to crystalline Ge under these conditions. Octanol is added to control particle growth, which appears to serve as a capping ligand. The average nanocrystal diameter could be changed from ~ 2 nm to ~70 nm by varying the reaction temperature and precursor concentration. Relatively size-monodisperse nanocrystals could be produced, with standard deviations about the mean diameter as low as ~10%. UV-visible absorbance and PL spectra of Ge nanocrystals in the 3 to 4 nm diameter size range exhibit optical absorbance and PL spectra blue-shifted by approximately 1.7 eV relative to band gap of bulk Ge, with quantum yields up to 6.6%.

---

* Portions of this chapter have been previously published as Lu, Xianmao; Ziegler, Kirk J.; Ghezelbash, Ali; Johnston, Keith P.; and Korgel, Brian A.; *Nano Lett.*, **2004**, 16, 389-394.

3.1 INTRODUCTION

A variety of metal and semiconductor nanocrystal materials can be produced by solution-phase arrested precipitation.[1] In this process, molecular precursors are degraded either by reduction/oxidation or thermolysis in the presence of capping ligands that bind to nucleating and growing particles and inhibit growth, and also provide redispersibility in compatible solvents. Interest in these "free-standing" nanocrystals derives from their unique size-tunable physical properties, relative chemical stability, redispersibility in various solvents, and chemically functionalizable surfaces. Group IV nanocrystals, such as Si and Ge, have been particularly challenging to synthesize by solution-phase methods, primarily due to their strong covalent bonding and the need for high temperatures to promote crystallization. Although a few research groups have reported crystalline Ge nanocrystal synthesis in solution at temperatures lower than 300ºC[2-4], chemical vapor deposition of Ge typically requires temperatures exceeding 415ºC to crystallize the films[5] without the aid of a catalyst, such as gold.[6] Since this temperature range exceeds the boiling point of conventional solvents under ambient conditions, we have been exploring high temperature pressurized solvents as reaction media for nanostructure synthesis.[7-13] For example,

these solvents—called supercritical fluids (SCF) when the temperature and pressure exceed the critical temperature and pressure—have been vital to the formation of Si[7,14,15] nanocrystals and Si[9,10], Ge[11,12] and GaAs[13] nanowires. In this chapter, we report the arrested precipitation synthesis of Ge nanocrystals utilizing a SCF as a solvent in a high-pressure high-temperature continuous flow reactor.

3.2 EXPERIMENTAL

3.2.1 Nanocrystal synthesis

Ge nanocrystals were synthesized by thermally degrading either tetraethylgermane (TEG) or diphenylgermane (DPG), in the presence of octanol at temperatures ranging from 400ºC to 550ºC at 20.7 MPa. The reactions were carried out using a flow reactor system like that described in detail by Lu *et al.*[10] The precursor solutions were either TEG (Gelest) in a 1:3 (volume ratio) mixture of octanol (T_c = 385°C, P_c = 3.45 MPa) and hexane (T_c = 235°C, P_c = 3.0 MPa), or DPG (Gelest) in pure octanol. Table 3.1 lists the TEG and DPG concentrations studied. The solutions were prepared in a nitrogen-filled glove box using solvents that were purchased anhydrous and packaged under nitrogen (Aldrich Chemical Co.). The reactants are fed from

a variable volume stainless steel cylinder with an HPLC pump—to control the reactor pressure and flow rate—into a 2 mL (0.5 cm i.d., 2.0 cm o.d., and 12.5 cm long) high-pressure titanium grade-2 cell with both ends connected to 1/16 in. o.d. and 0.03 in. i.d. stainless steel high-pressure tubing via titanium grade-2 LM-6 HIP reducers (High Pressure Equipment). The inlet stream was preheated to ~300^{o}C prior to entering the reactor. An SS-4R3A back-pressure regulator (Swagelok) connected after the reaction cell and a digital pressure gauge (Stratford) between the preheater tubing and the cell maintained the pressure at 20.7 MPa. The product is collected as it exits the back-pressure regulator of the reactor.

3.2.2. Characterization methods

After collection from the reactor, the Ge nanocrystals were purified for characterization. The sample was first dried on a rotary evaporator for 2 hours and then vacuum distilled overnight to remove the light organic and oily byproducts, resulting in a weight loss of more than 95%. The Ge nanocrystals are then redispersed in 0.1 ml chloroform and precipitated with 10 ml ethanol for further purification. The precipitated nanocrystals are collected by centrifugation at 10,000 rpm for 5 min. This step yields a dry residue of nanocrystals that can be redispersed in various organic solvents,

including chloroform and hexane. The nanocrystals were characterized by transmission electron microscopy (TEM), X-ray diffraction (XRD), Fourier transform infrared spectroscopy (FTIR), UV-visible absorbance and photoluminescence emission (PL) and excitation (PLE) spectroscopy.

3.3 RESULTS AND DISCUSSIONS

Reactor	Precursor (mM)	T (ºC)	τ (sec)	N	$\overline{d_p}$ (nm)	σ (%)
Flow	[TEG]=62.5	450	300	86	4.2	10
Flow	[TEG]=62.5	550	300	165	4.8	19
Flow	[TEG]=25.0	450	300	148	2.0	20
Batch	[TEG]=62.5	450	300	71	3.5	54
Flow	[DPG]=100.0	400	20	326	71.4	28
Flow	[DPG]=50.0	400	20	474	49.8	23
Flow	[DPG]=25.0	400	20	217	3.8	24
Flow	[DPG]=12.5	400	20	125	3.1	31
Batch	[DPG]=25.0	400	20	162	6.5	52

Table 3.1 Summary of the mean diameter $\overline{d_p}$, and standard deviation about the mean diameter σ, of Ge nanocrystals synthesized at various temperatures, residence times τ, and Ge precursor concentrations. *N* is the number of Ge nanocrystals counted for each sample to construct the histrograms used to determine the $\overline{d_p}$ and σ.

Decomposition of TEG in pure hexane at 450°C and 20.7 MPa produces micrometer-size bulk polycrystalline Ge particulates. Figure 3.1 shows a representative TEM image and XRD pattern from the material produced. Similar results are obtained for DPG composition in pure hexane. In contrast, when octanol is added to the reaction mixture, much smaller, nanometer-size Ge nanocrystals are obtained. Figure 3.2 shows TEM images[16] of Ge nanocrystals made from TEG in the presence of octanol at varying reaction temperature and TEG concentration. Of the conditions explored, the nanocrystals synthesized at [TEG] = 62.5 mM and 450°C had the narrowest size distribution, with an average diameter of 4.2±0.4 nm. The HRTEM image in Figure 3.2B shows the internal crystallinity for one Ge nanocrystal of the sample imaged in Figure 3.2A. The particle appears to consist of a single crystal domain and exhibits a 0.20 nm d-spacing corresponding to the {220} lattice spacing of diamond cubic Ge. An increase in reaction temperature to 550°C at this TEG concentration did not significantly increase the nanocrystal diameter, but did increase the size distribution with $\overline{d_p}$ = 4.8±0.93 nm (Figure 3.2C). The standard deviation about the mean diameter of ±19% is nearly twice as broad as obtained at 450°C (±10%). The TEG concentration, however, does have a significant

influence on the particle diameter. Ge nanocrystals produced at 450°C at lower TEG concentration, with [TEG] = 25.0 mM (Figure 3.2D), were much smaller, with particle diameters of 2.0±0.40 nm.

Ge nanocrystals could also be synthesized using DPG as the reactant. The particle size, however, was more difficult to limit than when TEG was used. Nanometer-size particles could be obtained only when pure octanol was used as the solvent, with slightly lower reaction temperature (400ºC) and shorter residence time (20 sec). Even at these lower reaction temperatures, residence times on the order of minutes yielded bulk polycrystalline Ge. The greater DPG reactivity provided access to a wider range of nanocrystal sizes. With relatively small changes in DPG concentration, nanocrystals could be formed with diameters as large as ~70 nm or as small as ~3 nm at the same reaction temperature. Figure 3.3 shows Ge nanocrystals made from DPG at 400ºC in octanol at 20.7 MPa at different DPG concentrations. As summarized in Table 3.1, the Ge nanocrystals made from DPG exhibit somewhat broader size distributions than those formed using TEG.

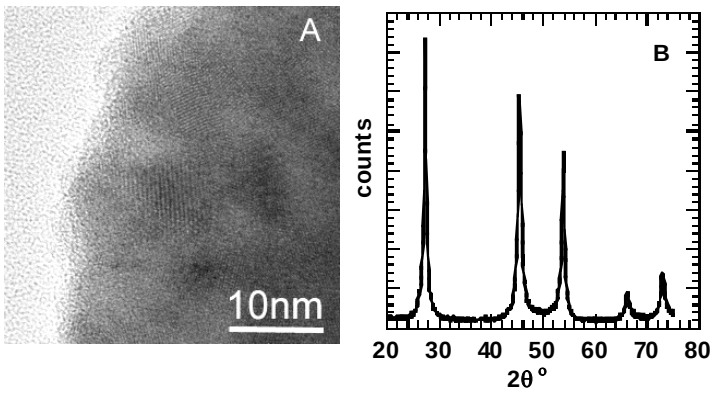

Figure 3.1 (A) TEM image of polycrystalline Ge formed from TEG pyrolysis in hexane at 450ºC and 20.7 MPa. (B) The XRD pattern indexes to diamond cubic Ge and indicates from the peak breadth a crystal domain size of ~60 nm.

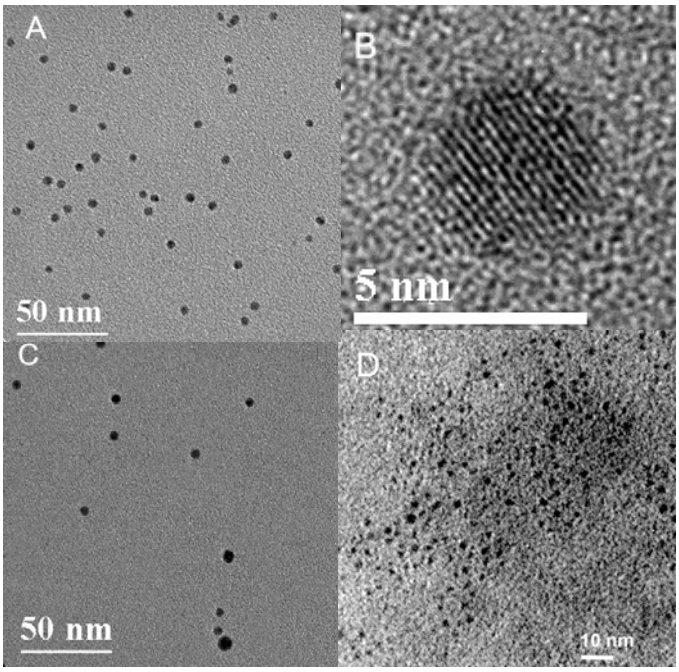

Figure 3.2 TEM images of octanol-stabilized Ge nanocrystals synthesized by TEG thermolysis in 1:3 v/v octanol:hexane with a reactor residence time of τ=5 min: (A) T = 450°C, [TEG] = 62.5mM, $\overline{d_p}$ = 4.2 ± 0.42 nm; (B) HRTEM image of a Ge nanocrystal from the sample in (A); (C) T = 550°C, [TEG] = 62.5 mM, $\overline{d_p}$ = 4.8 ± 0.93 nm; (D) T = 450°C, [TEG] = 25.0 mM, $\overline{d_p}$ = 2.0 ± 0.40 nm.

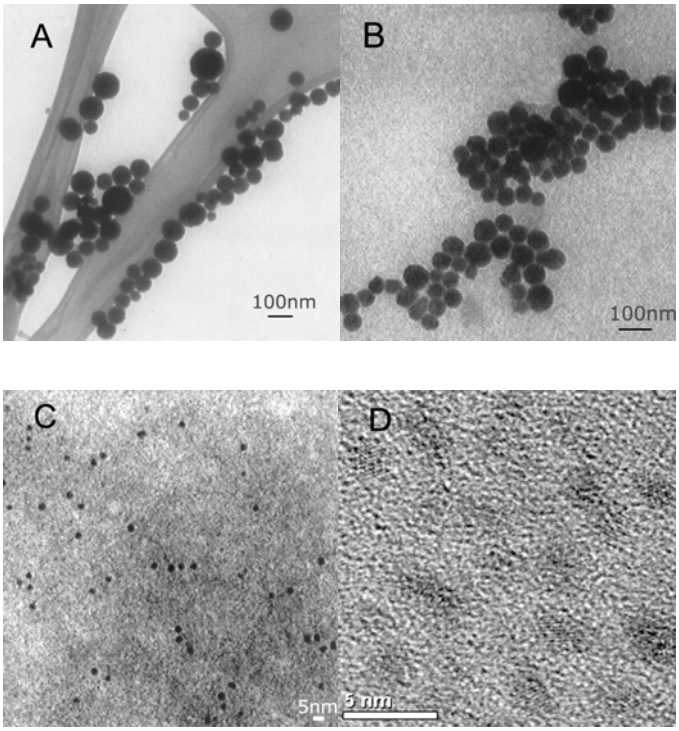

Figure 3.3 TEM images of Ge nanocrystals synthesized in pure octanol at 400°C, 20.7 MPa, and a reactor residence time of 20 sec: (A) [DPG]=100 mM, $\overline{d_p}$ = 71.4 ± 19.8 nm; (B) [DPG]=50 mM, $\overline{d_p}$ =49.8±11.5 nm; (C) [DPG]=25 mM, $\overline{d_p}$ = 3.8 ± 0.9 nm; (D) [DPG]=12.5 mM, $\overline{d_p}$ =3.1±0.9 nm.

We also explored Ge nanocrystal synthesis using a batch reactor setup. Batch reactions[17] were carried out for [TEG] = 62.5 mM and [DPG] = 25.0 mM (Table 3.1). The heat-up time was 2 minutes and the time at temperature was 5 minutes and 20 seconds for TEG and DPG, respectively. At 450ºC and [TEG] = 62.5 mM, the diameter of the Ge nanoparticles obtained from batch reaction was $\overline{d_p}$ = 3.5±1.9 nm, which is close to that of the particles produced in flow reactor at the same temperature and TEG concentration (4.2 nm). However, the standard deviation of the particles was much higher for the batch reaction than the flow reaction (±54% versus ±10%). This increase in polydispersity was also observed for the batch reaction of DPG. For [DPG] = 25.0 mM at 400ºC, the diameter of the Ge particles was $\overline{d_p}$ = 6.5 nm with a standard deviation of ±52%, which is also higher than in the flow reaction (±24%). The lower polydispersity produced using the flow-through reactor setup reflects the greater temperature and pressure control compared to the batch reactor setup.

The 3 nm and 4 nm diameter Ge nanocrystals synthesized using DPG (12.5 mM and 25 mM, respectively) exhibited primarily single crystal domains in their TEM images. Figure 3.3D, for example, shows a field of crystalline Ge nanocrystals where many display the characteristic 0.2 nm d-

spacing of the {220} planes in diamond cubic Ge. Figure 3.4A shows a selected area electron diffraction (SAED) pattern obtained from a 4 nm diameter Ge nanocrystal, exhibiting the characteristic spot pattern of a single crystal domain and the hexagonal symmetry of the {111} lattice plane of Ge. In contrast, SAED patterns from Ge nanocrystals in the larger size range—50 nm to 70 nm diameter—made from higher DPG concentrations (50 mM and 70 mM, respectively) exhibit ring patterns, characteristic of internal polycrystallinity. For example, Figure 3.4B shows an SAED pattern obtained from the larger nanocrystals with rings corresponding to the d-spacing between the {220} and {422} lattice planes in diamond cubic Ge. From XRD patterns obtained for the nanocrystals in this size range, the average crystalline domain size is ~40 nm for ~70 nm diameter nanocrystals (Figure 3.5B). In contrast, the crystal domain size determined from peak broadening in the XRD patterns from 3 to 4 nm diameter nanocrystals matches the particle diameter within experimental error (Figure 3.5B). Both XRD and elemental analysis of fields of nanocrystals by energy dispersive X-ray spectroscopy (EDS) (Figure 3.5A) confirm that the nanocrystals are composed of crystalline Ge.

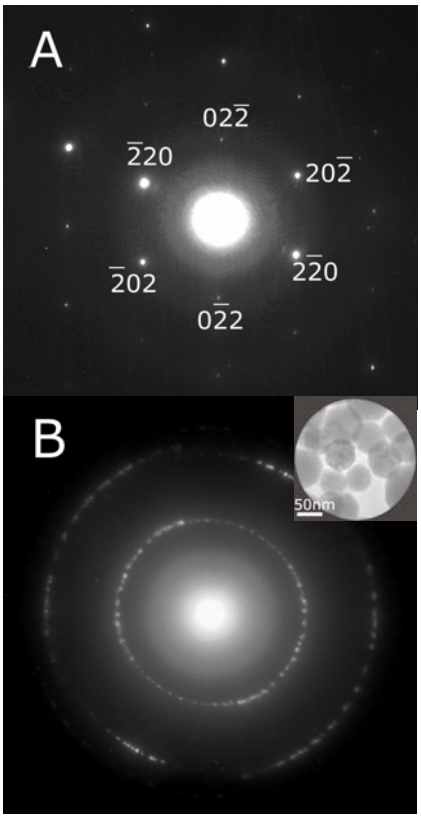

Figure 3.4 SAED from Ge nanocrystals synthesized by degrading DPG in octanol at 400°C with a 20 sec residence time: (A) SAED pattern obtained from an individual 4 nm diameter particle synthesized with [DPG]=12.5 mM; (B) an SAED pattern obtained from 70 nm diameter Ge nanocrystals synthesized with [DPG]=100 mM. The d-spacings in (B) of the two rings—0.199 nm and 0.116 nm—are consistent with the reference values (0.200 nm and 0.115) for Ge {220} and {422}. The spacings were determined using Bragg's equation[18], $r = \lambda L/d$, where the radius r=1.51 cm for the first diffraction ring and r=2.59 cm for the second ring, the electron wavelength is λ=0.0025079 nm for 200 keV accelerating voltage, and the camera length is L=120 cm.

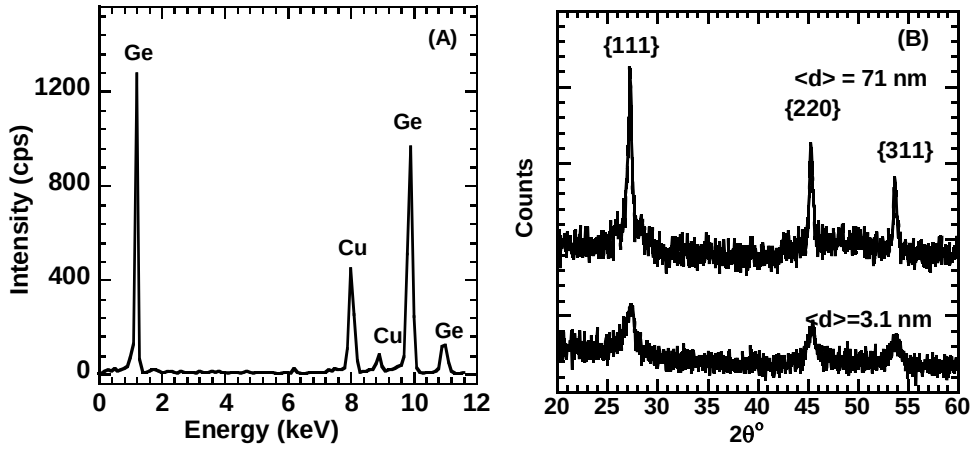

Figure 3.5 (A) EDS data obtained for the nanocrystals imaged by TEM in Figure 3.1C. The copper peaks result from the copper TEM grid used as the material support. (B) Powder XRD patterns of Ge nanocrystals made from 100 mM DPG ($\overline{d}$ =71.4 nm) and 12.5 mM DPG ($\overline{d}$ =3.1 nm) at 400ºC. XRD was performed using a Phillips vertical scanning diffractometer, with Cu Kα radiation (λ = 1.54 Å) and a scintillation detector. The sample was cleaned with rotary evaporator and vacuum oven and then dried as powders onto quartz slides (The Gem Dugout, State College, PA) in nitrogen glovebox. The crystal domain size was estimated from the peak width by the Scherrer formula[19] $t = \frac{0.9\lambda}{B\cos\theta_B}$.

The broadening of the Ge {111} reflection ($2\theta_B$=27.28º) is $B \approx$ 0.21º (fwhm) for the 71.4 nm Ge nanoparticles, and the calculated size from Scherrer equation is 38.9 nm, which is smaller than the average diameter measured by TEM, indicating that the nanocrystals are polycrystalline. The peak broadening for the 3.1 nm Ge nanoparticles is 1.96º (fwhm), and the corresponding Scherrer diameter is 4.1 nm, which is close to the mean size determined from TEM images.

FTIR spectra (Thermo Mattson Infinity Gold FTIR spectrometer) of the Ge nanocrystals can provide a qualitative measure of what is coating the nanocrystal surfaces. As mentioned previously, if DPG or TEG are degraded in the absence of octanol, bulk polycrystalline Ge is produced. The octanol helps stabilize the particle size, presumably by serving as a capping ligand. FTIR measurements were performed on purified Ge nanocrystals that were drop cast in air from chloroform onto intrinsic Si substrates. Three peaks appear in the FTIR spectra in Figure 3.6 at 2958, 2928, and 2858 cm^{-1}, characteristic of C-H stretching modes for CH_2 and CH_3 groups, indicating that hydrocarbon species coat the Ge nanocrystals. The peaks at 1468 and 1380 cm^{-1} are also consistent with the CH_3 bending vibrations. As we expect that the physisorbed and solution-phase organic species are removed in the rigorous washing steps prior to the measurement, the FTIR spectra provide a strong indication that a hydrocarbon layer is chemisorbed to the particle surface. The hydroxyl stretch for octanol (3300 cm^{-1}) is notably absent from the spectra. The peaks at 1068 and 698 cm^{-1} could correspond to Ge-O-C species[20-22], which would suggest covalent alkoxide bonding of the capping ligands to the Ge nanocrystal surface although other possibilities, such as CH-O- (1100 cm^{-1}) and CH_2-O- (1050 cm^{-1}), cannot be excluded. The peak at 850 cm^{-1} (Ge-O/Ge-C stretches) indicates that the surface is also covered with

either residual oxide or direct bonding between Ge and the hydrocarbon coating. But as FTIR is very sensitive to Ge-O and Ge-C stretches, the presence of these species would have to be in very small amount. Although it does not provide definitive proof of the nature of the ligand bonding to the nanocrystal surface, the FTIR spectra indicate that hydrocarbon species coat the nanocrystal surfaces, potentially through alkoxide bonding with the Ge surface.

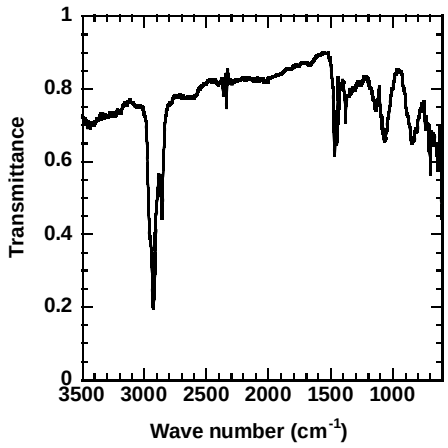

Figure 3.6 FTIR spectrum of Ge nanocrystals made from TEG at 400ºC on an intrinsic Si substrate.

Ge is an indirect band gap semiconductor unsuitable for light emitting applications as a bulk material, yet can produce relatively high photoluminescence at the nanoscale.[2,23] Figure 3.7 shows the room temperature UV-visible absorbance and PL/PLE spectra for 3.1 nm ([DPG]=12.5 mM, 400ºC) and 4.2 nm ([TEG]=62.5 mM, 450ºC) Ge nanocrystals. Bulk Ge has a band gap of 0.6 eV and according to the band structure of Ge,[2,4] the absorption coefficient of bulk Ge has distinct peaks at 550 nm (2.1 eV) and 280 nm (4.3 eV), associated with direct band transitions at *L* and *X* respectively. Quantum confinement effects are expected to shift the energy levels in Ge nanocrystals smaller than 23 nm in diameter, since the Bohr radius for Ge is 11.5 nm.[2] The absorption edges in Figure 3.7 for 3.1 nm and 4.2 nm diameter Ge nanocrystals were significantly blue-shifted relative to the bulk Ge band gap. In fact, these absorption edge are close to those of Si nanocrystals of similar diameter[7,14,15] as expected from predictions by several groups.[24-26] Our observed size shifts are also qualitatively consistent with those of Ge nanocrystals synthesized by Wilcoxon[2] and Heath[4]. The PL spectrum for the 4.2 nm Ge nanocrystals excited with 360 nm (3.4 eV) light shows a broad peak at 536 nm (2.3 eV), and the PLE spectrum (λ_{em} = 536 nm) shows strong absorption near 360 nm which is responsible for the majority of light emission. The PL spectrum for the 3.1

nm Ge nanoparticles excited at 340 nm (3.7 eV) shows a major peak at 476 nm (2.6 eV) that is blue-shifted relative to the 4.2 nm particles. The observed ~60 nm blue shift is greater than the difference in excitation wavelength (~20 nm), indicating that the effect of quantum confinement is likely playing a role in the optical properties of the nanocrystals. The PL quantum yields for the 3.1 nm and 4.2 nm Ge nanocrystals are 6.6% (at 340 nm) and 4.6% (at 360 nm) respectively, determined using a reference solution of quinine bisulfate (quantum yield=0.55, Sigma-Aldrich) in 0.1M sulfuric acid. However, the Ge nanocrystal PL can be very sensitive to the surface chemistry,[27,28] and must be more thoroughly examined in future experimental work to fully understand the nature of the observed size-dependent blue shifts in the absorption and PL spectra.

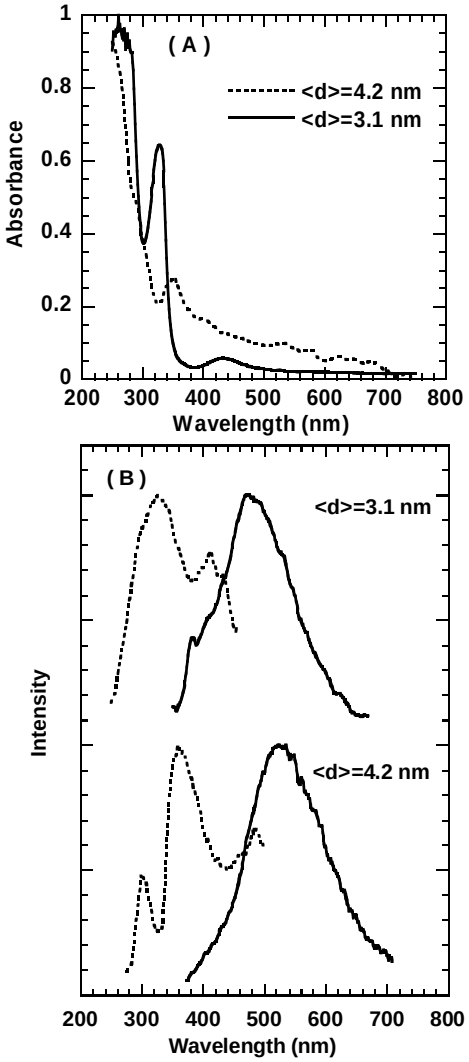

Figure 3.7 Room temperature UV-visible (A) absorbance and (B) PL (solid lines, excitation wavelength λ_{ex}=340 nm for $\overline{d_p}$ = 3.1±0.9 nm particles and λ_{ex}=360 nm for $\overline{d_p}$ = 4.2±0.4 nm particles) and PLE (dashed lines, emission wavelength λ_{em}=536 nm for 4.2 nm particles and λ_{em}=476 nm for 3.1 nm particles) spectra of 3.1 nm and 4.2 nm Ge nanoparticles dispersed in chloroform.

3.4 CONCLUSIONS

The window of potential reaction conditions for producing Ge nanocrystals depends sensitively on the Ge precursor chemistry. Significantly lower temperatures and residence times, and higher octanol concentrations, are required when DPG is used (400^{o}C, 20 sec) compared to TEG (450^{o}C, 5 min). This significant difference relates to the much lower kinetic stability of the Ge-phenyl bond compared to the Ge-alkyl bond[29]. These observations for nanocrystal growth are consistent with our findings for Ge nanowires, in which DPG is a more reactive precursor than TEG, requiring lower temperatures to produce nanowires in supercritical solvents.[11] The greater reactivity of DPG provides a narrower range of conditions that will yield nanometer-size particles, yet enables a broader range of sizes to be produced, simply by varying the precursor concentration.

Although the quality of the nanocrystal product is relatively high, with nanocrystal diameter being tunable over a wide range, from 2.0 nm to 71 nm, with crystalline cores and in many cases relatively narrow size distributions (<~10), along with visible photoluminescence with reasonably high quantum yields of 4~6%—which incidentally is higher than the reported quantum yields of 1.5% for 3.7 nm Ge nanoparticles[3] and 0.5% for 4 nm Ge

nanoparticles in a SiO_2 matrix[30]—the yield (or conversion) of Ge reactant to Ge nanocrystals, is relatively low. The highest yield was achieved for the 100 mM DPG at 400ºC, which was 6.9%. We found that low precursor concentrations were necessary to form smaller nanocrystals; however, under these conditions the yield decreased significantly. TEG degradation at 100 mM at higher temperature (450ºC) gave a lower reaction yield (<1.0%) than DPG at the same reactant concentration. Yields of this magnitude are simply not scalable to commercial production and must be improved if possible. The relatively low yield of the Ge nanocrystals appears to be due to the many competing molecular and oligomeric side reactions that lead to a high ratio of by-product to Ge nanocrystals that is difficult to overcome in this reaction system. Improvements in reaction yield using this approach require the identification of more suitable organogermane precursor, organic solvent, and capping ligand combinations. Fundamental calculations accounting for precursor degradation kinetics, capping ligand surface binding interactions, and particle nucleation and growth kinetics, would certainly be a useful guide to optimizing this synthetic system.

3.5 REFERENCES AND NOTES

(1) Klimov, V. I., Ed. *Semiconductor and Metal Nanocrystals: Synthesis, Electronic and Optical Properties;* Marcel Dekker: New York, 2003.

(2) Wilcoxon, J. P.; Provencio, P. P.; Samara, G. A. *Phys. Rev. B.* **2001**, *64*, 035417.

(3) Tanke, R. S.; Kauzlarich, S. M.; Patten, T. E.; Pettigrew, K. A.; Murphy, D. L.; Thompson, M. E.; Lee, H. W. H. *Chem. Mater.* **2003**, *15*, 1682.

(4) Heath, J. R.; Shiang, J. J.; Alivisatos, A. P. *J. Chem. Phys.* **1994**, *101*, 1607.

(5) Dutta, A. K. *Appl. Phys. Lett*. **1996**, *68*, 1189.

(6) Wang, D.; Dai, H. *Angew. Chem. Int. Ed*. **2002**, *41*, 4783.

(7) Holmes, J. D.; Ziegler, K. J.; Doty, R. C.; Pell, L. E.; Johnston, K. P.; Korgel, B. A. *J. Am. Chem. Soc.* **2001**, *123*, 3743.

(8) Ziegler, K. J.; Doty, R. C.; Johnston, K. P.; Korgel, B. A. *J. Am. Chem. Soc.* **2001**, *123*, 7797-7803.

(9) Holmes, J. D.; Johnston, K. P.; Doty, R. C.; Korgel, B. A. *Science* **2000**, *287*, 1471.

(10) Lu, X.; Hanrath, T.; Johnston, K. P.; Korgel, B. A. *Nano Lett.* **2003**, *3*, 93.

(11) Hanrath, T.; Korgel, B. A. *J. Am. Chem. Soc*. **2002**, *124*, 1424.

(12) Hanrath, T.; Korgel, B. A. *Adv. Mater*. **2003**, *15*, 437.

(13) Davidson, T. M.; Schricker, A. D.; Wiacek, R. J.; Korgel, B. A. *Adv. Mater*. **2004**, *167*,646.

(14) English, D. S.; Pell, L. E.; Yu, Z.; Barbara, P. F.; Korgel, B. A. *Nano Lett.* **2002**, *2*, 681.

(15) Ding, Z.; Quinn, B. M.; Haram, S. K.; Pell, L. E.; Korgel, B. A.; Bard, A. J. *Science* **2002**, *296*, 1293.

(16) TEM and selected area electron diffraction (SAED) were performed using a JEOL 2010F TEM operating at 200 kV equipped with a GATAN digital photography system. TEM samples were prepared by drop casting nanocrystals from chloroform dispersions onto 200 mesh copper grids with ultra-thin carbon film (Ladd Research, VT) or lacy carbon film (Electron Microscopy Sciences, PA). Energy-dispersive X-ray spectroscopy (EDS) was performed on the JEOL 2010F HRTEM equipped with an Oxford spectrometer.

(17) The Ge precursor solution was loaded into a 1 mL titanium grade-2 cell (0.5 cm I.D., 2.0 cm O.D. and 7.0 cm long with a titanium grade-2 LM6 HIP gland and plug, High Pressure Equipment, Inc) in a nitrogen glovebox. A brass block

(7X25X17 cm) was used to heat the reactor. The block was thermostatted with a thermocouple (Omega, Inc.) and a temperature controller, and heated by four 300 watt 1/4" diameter by 4.5" long cartridge heaters (Omega). The block was heated to the desired reaction temperature prior to inserting the cell. The cell was inserted into the preheated block and reached the synthesis temperature in 2 minutes. The reaction proceeded another 5 minutes for TEG and 20 seconds for DPG at this temperature.

(18) Cowley, J. M. *Electron Diffraction Techniques*; Oxford Science University Press: New York, **1992**; Vol. 1.

(19) Cullity, B. D. *Elements of X-Ray Diffraction*; Addison-Wesley Publishing Company, Inc.: Reading, MA, **1956**.

(20) Inagaki, N.; Mitsuuchi, M. *J. Poly. Sci.* **1983**, *21*, 2887.

(21) Pretsch, E.; Clerc, T.; Seibl, J.; Simon, W. *Tables of Spectral Data for Structure Determination of Organic Compounds*; Springer-Verlag: Berlin, **1983**.

(22) Socrates, G. *Infrared Characteristic Group Frequencies: Tables and Charts*; 2nd ed.; John Wiley & Sons: New York, **1994**.

(23) Taylor, B. R.; Kauzlarich, S. M.; Delgado, G. R.; Lee, H. W. *Chem. Mater.* **1999**, *11*, 2493.

(24) Melnikov, D. V.; Chelikowsky, J. R. *Solid State Commun.* **2003**, *127*, 361.

(25) Reboredo, F. A.; Zunger, A. *Phys. Rev. B*. **2000**, *62*, R2275.

(26) Takagahara, T.; Takeda, K. *Phys. Rev. B*. **1996**, *53*, R4205.

(27) Okamoto, S.; Kanemitsu, Y. *Phys. Rev. B*. **1996**, *54*, 16421.

(28) Reboredo, F. A.; Zunger, A. *Phys. Rev. B*. **2001**, *63*, 235314.

(29) Rappoport, Z., Ed. *The Chemistry of Organic Germanium, Tin and Lead Compounds*, Volume 2 (Part 1); John Wiley & Sons:Chichester, England, **2002**; Vol. 2.

(30) Kanemitsu, Y.; Uto, H.; Masumoto, Y.; Maeda, Y. *Appl. Phys. Lett.* **1992**, *61*, 2187.

Chapter 4: Synthesis of Germanium Nanocrystals in High Temperature Supercritical CO_2[*]

Germanium nanocrystals were synthesized in supercritical (sc) CO_2 by thermolysis of diphenylgermane (DPG) or tetraethylgermane (TEG) with octanol as a capping ligand at 500°C and 27.6 MPa. The Ge nanocrystals were characterized with HRTEM, energy-dispersive X-ray spectroscopy (EDS), and X-ray diffraction (XRD). On the basis of TEM, the mean diameters of the nanocrystals made from DPG and TEG were 10.1 and 5.6nm, respectively. The synthesis in sc-CO_2 produced much less organic contamination compared with similar reactions in organic supercritical fluids. When the same reaction of DPG with octanol was performed in the gas phase without CO_2 present, bulk Ge crystals were formed instead of nanocrystals. Thus, the solvation of the hydrocarbon ligands by CO_2 was sufficient to provide steric stabilization. The presence of steric stabilization in CO_2 at a reduced temperature of 2.5, with a reduced solvent density of only 0.4, may be attributed to a reduction in the differences between ligand-ligand interactions and ligand-CO_2 interactions relative to thermal energy.

---

[*] Portions of this chapter have been previously published as Lu, Xianmao; Korgel, Brian A.; and Johnston, Keith P.; *Nanotechnology*, **2005**, 4, 969-974. Copyright 2005 IOP Publishing Ltd.

4.1 INTRODUCTION

The size-tunable optical and electronic properties of semiconductor nanocrystals are attractive for both theoretical study and a variety of practical applications[1,2]. Among a variety of synthetic methods developed in the past decade[3-7], arrested precipitation has been particularly successful for controlling the size of the nanocrystals. In these solution-phase reactions, molecular precursors form nuclei followed by surface passivation of the growing particles with capping ligands. The ligands provide chemical stability and the potential for redispersibility in solvents. This method has proven to be very successful for synthesizing a variety of metal[8-10], group II-VI[11] and group III-V[12] semiconductor "free-standing" nanocrystals. However, synthesis of group IV nanocrystals, such as Si and Ge, requires high temperatures for crystallization due to their covalent bonding[13-16]. In the gas-phase, Ge crystallization requires temperatures typically above 350° C[17], well above the normal boiling point and critical temperature of most liquid solvents. However, capping ligands can be stabilized at elevated pressures in supercritical fluids[18]. Supercritical organic solvents, such as hexane (sc-hexane), have been utilized to synthesize Si[19,20]and Ge[21] nanocrystals, and Si[22,23], Ge[24,25] and GaAs[26] nanowires.

Compared to organic supercritical solvents such as hexane and octanol, supercritical carbon dioxide (sc-CO_2) exhibits many unique features for the synthesis of nanocrystals. CO_2 is non-flammable, environmentally benign, and it is chemically stable even at 600°C. Watkins et al. reported that reduction of organometallic precursors with hydrogen in sc-CO_2 at 80°C leads to highly uniform thin metal films[27,28]. Well-ordered mesoporous silicate films can be produced in sc-CO_2 at 60°C by catalyzed condensation of silicon alkoxides within block co-polymer templates[29]. Shah and coworkers synthesized silver, platinum and iridium nanocrystals by arrested precipitation in sc-CO_2 at temperatures up to 80°C with fluorinated ligands[30]. Each of these studies utilized temperatures below 100^{o} C. In contrast, Ryan et al. demonstrated that sc-CO_2 can be used at ~600°C to synthesize ultrahigh density semiconductor nanowires in a clean and fast process[31].

The stabilities of colloids in supercritical fluids have been related to the conformations of oligomeric stabilizers with Monte Carlo simulation[32-36]. A single oligomeric chain in a supercritical fluid at a reduced pressure, $P_r = P/P_c$, of 3.5, collapses upon heating to a $T_r = T/T_c$ of 1.25, but re-expands upon further heating to $T_r > 1.85$ at the coil-globule transition (C-GT) temperature. The critical flocculation density, above which colloids are stable, has been shown to be equivalent to the C-GT density[33]. Therefore, these simulations

suggest that it should be possible to form stable colloids in CO_2 at high reduced temperatures of interest in our study. If these predictions of simulation can be verified experimentally, large new classes of colloids in supercritical fluid CO_2 may be discovered at high temperatures. Furthermore, these conditions could be used for synthesis of nanocrystals.

In the previous chapter, we reported synthesis of Ge nanoparticles by decomposing TEG or DPG in the presence of octanol as a capping ligand in sc-hexane at 400-500°C[21,37]. Crystalline Ge nanoparticles 3~4nm in diameter produced in this method exhibit blue-shifted photoluminescence with relatively high quantum yield of ~6%. Due to the degradation of the organic solvents at the high reaction temperatures, however, extensive cleaning of the Ge nanoparticles was required to remove the organic by-products. In addition the yield of Ge was less than 1%.

Here, we report the synthesis of crystalline Ge nanocrystals at 500°C in sc-CO_2 with greatly reduced organic contamination relative to the case for organic supercritical fluids. By replacing the organic solvent with CO_2, the total amount of organic carbon is lowered by ~90%. The nanocrystals are characterized with a variety of techniques to determine the composition, morphology and crystallinity. Control experiments performed in the gas

phase without CO_2 are utilized to show how CO_2 influences the particle size due to steric stabilization. The ability to achieve steric stabilization at high reduced temperatures is explained based on the simulations noted above of the coil-globule transition density, phase behavior for oligomer chains, and flocculation of colloids in high temperature supercritical fluids. The results appear to confirm the prediction of the MC simulations that steric stabilization is possible at lower solvent densities at high temperatures than at ambient temperature, due to a reduction in the differences between ligand-ligand interactions and ligand-CO_2 interactions relative to thermal energy.

4.2 EXPERIMENTAL

4.2.1 Nanocrystal synthesis

Ge nanocrystals were synthesized by thermally degrading a Ge precursor, either tetraethylgermane (TEG, Aldrich Chemical Co.) or diphenylgermane (DPG, Gelest), in the presence of octanol (Aldrich Chemical Co.) at 500ºC and 27.6 MPa in sc-CO_2 (purity > 99.99%, Matheson Gas Products). The reactions were carried out using a 1mL (0.5cm i.d., 2.0cm o.d., 7cm long) high pressure titanium grade-2 reaction cell. In a typical experiment, 10μL of octanol with 50μL TEG or DPG was loaded into the

reaction cell in the glovebox under nitrogen. All chemicals in the reaction were anhydrous and packed under nitrogen upon purchase and used as received. The cell was sealed with a titanium grade-2 LM-6 HIP reducer (High Pressure Equipment) and a two-way stainless steel high pressure valve (High Pressure Equipment) and then connected to a Dionex Model 501 Computer Controlled Syringe Pump via 1/16 in. o.d. and 0.03 in. i.d. stainless steel high pressure tubing. A brass block (7×25×17 cm), which was thermostatted with a thermocouple and a temperature controller (Omega, Inc.) and heated by four 300 watt 1/4" diameter by 4.5" long cartridge heaters (Omega), was used to heat the reactor. Before the reaction, CO_2 was pumped with the syringe pump into the reactor at 20°C to 5.5MPa. With the valve between the pump and reactor closed, the reactor was then placed into the block heater, which had been preheated to 10°C above the desired reaction temperature. For safety, it was moved remotely with a long set of tongs and shielding from the high pressure. The reaction cell was heated to the reaction temperature, usually 500°C, in about 30 s. As the pressure increased to 20 MPa, the valve was opened with the pressure preset at a higher value on the pump side. The pressure was then controlled at 27.6 MPa with the pump. The reaction proceeded for another 5 minutes at the reaction temperature and the reactor was removed remotely from the block heater and cooled down to

room temperature with water and depressurized. CO_2 was then vented as a vapor, leaving most of the other components in the cell. The nanocrystals were collected from the reactor with chloroform. The samples were centrifuged at 6000 rpm for 4 minutes to remove the precipitate containing by-products and then dried with a rotary evaporator. The resulting black powder was then re-dispersed in chloroform.

4.2.2 Characterization methods

High resolution transmission electron microscopy (HRTEM) was performed using a JEOL 2010F TEM with energy-dispersive X-ray spectroscopy (EDS) operating at 200kV; images were obtained primarily with a GATAN digital photography system. Low resolution TEM images were obtained with a Philips EM201 TEM operating at 80kV. The TEM grid was prepared by dropping the Ge nanocrystals dispersion onto the 200 mesh copper grid with ultra-thin carbon film (Ladd Research Co.). X-ray diffraction (XRD) spectra were obtained on quartz slides (The Gem Dugout, State College, PA**)** using a Phillips vertical scanning diffractometer, with Cu Kα radiation (λ=1.54Å) and a scintillation detector.

4.3 RESULTS AND DISCUSSION

4.3.1 Nanocrystal morphology

Figure 4.1A shows a TEM image of Ge nanoparticles made from 50μL DPG with 10μL octanol (molar ratio of DPG:octanol = 4:1) at 500°C in sc-CO_2 at 27.6MPa. The diameter of the Ge nanoparticles ranges from 2 to 50nm with an average of 10.1±5.5nm based on the TEM measurement of more than 500 nanoparticles. The Ge nanoparticles (Figure 4.1B) made from TEG at the same molar ratio (TEG:octanol=4:1) with octanol in sc-CO_2 at the same reaction temperature and pressure had an average diameter of 5.6±3.5nm. The standard deviation/mean for the nanoparticles made from DPG and TEG are 54% and 63%, respectively. Similar to what has been observed in our previous work[21] in other supercritical solvents, including octanol and hexane the sizes of the nanocrystals made from TEG are smaller than those made from DPG at the same reaction conditions. For the Ge nanoparticles made in these supercritical organic solvents, the standard deviation about the mean ranged from 10 to 30%[21]. The broader size distribution in CO_2 is consistent with weaker solvation of the stabilizing ligands as discussed in detail later.

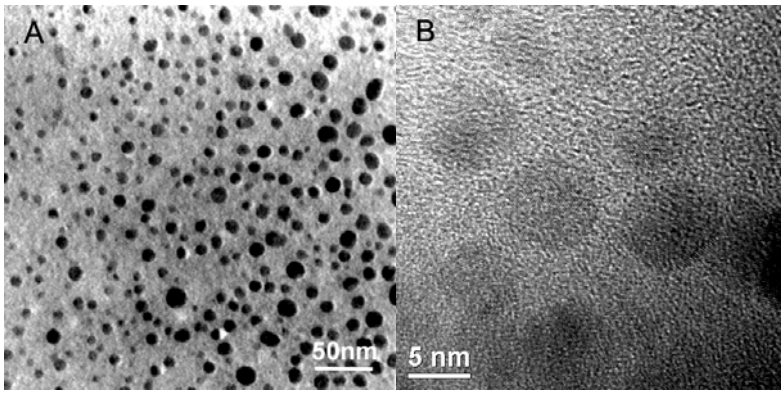

Figure 4.1 TEM images of Ge nanoparticles made from (A) DPG and (B) TEG with octanol at 500°C at 27.6MPa in sc-CO_2.

HRTEM results indicate that the nanoparticles synthesized with DPG or TEG are crystalline as shown in Figure 4.2. Both the {111} and {220} lattice fringes are visible, with the expected d-spacings of 3.27 and 2.00Å respectively, for diamond cubic Ge. The fast Fourier transform (FFT) of the HRTEM image of a singe nanoparticle (Figure 4.2B) exhibited spots with hexagonal symmetry and spacings consistent with the {111} lattice planes in diamond cubic Ge. The EDS spectrum obtained with the TEM (Figure 4.3) also confirms the presence of Ge in the sample. Although HRTEM images of many nanoparticles show a single crystalline core, others revealed polycrystalliny (Figure 4.2C), indicating that coagulative growth occurred in some Ge particles. The coagulation may indicate that CO_2 provided only partial solvation of the stabilizing ligands, such that steric stabilization was somewhat limited. Likewise, high quality Ag nanocrystals could be synthesized in sc-CO_2, even when these particles were only partially coated with ligands[38].

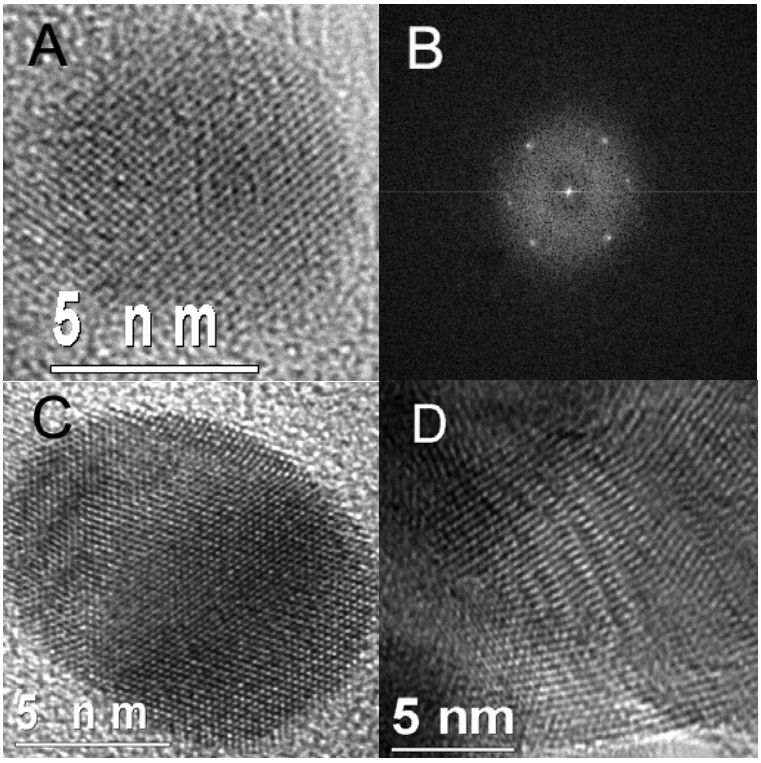

Figure 4.2 HRTEM images of Ge nanoparticles. (A) nanoparticle made from TEG; (B) is the FFT of image (A); (C) and (D) are the particles made from DPG with octanol in sc-CO_2 and without CO_2, respectively.

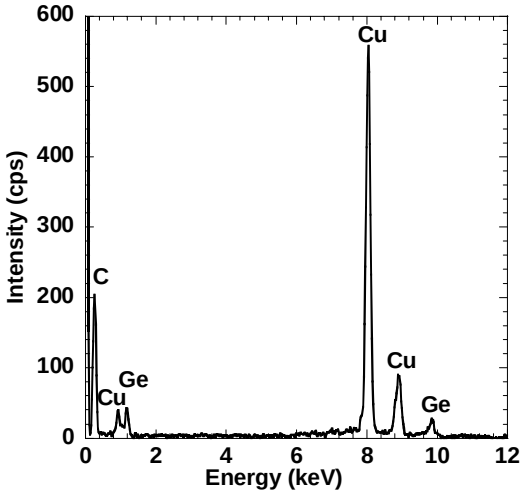

Figure 4.3 EDS data of the Ge nanoparticles. The peaks at 1.2 and 9.8 keV correspond to the *Lα and Kα* lines of Ge, respectively. The copper peaks result from the copper TEM grid.

The powder XRD pattern of Ge nanocrystals made from DPG in sc-CO_2 at 500ºC (Figure 4.4B) shows peaks of crystalline Ge with a diamond cubic structure. The sample was cast onto quartz slides to form a thin layer of powder. For the {111} reflection ($2\theta_B$=27.28º), the size calculated from the peak width $B \approx 0.7º$ (fwhm) and the Scherrer equation is 11.5nm, which is close to the average diameter of 10.1 nm measured by TEM.

A control experiment was performed with 50μL DPG and 10μL octanol in the 1mL reaction cell at 500°C, and a calculated pressure of 0.4MPa, without the presence of CO_2. The XRD pattern (Figure 4.4A) shows only very sharp peaks of bulk polycrystalline Ge, indicating that Ge nanocrystals were not produced without CO_2. The formation of bulk Ge is to be expected in the gas phase without CO_2 as solvation of the ligands was not present. The unstabilized Ge crystals formed in the gas phase (Figure 4.3D) were observed to coat the reactor walls and were highly aggregated. In contrast nanocrystals were formed with CO_2 present, as illustrated by the broad peaks in Figure 4.4B and the HRTEMs.

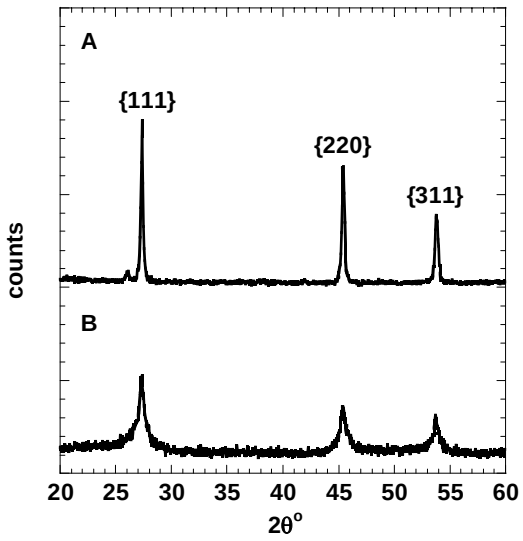

Figure 4.4 XRD of the Ge nanoparticles made from 50μL DPG with 10μL octanol at 500°C, (A) without CO_2 at a calculated pressure of 0.4MPa, and (B) in sc-CO_2 at 27.6MPa.

A major goal for the synthesis of Ge nanoparticles in sc-CO_2, instead of an organic solvent, such as hexane, is to reduce the organic contaminants formed by solvent degradation at the high temperature required to activate the reaction and crystallization. Figure 4.5 compares the appearance of the products made from the same concentrations of TEG and octanol in sc-hexane (Figure 4.5A) and in sc-CO_2 (Figure 4.5B) at 500°C and at similar pressures. No cleaning was performed on these two samples. The product made in sc-hexane is brown with a significant amount of oily yellow by-product, after evaporating off the solvent at room temperature. A weight loss of more than 90% was observed when the sample was dried in a vacuum oven at 180°C[21]. The sample made in sc-CO_2, however, was very clear with much less by-product. Only black dry powder was obtained, without an oily yellow phase, after drying with a rotary evaporator at room temperature. The weight loss was less than 10% when heated at 180°C under vacuum. For the reaction in hexane, the number of moles of carbon in the precursor, ligand and solvent were 0.002, 0.0005, and 0.023, respectively. The larger amount of byproduct is consistent with the large amount of carbon in the hexane. Although the formation of by-products from the decomposition of Ge precursors and the capping ligand cannot be completely avoided, they were reduced substantially when sc-CO_2, rather than sc-hexane, was used as the solvent.

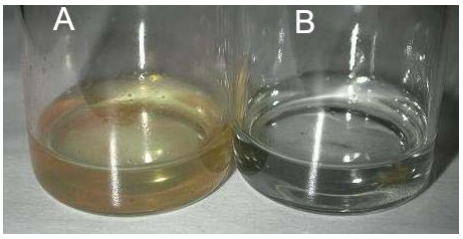

Figure 4.5 Digital image of the reaction mixtures made from 50μL TEG with 10μL octanol at 500°C in (A) sc-hexane at a calculated pressure of 29.5 MPa and (B) sc-CO_2 at 27.6MPa. The products were collected with 2mL chloroform. From the TEM observation, the concentrations of nanoparticles in (A) and (B) are about the same and very dilute.

4.3.2 Mechanism of steric stabilization at high reduced temperatures

The stability of the nanocrystals in sc-CO_2 depends on the balance between attractive and repulsive forces between particles. The particle core-core attractive van der Waals interaction is given by

$$\Phi_{vdW} = -\frac{A_{121}}{6}\left[\frac{2r^2}{d^2-4r^2}+\frac{2r^2}{d^2}+\ln\left(\frac{d^2-4r^2}{d^2}\right)\right] \qquad (4.1)$$

where r is the radius of the particles, d is the particle edge-to-edge separation and A_{121} is Hamaker constant between the Ge cores (1) through the CO_2 medium (2). The Hamaker constant is a function of the pure component values according to the relationship

$$A_{121} = (\sqrt{A_{11}} - \sqrt{A_{22}})^2 \qquad (4.2)$$

For CO_2, A_{22} can be estimated from simplified Lifshitz theory[39]:

$$A_{22} = \frac{3}{4}k_bT\left(\frac{\varepsilon_2-1}{\varepsilon_2+1}\right)^2 + \frac{2hv_e}{16\sqrt{2}}\frac{(n_2-1)^2}{(n_2+1)^{3/2}} \qquad (4.3)$$

where k_b is Boltzmann's constant, T is temperature, h is Plank's constant, and v_e is the maximum electronic ultraviolet adsorption frequency usually taken to be 3×10^{15} s^{-1}. The dielectric constant ε_2 and the refractive index n_2 can be obtained from an equation of state[40] and the literature values[41] of

$(\varepsilon_2 - 1)V/(\varepsilon_2 - 2)$ and $(n_2^2 - 1)V/(n_2^2 - 2)$ for CO_2, where V is the molar volume. The dielectric constant of the Ge nanoparticles varies with the particle size. However, the known values for bulk Ge were used resulting in A_{11}=5.3eV with ε_1=16.6 and n_1=4.0.

Under the reaction condition of 500°C and 27.6MPa, the estimated A_{121} for Ge in CO_2 is 5.0eV, only 16% higher than the Hamaker constant of 4.3eV at 80°C and 27.6MPa, a reaction condition proven to be effective for the synthesis of silver, platinum and iridium nanocrystals in sc-CO_2. It is about 40% larger than the value of 3.6eV in hexane at ambient conditions. This increased attractive force and the resulting higher degree of aggregation accounts in part for the broader size distribution of the Ge nanoparticles synthesized in sc-CO_2 relative to organic solvents.

The Waals attraction between nanocrystal cores is screened by steric repulsion from the capping ligands on the nanocrystals[30]. The repulsive forces of the surface passivated nanoparticles are determined by the surface coverage of the capping ligands, the length of the ligand tail and the solvent quality. In good solvent, such as toluene, hydrocarbon ligands are solvated, and extend into the solvent to minimize attraction between the nanocrystal cores[42]. In a poor solvent, the capping ligands collapse partially and the overall interaction

between particles becomes attractive resulting in aggregation of the particles and broad size distributions.

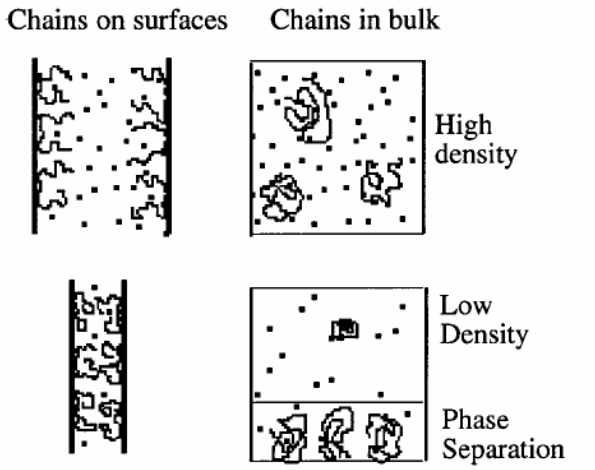

Figure 4.6 Analogy between flocculation of oligomer chains grafted to a surface at a high density above and low density below: (1) the critical flocculation density (CFD), (2)the coil-globule transition density(C-GTD) of the chain and (3) the upper critical solution density (UCSD) on the bulk polymer-solvent phase diagram (Adapted from Figure 1 in ref[43]).

According to lattice fluid theory and Monte Carlo simulation, the force between colloidal particles in supercritical fluids[34] has been shown to be related directly to the conformation of the oligomeric stabilizer chains[33] and the stabilizer chain-solvent phase behavior[32]. Each of these properties is a strong function of the solvent density, which influences the solvent quality as shown in Figure 4.6. At high density the oligomer coils are extended and are miscible with the solvent. The chains collapse from a coil-like conformation to a globular structure when the solvent density is reduced below the coil-to-globule transition density (C-GTD), where attractive and repulsive intrachain interactions are balanced[33]. The dimensions of the polymer chain are determined by the intrachain attractive forces which collapse the chain and the entropic forces which expand the chain to a random coil-like structure. The solvent screens the intrachain attractive interactions. At a given temperature, the screening favors a more extended polymer chain as the solvent density increases. Likewise, at a given solvent density, the chain dimensions increase with temperature. The temperature effect is apparent in the χ parameter

$$\chi = \frac{\varepsilon_{11} + \varepsilon_{22} - 2\varepsilon_{12}}{k_b T} \qquad (4.4)$$

where ε_{ij} is the interaction energy between component i and j. Notice that the effect of attractive energetics becomes weaker at high temperature (ε/k_bT).

Monte Carlo simulation shows that a closed immiscibilty loop is formed in the binary oligomer-solvent phase diagram at a P_r of 3.5 (Figure 4.7), which is of interest in our study. At temperatures below the low critical solvent temperature (LCST), which corresponds to the C-GTD of the solvent, the chain is expanded due to the good solvent conditions.[33] The nanocrystals studied in CO_2 below 100° C[18,30,44] are at or are close to this condition. When the temperature is increased above the LCST at a constant P_r, chain contraction occurs because of the low density of the solvent. However, at a T_r of 1.85, the attractive interactions in equation (4.4) become less important than the thermal energy, k_bT, resulting in a one-phase region[32] where the chains are re-expanded[33]. Similarly, Gromov et al. also found that for a polymer-supercritical mixture, both LCST and upper critical solvent temperature (UCST) are observed at certain pressures (Figure 6 in ref[32]).

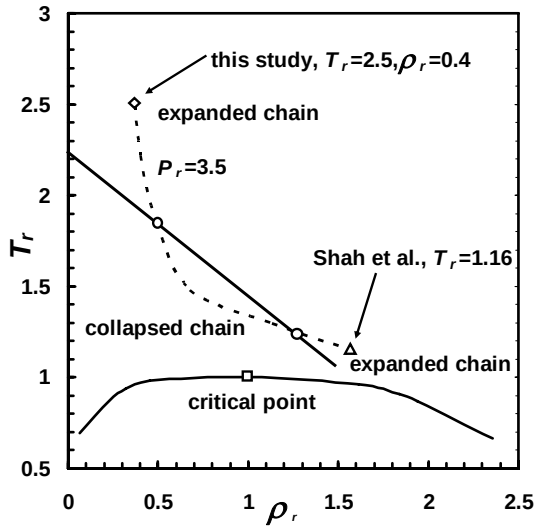

Figure 4.7 Variation of the C-GTD ρ_r with reduced temperature T_r. The dotted line is the solvent isobar at P_r=3.5, which is the pressure used in this study. Taken from ref [33].

The force between surfaces with grafted chains is related closely to the C-GTD and the UCSD. Lattice-fluid self-consistent field theory (LFSCF) shows that the force between surfaces becomes attractive at densities below the critical flocculation density (CFD)[34]， Here the solvent molecules leave the polymer chains to raise the volume and the entropy of the system, and attractive forces between polymer chains cannot be screened by the solvent molecules. Luna-Barcenas et al.[33] found that at a certain T_r, the CFD is about the same as the UCSD of the bulk polymer solution, and the C-GTD of a single Lennard-Jones polymer chain in supercritical solvent (Table II in ref[33]). In all these cases, the polymer chain collapse plays a central role in the polymer flocculation and polymer-solvent phase separation, as shown in Figure 4.6. In experimental studies of the flocculation of poly(2-ethylhexyl acrylate) in sc-CO_2, the CFD was shown to correspond to the UCSD based on light scattering measurement[45]. Together these studies suggest that it should be possible to stabilize colloids coated with oliomeric chains in CO_2 at the high temperatures investigated in our study even at the relatively low solvent densities.

A recent study demonstrated that CO_2 may be utilized at high temperatures for inorganic synthesis of nanowires. Ryan et al.[31] decomposed

DPG to form Ge nanowires at 600°C. The sc-CO_2 acts as a solvent to enable the rapid transport of Ge precursor, DPG, into the mesopores of the silica growth template.

In our study, the formation of nanocrystals on the order of 10 nm indicated that C_8 hydrocarbon chains provide some degree of steric stabilization. Although the density of CO_2 is lower than in the previous studies of nanocrystal stabilization below 100^o C[30], it must still above the C-GTD, given that steric stabilization is present. According to simulation, the C-GTD is only 0.3 at a T_r of 2.0 versus 1.4 at a T_r of 1.16 in previous low temperature studies (Figure 4.7) [33]. At high Ts, the effect of the attractive interactions in eq. (4) becomes less important relative to thermal energy and χ decreases. Therefore, these experimental results appear to confirm the prediction of the simulations that colloidal stabilization is possible in supercritical fluids when the reduced temperature is above 1.85 (T_r=2.5 in this study) despite the lower solvent densities than at near ambient temperatures. Moreover, CO_2 can provide a degree of stabilization of colloids with hydrocarbon ligands at high reduced temperatures, whereas fluorocarbon tails, with unusually weak tail-tail interactions, have been required at temperatures below 100^o C.

4.4 CONCLUSIONS

Highly crystalline germanium nanoparticles either 5.6 or 10.1 nm in diameter were synthesized in supercritical (sc) CO_2 by thermolysis of organogermanes with octanol as a capping ligand at 500^{o}C and 27.6 MPa. The use of CO_2, which is relatively inert, rather than organic supercritical fluids reduces the amount of organic byproduct contaminants markedly. Without CO_2, the gas phase reaction did not produce nanocrystals, indicating that CO_2 provides sufficient solvation of the capping ligands to achieve steric stabilization. The stabilization of the nanocrystals coated with hydrocarbon ligands in CO_2 at a reduced temperature of 2.5 with a reduced solvent density of only 0.4 may be attributed to a reduction in the differences between ligand-ligand interactions and ligand-CO_2 interactions relative to thermal energy, consistent with previous conclusions from computer simulation. This general result suggests that a variety of new classes of colloids should be stable in CO_2 at high reduced temperatures at lower densities than required at near ambient temperatures.

4.5 REFERENCES

(1) Heath, J. R. *Chem. Soc. Rev.* **1998**, *27*, 65.

(2) Alivisatos, A. P. *Science* **1996**, *271*, 933.

(3) Bley, R. A.; Kauzlarich, S. M.; Davis, J. E.; Lee, H. W. *Chem. Mater.* **1996**, *8*, 1881.

(4) Bley, R. A.; Kauzlarich, S. M. *J. Am. Chem. Soc.* **1996**, *118*, 12461.

(5) Littau, K. A.; Szajowski, P. J.; Muller, A. J.; Kortan, A. R.; Brus, L. E. *J. Phys. Chem.* **1993**, *97*, 1224.

(6) Kornowski, A.; Giersig, M.; Vogel, R.; Chemseddine, A.; Weller, H. *Adv. Mater.* **1993**, *5*, 634.

(7) Maeda, Y.; Tsukamoto, N.; Yazawa, Y.; Kanemitsu, Y.; Masumoto, Y. *Appl. Phys. Lett.* **1991**, *59*, 3168.

(8) Sigman, M. B., Jr.; Saunders, A. E.; Korgel, B. A. *Langmuir* **2004**, *20*, 978.

(9) Saunders, A. E.; Sigman, M. B., Jr.; Korgel, B. A. *J. Phys. Chem. B* **2004**, *108*, 193.

(10) Son, S. U.; Jang, Y.; Yoon, K. Y.; Kang, E.; Hyeon, T. *Nano Lett.* **2004**, *4*, 1147.

(11) Murray, C. B.; Norris, D. J.; Bawendi, M. G. *J. Am. Chem. Soc.* **1993**, *115*, 8706.

(12) Stowell, C. A.; Wiacek, R. J.; Saunders, A. E.; Korgel, B. A. *Nano Lett.* **2003**, *3*, 1441.

(13) Heath, J. R. *Science* **1992**, *258*, 1131.

(14) Heath, J. R.; Shiang, J. J.; Alivisatos, A. P. *J. Chem. Phys.* **1994**, *101*, 1607.

(15) Taylor, B. R.; Kauzlarich, S. M.; Delgado, G. R.; Lee, H. W. H. *Chem. Mater.* **1999**, *11*, 2493.

(16) Wilcoxon, J. P.; Provencio, P. P.; Samara, G. A. *Phys. Rev. B* **2001**, *64*, 035417.

(17) Jiang, J.; Chen, K.; Huang, X.; Li, Z.; Feng, D. *Appl. Phys. Lett.* **1994**, *65*, 1799.

(18) Shah, P. S.; Hanrath, T.; Johnston, K. P.; Korgel, B. A. *J. Phys. Chem. B* **2004**, *108*, 9574.

(19) Holmes, J. D.; Ziegler, K. J.; Doty, R. C.; Pell, L. E.; Johnston, K. P.; Korgel, B. A. *J. Am. Chem. Soc.* **2001**, *123*, 3743.

(20) Pell, L. E.; Schricker, A. D.; Mikulec, F. V.; Korgel, B. A. *Langmuir* **2004**, *20*, 6546.

(21) Lu, X.; Ziegler, K. J.; Ghezelbash, A.; Johnston, K. P.; Korgel, B. A. *Nano Lett.* **2004**, *4*, 969.

(22) Lu, X.; Hanrath, T.; Johnston, K. P.; Korgel, B. A. *Nano Lett.* **2003**, *3*, 93.

(23) Holmes, J. D.; Johnston, K. P.; Doty, R. C.; Korgel, B. A. *Science* **2000**, *287*, 1471.

(24) Hanrath, T.; Korgel, B. A. *J. Am. Chem. Soc.* **2002**, *124*, 1424.

(25) Hanrath, T.; Korgel, B. A. *Adv. Mater.* **2003**, *15*, 437.

(26) Davidson, F. M.; Schricker, A. D.; Wiacek, R. J.; Korgel, B. A. *Adv. Mater.* **2004**, *16*, 646.

(27) Watkins, J. J.; McCarthy, T. J. *Chem. Mater.* **1995**, *7*, 1991.

(28) Watkins, J. J.; Blackburn, J. M.; McCarthy, T. J. *Chem. Mater.* **1999**, *11*, 213.

(29) Pai, R. A.; Humayun, R.; Schulberg, M. T.; Sengupta, A.; Sun, J.-N.; Watkins, J. J. *Science* **2004**, *303*, 507.

(30) Shah, P. S.; Husain, S.; Johnston, K. P.; Korgel, B. A. *J. Phys. Chem. B* **2001**, *105*, 9433.

(31) Ryan, K. M.; Erts, D.; Olin, H.; Morris, M. A.; Holmes, J. D. *J. Am. Chem. Soc.* **2003**, *125*, 6284.

(32) Gromov, D. G.; de Pablo, J. J.; Luna-Barcenas, G.; Sanchez, I. C.; Johnston, K. P. *J. Chem. Phys.* **1998**, *108*, 4647.

(33) Luna-Barcenas, G.; Meredith, J. C.; Sanchez, I. C.; Johnston, K. P.; Gromov, D. G.; de Pablo, J. J. *J. Chem. Phys.* **1997**, *107*, 10782.

(34) Meredith, J. C.; Sanchez, I. C.; Johnston, K. P.; de Pablo, J. J. *J. Chem. Phys.* **1998**, *109*, 6424.

(35) Condo, P. D.; Sumpter, S. R.; Lee, M. L.; Johnston, K. P. *Ind. Eng. Chem. Res.* **1996**, *35*, 1115.

(36) Sirard, S. M.; Gupta, R. R.; Russell, T. P.; Watkins, J. J.; Green, P. F.; Johnston, K. P. *Macromolecules* **2003**, *36*, 3365.

(37) Myung, N.; Lu, X.; Johnston, K. P.; Bard, A. J. *Nano Lett.* **2004**, *4*, 183.

(38) Shah, P. S.; Husain, S.; Johnston, K. P.; Korgel, B. A. *J. Phys. Chem. B* **2002**, *106*, 12178.

(39) Israelachvili, J. N. *Intermolecular and Surface Forces: With Applications to Colloidal and Biological Systems*, 1985.

(40) Yaws, C. L. *Handbook of Thermodynamics Diagrams*; Gulf Publishing Company: Houston, Texas, 1996; Vol. 1-3.

(41) Johnston, D. R.; Cole, R. H. *J. Chem. Phys.* **1962**, *36*, 318.

(42) Saunders, A. E.; Korgel, B. A. *J. Phys. Chem. B* **2004**, *108*, 16732.

(43) Meredith, J. C.; Johnston, K. P. *Macromolecules* **1998**, *31*, 5507.

(44) Saunders, A. E.; Shah, P. S.; Park, E. J.; Lim, K. T.; Johnston, K. P.; Korgel, B. A. *J. Phys. Chem. B* **2004**, *108*, 15969.

(45) Yates, M. Z.; ONeill, M. L.; Johnston, K. P.; Webber, S.; Canelas, D. A.; Betts, D. E.; DeSimone, J. M. *Macromolecules* **1997**, *30*, 5060.

Chapter 5: High Yield of Germanium Nanocrystals Synthesized from Germanium Diiodide in Solution*

High chemical yields, up to 73%, were achieved for germanium (Ge) nanocrystals synthesized in solution with germanium diiodide (GeI_2) and $LiAlH_4$ as a reducing agent in tri-n-octylphosphine (TOP) or tri-n-butylphosphine (TBP). Ge nanocrystals were characterized by TEM, energy dispersive X-ray spectroscopy (EDS), X-ray diffraction (XRD), FTIR spectroscopy and X-ray photoelectron spectroscopy (XPS). Reactions in TOP at 300°C yielded Ge nanocrystals with moderate size polydispersity and good crystallinity with average diameters that could be manipulated by varying the precursor concentration from ~3 nm to ~11 nm. High chemical yields are enabled by the high reactivity of GeI_2, high GeI_2 solubility in alkyl phosphines and relatively mild reaction temperature, which minimizes byproduct formation and solvent degradation. The presence of alkyl groups in the FTIR spectra, the small and controllable particle diameters and lack of significant Ge oxidation revealed by XPS indicate that the nanocrystals were chemically passivated with an organic layer.

---

* Portions of this chapter have been previously published as Lu, Xianmao; Korgel, Brian A.; Johnston, Keith P. *Chem. Mater.*, **2005**, *17*, 6479-6485. Copyright 2005 American Chemical Society.

5.1 INTRODUCTION

Semiconductor nanocrystals exhibit size-tunable optical and electronic properties that are of interest in solid state lighting, sensors and other electronic and optoelectronic devices[1,2]. Solution-phase methods have been developed to produce a wide range of materials, including metal[3-5], Group II-VI[6], III-V[7], and IV[8] semiconductor nanocrystals by reacting precursors in the presence of organic capping ligands. For Ge nanocrystals, it has been challenging to identify appropriate precursors that readily decompose in the presence of organic ligands and sustain controlled crystalline particle growth. Many synthetic approaches have been explored, including $GeCl_4$ reduction with reducing agents such as NaK alloy[9] and sodium or lithium naphthalenide[10], reduction of $GeCl_4$ in inverse micelles combined with separation using HPLC[11], metathesis reactions of NaGe, KGe or Mg_2Ge with $GeCl_4$[12-15], thermally initiated hydrogermylation of GeI_4[16], organogermane thermolysis (for example, tetraethylgermane TEG and diphenylgermane DPG) in high temperature organic solvent[17] or in supercritical solvents[18-20], thermal reduction of $Ge[N(SiMe_3)_2]_2$ in a non-coordinating solvent[21], and reduction of $GeCl_4$ in inverse micelles to make Ge nanocubes[22]. These methods have not been able to achieve simultaneously a high yield of crystalline well-passivated Ge nanocrystals with controlled size and low polydispersity, due to limitations of limited precursor reactivity, particularly for

$GeCl_4$, byproduct formation, for example, from organogermanes, and poor ligand stabilization.

In this chapter, we report the synthesis of Ge nanocrystals by reduction of germanium diiodide (GeI_2) with $LiAlH_4$ in coordinating solvents, tri-n-octylphosphine (TOP) or tri-n-butylphospine (TBP) with high chemical yields. GeI_2 disproportionates to Ge and GeI_4 at ~330°C and this reaction has been used to grow Ge films by chemical vapor deposition at higher temperatures[23,24]. Wu et al. recently synthesized single crystalline Ge nanowires from GeI_2 by a vapor transport method at temperatures about 1000°C[25]. When mixed with alkyl phosphines R_3P, such as TOP and TBP, GeI_2 and R_3P react to form adducts of $(GeI_2)\cdot R_3P$[26]. The TOP·(GeI_2) and TBP·(GeI_2) complexes are soluble in organic solvents, offering the opportunity for Ge synthesis in solution under mild reaction temperature of 300°C and atmospheric pressure. The goal was to achieve a high chemical yield of Ge nanocrystals by taking advantage of the high reactivity of GeI_2 and high GeI_2 solubility in alkyl phosphines and to use mild reaction temperatures to minimize solvent degradation byproducts. The coordinating solvents (i.e., TOP and TBP) control the rate of precursor decomposition and serve as capping ligands to prevent particle aggregation, leading to relatively monodisperse nanocrystals. Preliminary experiments performed by heating GeI_2 in TOP at 330° gave observable quantities of Ge nanocrystals. However, the nanocrystal surfaces were heavily oxidized and the yield was low. The addition

of $LiAlH_4$ as a reducing agent was found to prevent surface oxidation and increase the reaction yield significantly, resulting in chemical yields of up to 73%. The method of addition of the precursor and $LiAlH_4$ and the temperature profile were designed to produce high nucleation rates and to control the particle size. The Ge nanocrystals were crystalline with moderate polydispersity. Coarse size control can be achieved by varying the precursor concentration, with higher GeI_2 concentrations giving larger particles. In addition to the high yield of Ge nanocrystals, this report also describes the effect of precursor concentration and different solvents on the nanocrystal size and the growth mechanism. The competition between growth by condensation and aggregation is analyzed based on the moments in the size distribution. The results are compared with previous synthetic methods, which have explored a wide range of temperatures with various types of precursors, reducing agents, stabilizing ligands, and solvents.

5.2 EXPERIMENTAL

5.2.1 Synthesis

Ge nanocrystals were synthesized under nitrogen in a three-neck flask on a Schlenk line. GeI_2 (Strem Chemicals, packed under argon) were stored in a nitrogen-filled glovebox upon purchase. Both TOP and TBP (Aldrich, tech. grade) were degassed through a freeze-pump-thaw technique and TOP was

distilled at 200°C and 0.3 Torr. TBP and vacuum distilled TOP were then transferred into the glovebox, and 4 Å molecular sieves were used to absorb the water in the solvents. The precursor solutions were prepared in the glovebox. Amounts of 0.215, 0.43 and 0.86 g GeI_2 were added to 5ml TOP or TBP and stirred for 10 hours to form clear yellow solutions with concentrations of 130, 260 and 520 mM, respectively. Amounts of 0.0125, 0.025 and 0.05 g $LiAlH_4$ (Aldrich) were added to 5 ml TOP or TBP and also stirred for 10 hours to form 65, 130, and 260 mM dispersions. The GeI_2 and $LiAlH_4$ mixtures were loaded separately into 10 ml glass syringes. 5 ml of GeI_2 solution was injected into the flask through a rubber septum and heated to 120°C with stirring, followed by the injection of 5 ml of the corresponding $LiAlH_4$ dispersion. The $LiAlH_4$ concentration was about half that of GeI_2. The introduction of $LiAlH_4$ immediately produced a brown solution. The temperature was raised to 300°C for reaction in TOP and 240°C in TBP within 5 min, and the solution gradually turned black in 2 min. After 60 min, the heating mantle was removed and the products were allowed to cool to room temperature. 10 ml acetone was added to the mixture to form a black precipitate containing Ge, and the mixture was centrifuged. The Ge nanocrystals were redispersed in 10 ml of chloroform and reprecipitated with 10 ml of acetone, and centrifuged again at 9,000 rpm for 5 min. This purification step was repeated again. A final centrifugation of redispersed nanocrystals in 10 ml of chloroform at 6,000 rpm for 5 min resulted in

a dark grey solution of Ge nanocrystals and precipitate containing impurities. The Ge nanocrystals were vacuum dried on a rotary evaporator at room temperature. About 23, 70 and 95 mg of black powder consisting of Ge nanocrystals was obtained after the purification steps for reactions of 130, 260 and 520 mM GeI_2 in TOP corresponding to chemical yields of 48%, 73% and 50%, respectively. The nanocrystals readily redisperse in chloroform and toluene.

5.2.2 Materials characterization

The nanocrystals were characterized by transmission electron microscopy (TEM), energy-dispersive X-ray spectroscopy (EDS), Fourier-transform infrared (FTIR) spectroscopy, and X-ray photoelectron spectroscopy (XPS). TEM specimens were prepared by drop casting dilute dispersions onto 200-mesh copper grids coated with ultra-thin carbon film (Ladd Research Co.). Low resolution TEM (LRTEM) images were obtained with a Philips EM201 TEM operating at 80kV. High resolution TEM (HRTEM) was performed on a JEOL 2010F TEM; images were obtained digitally with a GATAN digital photography system. EDS was performed on the JEOL 2010F HRTEM equipped with an Oxford spectrometer. XPS data was acquired using a Physical Electronics XPS 5700 ESCA spectrometer equipped with a monochromatic Al X-ray source (Al Kα, 1.4866 keV) and 11.7 eV path energy by drop casting 2 mg of nanoparticles from

chloroform onto a 1×1cm silicon substrate. X-ray diffraction (XRD) was obtained from ~10 mg nanocrystals deposited by drop casting on quartz slides (Gem Dugout, State College, PA**)** with continuous scan for 5 hours at a rate of 12°/min and 0.02° per step using a Bruker-Nonius D8 Advance powder diffractometer with Cu K_α radiation (λ=1.54 Å) and a rotary sample stage (30rpm). FTIR measurements were performed using Thermo Mattson Infinity Gold FTIR spectrometer for purified Ge nanocrystals that were drop cast in air from chloroform onto a KBr IR card (International Crystal Laboratories).

5.3 RESULTS

5.3.1 Nanocrystal synthesis in TOP

Figure 5.1 shows representative TEM images of Ge nanocrystals made from different GeI_2 concentrations in TOP: 130, 260 and 520 mM. The particles have not been size-selectively precipitated. The samples are relatively free of organic contamination, as oily species were not observed and the particles are distributed on the entire TEM grid, unlike the nanoparticles made from organogermanes at higher temperature, which contained large amount of organic by-products even after extensive washing[18]. The average nanocrystal diameters were obtained by counting 600 nanocrystals for each sample with Scion Image software (Scion Co.). 260 mM GeI_2 in TOP (at 300°C) gave nanocrystals with

an average diameter of 8.1±1.4 nm with 90% of the particles ranging between 6 nm and 10 nm. The nanocrystal diameter could be varied by changing the GeI_2 concentration. The diameter increased to 11.6±2.2 nm for 520 mM GeI_2 in TOP and decreased to 3.0±0.5 nm when the concentration of GeI_2 in TOP was decreased to 130 mM.

Figure 5.2 shows the Ge nanocrystal size distributions obtained from reactions with 130, 260 and 520 mM GeI_2 in TOP. The average particle diameter increases from 3.0 nm to 8.1 nm to 11.6 nm with the increased precursor concentration. The polydispersity, however, was relatively independent of the precursor concentration with the standard deviations about the mean diameter of 16.7%, 17.3% and 19.0%, respectively.

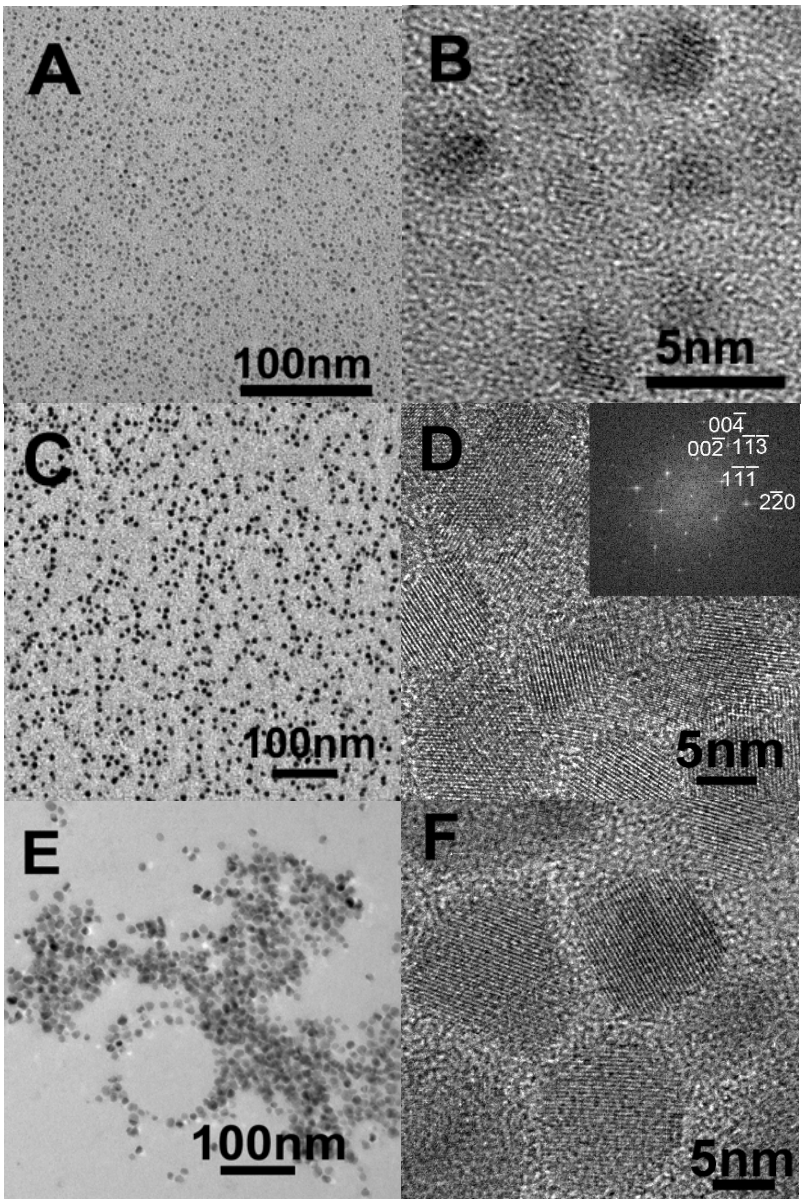

Figure 5.1 LRTEM and HRTEM images of (A,B) 3.0±0.5, (C,D) 8.1±1.4 and (E,F) 11.6±2.2 nm Ge nanoparticles synthesized from 130, 260, 520 mM GeI_2 solution in TOP at 300°C, respectively. HRTEM images show lattice fringes for most of the nanocrystals. The observed lattice spacings of 3.26 and 2.00Å correspond to the {111} and {220} planes of diamond cubic Ge. Inset of D) the FFT of a single nanoparticle imaged down the <110> zone axis. A forbidden spot [00-2] appears in the pattern, which can be attributed to double diffraction from [1-1-1] and [-11-1].

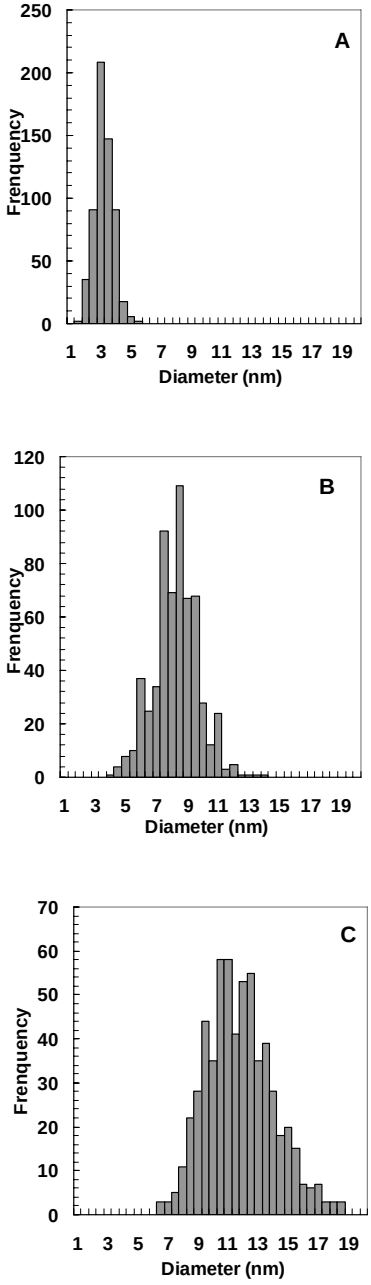

Figure 5.2 Size distribution for Ge nanoparticles with diameters of (A) 3.0±0.5 nm, (B) 8.1±1.4 nm, and (C) 11.6±2.2 nm.

High resolution TEM of fields of nanocrystals (Figure 5.1 B, D and F) and X-ray diffraction (XRD) (Figure 5.3) confirmed that the nanocrystals were crystalline with diamond cubic Ge structure. The Ge nanocrystals of different size exhibited primarily single crystal domains according to the HRTEM images. Figure 5.1B, for example, shows a field of crystalline 3 nm Ge nanocrystals with 3.26 and 2.00 Å d-spacings corresponding to the {111} and {220} planes in diamond cubic Ge. An example of a fast Fourier transform (FFT) of an HRTEM image of an individual particle is shown in the inset in Figure 5.1D. The 9 nm diameter particles shows diffraction spots corresponding d-spacings of 3.26, 2.00, 1.70, and 1.41 Å, which index to the Ge {111}, {220}, {311}, and {400} cubic phase reflections, respectively. The XRD peaks also match the expected {111}, {220} and {311} peaks for bulk Ge. The diffraction peak line broadening in the XRD pattern results from the small nanocrystal diameter. From the Scherrer equation, the peak broadening values of 2.58°, 1°, and 0.78° for the FWHM of the {111} peak of the nanocrystals made from 130, 260 and 520 mM GeI_2 in TOP indicate average diameters of 3.1, 8.0 and 10.3 nm, consistent with the average diameters determined from TEM images of 3.0, 8.1 and 11.6 nm, respectively.

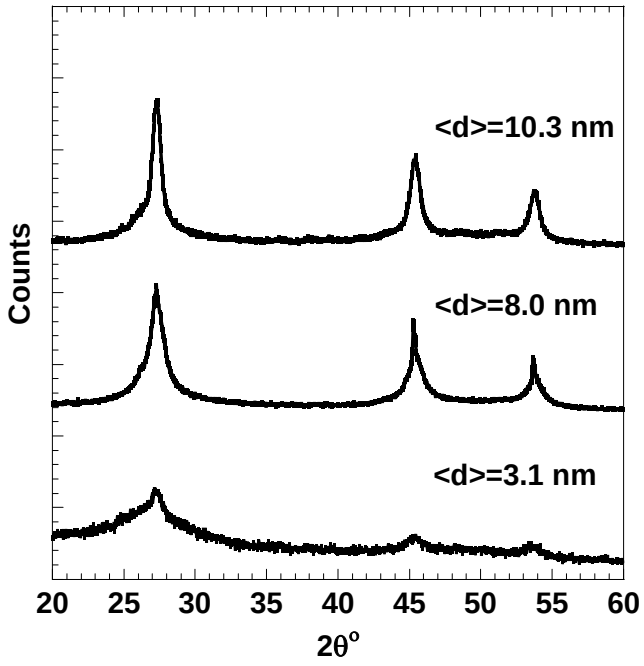

Figure 5.3 Powder XRD of three different Ge nanocrystal preparations with different average particle diameter. Each sample shows the characteristic {111}, {220} and {311} diffraction peaks for diamond cubic Ge. Increased peak broadening occurs for the smaller diameter nanocrystals. The FWHM of the {111} reflection is 2.58°, 1.0° and 0.78°, corresponding to Scherrer diameters of 3.1, 8.0 and 10.3 nm, which are consistent with the TEM measurements of 3.0, 8.1 and 11.6 nm, respectively.

EDS data (Figure 5.4) also confirmed the presence of Ge in the sample. In addition to Ge, small amounts of O, P and I are also observed by EDS. P is most likely from bound TOP and possibly trioctylphosphine oxide (TOPO), O could be from surface oxide or possibly TOPO, and I could be due to adsorbed precursor byproduct. Relative to the Ge signal, however, the intensity of O, P and I peaks are very low, indicating very small amounts of those species.

The FTIR spectrum in Figure 5.5 of 8.1 nm diameter Ge nanocrystals reveals three peaks at 2956, 2920, and 2854 cm^{-1} that correspond to C-H stretching modes for CH_2 and CH_3 groups, indicating that hydrocarbon species are present. The peaks at 1463 and 1378 cm^{-1} are also consistent with the CH_3 bending vibrations. The peaks ranging from 700 to 1100 cm^{-1} are very similar to the IR of TOP[27], consistent with the presence of TOP as a stabilizing ligand. Although FTIR does not provide definitive proof that organic ligands are bonded to the nanocrystal surface, the FTIR spectra are consistent with the presence of a hydrocarbon layer on the particle surface.

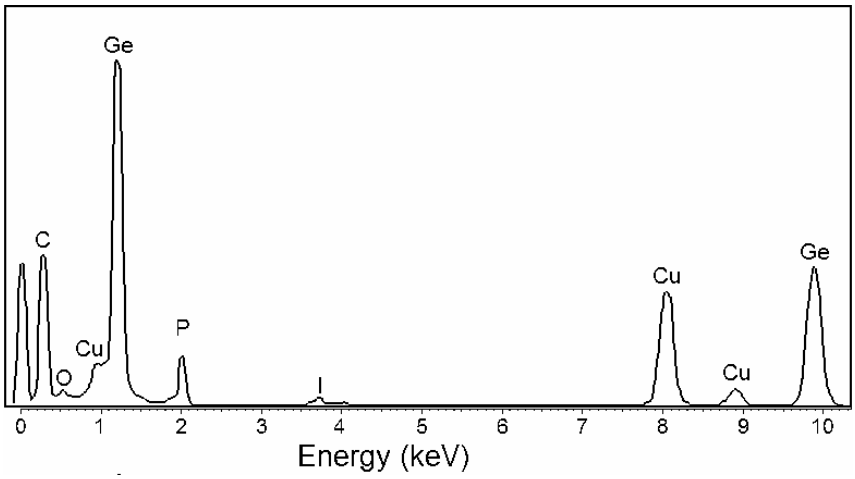

Figure 5.4 EDS spectrum obtained from the 11.6 nm Ge nanocrystals imaged by TEM in Figure 5.1E. The peaks at 1.2 and 9.8 keV correspond to the Lα and Kα lines of Ge. The copper and carbon peaks result from the copper TEM grid coated with carbon film.

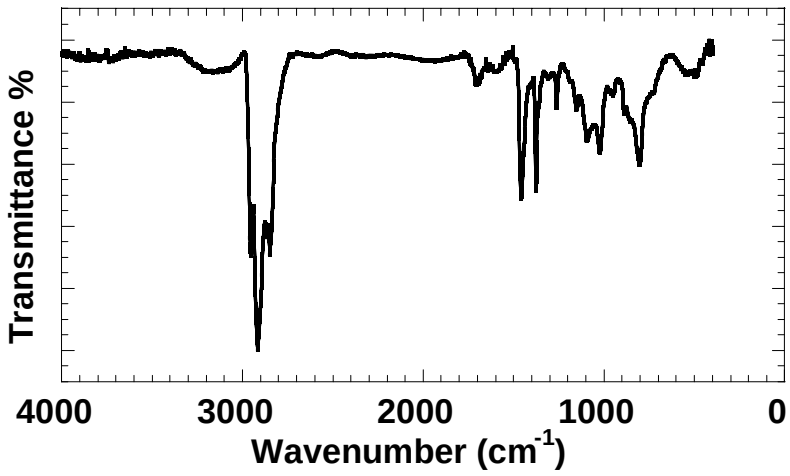

Figure 5.5 FTIR spectra of 8.1 nm Ge nanocrystals made from 260 mM GeI_2 in TOP at 300°C.

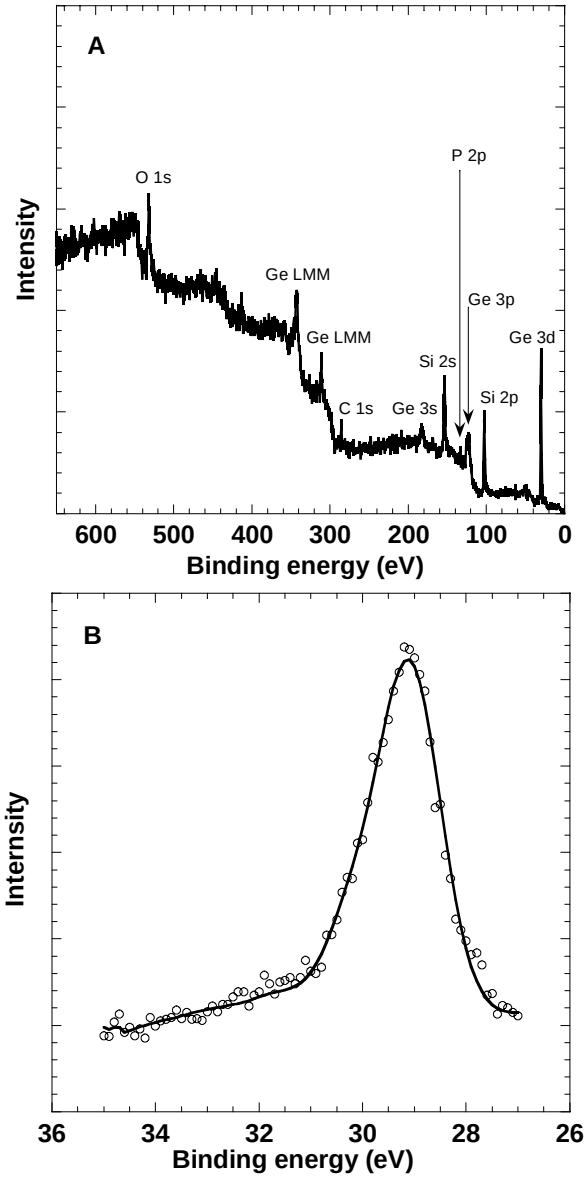

Figure 5.6 XPS spectra of 8.1 nm Ge nanocrystals. (A) Survey scan of the sample on Si substrate, the peaks of Si and O are from the substrate with an oxidation layer. (B) High resolution Ge 3d scan.

XPS was used to probe the extent of Ge nanocrystal surface oxidation. Like silicon, Ge is highly sensitive to oxidation. Various organic species have been studied as surface passivants for Ge that prevent or slow significantly surface oxidation, including alkenes, thiols and alkynes[28,29]. We are not aware of any studies that have examined TOP as a passivating ligand for Ge surfaces. XPS data was obtained from Ge nanocrystals drop cast from chloroform onto oxidized silicon substrates. Ge has signature peaks at 29.0 and 29.6 eV, attributed to $3d_{5/2}$ and $3d_{3/2}$, respectively[30]. Ge oxidation gives rise to satellite peaks associated with Ge^{1+}, Ge^{2+}, Ge^{3+} and Ge^{4+} oxidation states, each with an associated energy shift of 0.8, 1.8, 2.6 and 3.4 eV relative to the binding energy of 29.0 eV for Ge $3d_{5/2}$, respectively.[31] The native oxide of Ge, GeO_2, has a photoelectron peak maximum of 32.4 eV[30]. A low resolution scan for 8.1 nm Ge nanocrystals made from 260 mM GeI_2 in TOP at 300°C (Figure 5.6A) shows Ge 3d (29 eV) , 3p (123 eV), 3s (183 eV) and Ge LMM (311, 342 eV) peaks. Peaks at 130 eV and 285 eV correspond to P 2p and C 1s, indicating the presence of alkyl phosphines in the sample, which serve as the nanocrystal capping ligands in the synthesis. The absence of peaks from Al (2p 73 eV), I (3d 619 eV) and Li (1s, 55 eV) confirms minimal contamination from those species. Figure 5.6B shows a higher resolution XPS scan of the 3d Ge peak. Although the splitting of Ge 3d to $3d_{5/2}$ and

$3d_{3/2}$ was not well resolved, the peak centered at 29.2 eV was in good agreement with the expected value for elemental Ge. Barely noticeable photoelectron signals between 30.4 and 34.0 eV were observed, indicating that minimal surface oxidation occurs during the purification process.

5.3.2 Nanocrystal synthesis in TBP

TBP was also used as a coordinating solvent for synthesis of Ge nanocrystals from GeI_2. The reaction was carried out in TBP at lower temperature (240°C) due to its lower boiling point relative to TOP. Figure 5.7 shows a TEM image of Ge nanoparticles made from 130 mM GeI_2 in TBP with 65 mM $LiAlH_4$. The particles had an average diameter of 6.4 nm with a standard deviation of 55%. Compared to reactions in TOP with the same GeI_2 concentration, the Ge nanoparticles made in TBP exhibit larger average diameter (6.4 nm vs. 3.1 nm) with a broader size distribution (55% vs. 17%). This difference suggests that the higher steric barrier provided by the longer TOP alkyl chains offers better size control for Ge nanocrystals, similar to the case of CdSe nanoparticles synthesized in TBP and TOP[6].

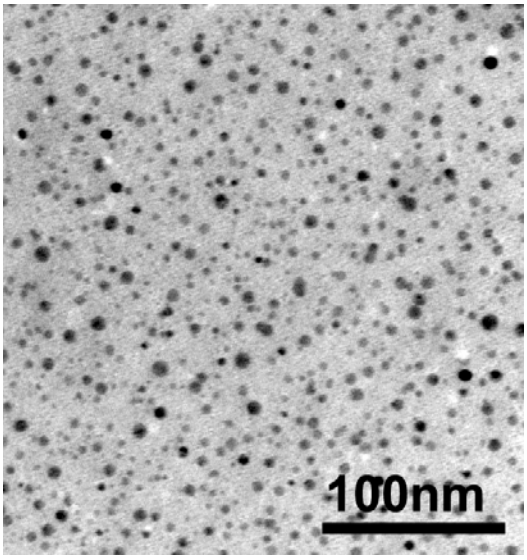

Figure 5.7 LRTEM of Ge nanocrystals with diameter of 6.4±3.5 nm made from 130 mM solution of GeI_2 in TBP at 240°C.

5.4 DISCUSSION

5.4.1 Ge precursor chemistry

$LiAlH_4$ reduction of GeI_2 in TOP at 300°C gives high chemical yields of Ge nanocrystals. To put these results in perspective, we have summarized in Table 5.1 other solution-phase synthetic methods for Ge nanocrystals from the literature. Compared to the widely used Ge(IV) precursors, GeX_4 (X=Cl, Br and I) and organogermanes, GeI_2 offers various advantages. First, the formation of the complex $(GeI_2)\cdot TOP$ makes GeI_2 highly soluble in TOP, up to a concentration of 0.5 M GeI_2 at room temperature. In contrast, the solubility of GeI_4 in hydrocarbon solvents is fairly low. The high Ge precursor concentration produces a large supersaturation of Ge atoms in the initial stages of the reaction to produce a high particle nucleation rate. The high nucleation rate is desirable for the potential formation of small crystals with low polydispersity. Second, the high boiling point of GeI_2 facilitates reactions at ambient pressure even at high temperatures, which favors the formation of elemental Ge. Attempts have been tried by many research groups to make Ge nanoparticles by reduction of $GeCl_4$ with $LiAlH_4$. However, the low boiling point of $GeCl_4$ (83°C) limits the reaction

temperature under atmospheric pressure and the highly corrosive by-products (*e.g.* HCl) can be undesirable. Most significantly, $LiAlH_4$ reduction of $GeCl_4$ at low temperature (<80°C) yields mostly GeH_4 and oligomeric germanes of Ge_xH_{2x+2} (such as Ge_5H_{12}, Ge_7H_{16}, etc.), instead of Ge[32,33], which can limit the Ge nanocrystal yield significantly. Although reduction of GeI_2 with $LiAlH_4$ may also form Ge_xH_{2x+2} species, they will decompose to elemental Ge and hydrogen at the higher reaction temperature (~300°C)[32]. GeI_2 is also easier to reduce to Ge than GeX_4. At 25°C, the reduction potential of Ge(II) to Ge(0) is greater than that of Ge(IV) to Ge(0) (0.247 vs. 0.124 eV) [21,34]. Furthermore, GeI_2 disproportionates to Ge and GeI_4 even without the presence of reducing agent at ~330°C. This high reactivity of GeI_2 enables a high chemical yield of Ge nanocrystals.

Ge precursor	Reducing agent	Temperature	Stabilizer	solvent	Reference
$GeCl_4$	NaK alloy	270°C	$RMCl_3$ (M=Si/Ge)	Heptane	Ref #9
$GeCl_4$	$Li[C_{10}H_8]$	Room T	CH_3SiCl	Tetrahydrofuran	Ref #10
GeX_4*	$LiAlH_4$	Room T	micelle	Octane	Ref #11
$GeCl_4$	NaGe/KGe/Mg_2Ge		Glyme/diglyme	Glyme/diglyme	Ref #12-15
GeI_4	$LiAlH_4$		n-alkene	Tetrahydrofuran	Ref #16
TEG*	Thermal reduction	400°C	Organic molecules	Hexane	Ref #17
TEG/DPG*	Thermal reduction	400-500°C	Octanol	Hexane	Ref#18-19
TEG/DPG*	Thermal reduction	500°C	Octanol	Supercritical CO_2	Ref# 20
$Ge[N(SiMe_3)_2]_2$	Thermal reduction	300°C	Oleylamine	Octadecene	Ref #21
GeI_2	$LiAlH_4$	300°C	TOP	TOP	This study

*X=Cl,Br or I; TEG=tetraethylgermane; DPG=diphenylgermane

Table 5.1 Summary of synthetic approaches for production of Ge nanocrystals in solution; only Refs. 14, 21, 22 and this study report yield.

Although the reaction mechanism for reduction of GeI_2 by $LiAlH_4$ in the presence of alkyl phosphines is not fully characterized, the following possible reactions are likely present: GeI_2 disproportionation to GeI_4 and Ge; GeI_2 reduction to Ge by $LiAlH_4$; and GeI_4 reduction to Ge or Ge(II) by $LiAlH_4$. The major by-products of those reactions are iodides, including LiI and AlI_3. EDS of the Ge nanocrystal product revealed only a limited presence of I, indicating that most of the iodide contaminants are removed in the purification step as expected: LiI is soluble in acetone and AlI_3 is not soluble in chloroform.

Approaches to control the Ge nanocrystal size include inverse micelles as templates[11,22] and covalent bonding of hydrocarbons with reactive functional groups[12,17,18]. In the later case, the possibility of forming long chain Ge compounds with polymerized hydrocarbon groups at high reaction temperature (>400°C) may in part account for the low yield of nanoparticles. In addition, hydrocarbon decomposition can occur at these temperatures, leading to oligomeric byproducts that can be very difficult to separate from the nanocrystals. An alternative approach is to minimize hydrocarbon decomposition byproducts by synthesizing Ge at 500°C in the chemically inert solvent, supercritical CO_2, which is capable of solvating octanol as a

capping ligand at this high temperature[20]. However, the particle sizes were significantly larger than in the present study.

Although TOP is one of the most commonly used coordinating solvents in the synthesis of colloidal Group II-VI semiconductor nanocrystals (e.g. CdSe[6]), this is the first report where it has been employed as a solvent to synthesize Ge nanoparticles. Since the reduction of GeI_2 with $LiAlH_4$ was conducted at a mild temperature (~300°C), the formation of hydrocarbon free radicals, which would lower the yield of nanoparticles by competing with Ge homogeneous nucleation to form organogermane oligomers, was minimized if not completely avoided. The mechanism for the passivation of the particles in this study is unknown, but would be influenced by the known coordination of TOP with GeI_2 to form the $(GeI_2)\cdot$TOP complex during reaction[32].

5.4.2 Ge nanocrystal growth

Colloidal nanocrystal formation involves two steps: nucleation, which relieves the excess free energy of the supersaturated solution, followed by particle growth. To achieve monodisperse size distributions, the nucleation and growth steps must be temporally separated to ensure that new nuclei are not forming during the growth stage[19,35,36]. Once nucleated, the particles may grow by either (1) reactant diffusion-limited growth with Ge atom

condensation on existing particles or (2) aggregation of existing particles. To determine which of these growth mechanisms is dominant in Ge nanocrystal synthesis, a similarity transformation technique was used to analyze the moments of the size distribution of the nanoparticles. This analysis of particle size distributions, developed by Friedlander *et al.*[37,38] to study the growth mechanism of aerosol particles, was extended recently by Shah *et al.*[39] to analyze the growth mechanism of colloidally-grown silver nanocrystals in supercritical carbon dioxide. At relatively long times after particle nucleation, the size distribution becomes independent of the initial nucleation event and will reflect the particle growth mechanism. The two growth mechanisms of condensation and aggregation may be in competition, with condensation narrowing the size distribution at long times and aggregation broadening it[40]. The extent to which aggregation and condensation control particle growth can be determined by examining the moments of the size distribution function $\mu_1 = r_3 / r_h$ and $\mu_3 = r_1 / r_3$, where r_1 is the arithmetic mean radius defined as $r_1 = \sum r_i / N_\infty$; r_3 is the cubic mean radius defined as $r_3 = (\sum r_1^3 / N_\infty)^{1/3}$; and r_h is the harmonic mean radius defined as $r_h = N_\infty / (\sum 1/r_i)$. For a monodisperse sample, $r_1 = r_3 = r_h$ and

$\mu_1 = \mu_3 = 1$. Significant deviations from 1, with $\mu_1 > 1.25$ and $\mu_3 < 0.905$, indicate that particles grow primarily by aggregation.

For the analysis, the total number of particles N_∞, were obtained by integrating the experimental size distributions determined by TEM, as a function of particle volume (i.e., $v_i = (4/3)\pi \cdot r_i^3$):

$$N_\infty = \int_0^\infty n(v)dv \qquad (5.1)$$

$n(v)$ is the number concentration of particles with volume between v and $v + dv$. Table 5.2 summarizes the calculated values of μ_1 and μ_3 of the Ge nanocrystals. For the three different nanocrystal preparations, both μ_1 and μ_3 are close to unity, indicating that the nanocrystals grow primarily by condensation (Table 5.2). The high concentration of passivating ligand TOP limits particle aggregation, as well as other factors in the reaction mechanism that favor growth by condensation. Upon the rapid introduction of $LiAlH_4$ into the GeI_2 solution at 120°C, germanes Ge_xH_{2x+2} and high supersaturation of elemental Ge are formed to produce rapid nucleation rates. With increasing temperature, more Ge atoms are supplied to the nuclei by

decomposition of $Ge_xH_{2x+2,}$ which sustains the growth of the nanoparticles by condensation.

5.5 CONCLUSIONS

High chemical yields up to 73% (mol recovered Ge/mol initial GeI_2, without including the weight of the capping ligands) of Ge nanocrystals, with sizes ranging from 3 to 11 nm, have been synthesized by reducing GeI_2 with $LiAlH_4$ in TOP at 300°C and in TBP at 240°C. The weight of ligands on the surface was unknown, but a full monolayer would change the total weight by less than 10% based on the short length of the ligands. The particle size increased monotonically with increased GeI_2 precursor concentration. 95 mg quantities of high quality Ge nanocrystals were obtained, and the simple batch process is suitable for scale-up to produce larger quantities. The high yield is due to a combination of advantages compared with previous syntheses including the higher reactivity of Ge(II) versus Ge(IV), high solubility of $(GeI_2)\cdot R_3P$ complexes, the lower concentration of byproducts and solvent degradation due to moderate temperatures, the lack of organic impurity atoms in the precursor, and passivation of the surface with TOP ligands. Reaction in TBP produced larger nanoparticles with much broader size distribution than TOP for a given concentration of GeI_2, presumably due to weaker steric

stabilization by the shorter alkyl chain of TBP. The moments of the size distribution of the Ge nanoparticles synthesized in TOP indicate condensation controlled growth. This result is consistent with the observation of single crystals by HRTEM and XRD and the moderate polydispersity. FTIR and XPS spectra of the nanoparticles showed the presence of hydrocarbon groups and the limited oxidation of the particles. Together, these results indicated that the TOP and TBP coated the surfaces of the particles to provide passivation against coagulation and oxidation.

particle diameter	μ_1	μ_3
3.0 nm	1.09	0.96
8.1 nm	1.07	0.97
11.6 nm	1.08	0.96

Table 5.2 Calculated moments of the size distribution for Ge nanocrystals synthesized in TOP.

5.6 REFERENCES

(1) Heath, J. R. *Chem. Soc. Rev.* **1998**, *27*, 65.

(2) Alivisatos, A. P. *Science* **1996**, *271*, 933.

(3) Sigman, M. B., Jr.; Saunders, A. E.; Korgel, B. A. *Langmuir* **2004**, *20*, 978.

(4) Saunders, A. E.; Sigman, M. B., Jr.; Korgel, B. A. *J. Phys. Chem. B* **2004**, *108*, 193.

(5) Son, S. U.; Jang, Y.; Yoon, K. Y.; Kang, E.; Hyeon, T. *Nano Lett.* **2004**, *4*, 1147.

(6) Murray, C. B.; Norris, D. J.; Bawendi, M. G. *J. Am. Chem. Soc.* **1993**, *115*, 8706.

(7) Stowell, C. A.; Wiacek, R. J.; Saunders, A. E.; Korgel, B. A. *Nano Lett.* **2003**, *3*, 1441.

(8) Holmes, J. D.; Ziegler, K. J.; Doty, R. C.; Pell, L. E.; Johnston, K. P.; Korgel, B. A. *J. Am. Chem. Soc.* **2001**, *123*, 3743.

(9) Heath, J. R.; Shiang, J. J.; Alivisatos, A. P. *J. Chem. Phys.* **1994**, *101*, 1607.

(10) Kornowski, A.; Giersig, M.; Vogel, R.; Chemseddine, A.; Weller, H. *Adv. Mater.* **1993**, *5*, 634.

(11) Wilcoxon, J. P.; Provencio, P. P.; Samara, G. A. *Phys. Rev. B* **2001**, *64*, 035417.

(12) Taylor, B. R.; Kauzlarich, S. M.; Delgado, G. R.; Lee, H. W. H. *Chem. Mater.* **1999**, *11*, 2493.

(13) Tanke, R. S.; Kauzlarich, S. M.; Patten, T. E.; Pettigrew, K. A.; Murphy, D. L.; Thompson, M. E.; Lee, H. W. H. *Chem. Mater.* **2003**, *15*, 1682.

(14) Taylor, B. R.; Fox, G. A.; Hope-Weeks, L. J.; Maxwell, R. S.; Kauzlarich, S. M.; Lee, H. W. H. *Mater. Sci. Eng. B-Solid State Mater. Adv. Technol.* **2002**, *96*, 90-93.

(15) Taylor, B. R.; Kauzlarich, S. M.; Lee, H. W. H.; Delgado, G. R. *Chem. Mater.* **1998**, *10*, 22-24.

(16) Fok, E.; Shih, M.; Meldrum, A.; Veinot, J. G. C. *Chem. Commun.* **2004**, 386.

(17) Gerion, D.; Zaitseva, N.; Saw, C.; Casula, M. F.; Fakra, S.; Van Buuren, T.; Galli, G. *Nano Lett.* **2004**, *4*, 597.

(18) Lu, X.; Ziegler, K. J.; Ghezelbash, A.; Johnston, K. P.; Korgel, B. A. *Nano Lett.* **2004**, *4*, 969.

(19) Myung, N.; Lu, X.; Johnston, K. P.; Bard, A. J. *Nano Lett.* **2004**, *4*, 183.

(20) Lu, X.; Korgel, B. A.; Johnston, K. P. *Nanotechnology* **2005**, *16*, S389.

(21) Gerung, H.; Bunge, S. D.; Boyle, T. J.; Brinker, C. J.; Han, S. M. *Chem. Commun.* **2005**, 1914.

(22) Wang, W. Z.; Huang, J. Y.; Ren, Z. F. *Langmuir* **2005**, *21*, 751-754.

(23) Newman, R. C.; Wake-field, J. *Solid State Phys. Electron. Telecomm., Proc.* **1960**, *1*, 160.

(24) Launay, J. C.; Debegnac, H.; Zappoli, B.; Mignon, C. *J. Cryst. Growth* **1988**, *92*, 323.

(25) Wu, Y.; Yang, P. *Chem. Mater.* **2000**, *12*, 605.

(26) King, R. B. *Inorg. Chem.* **1963**, *2*, 199.

(27) Pouchert, C. J. *The Aldrich Library of FT-IR spectra*; 2nd ed. Milwaukee, Wis., 1997.

(28) Hanrath, T.; Korgel, B. A. *J. Am. Chem. Soc.* **2004**, *126*, 15466.

(29) Choi, K.; Buriak, J. M. *Langmuir* **2000**, *16*, 7737.

(30) Oh, J.; Campbell, J. C. *J. Electron. Mater.* **2004**, *33*, 364.

(31) Schmeisser, D.; Schnell, R. D.; Bogen, A.; Himpsel, F. J.; Rieger, D.; Landgren, G.; Morar, J. F. *Surf. Sci.* **1986**, *172*, 455-465.

(32) Stone, F. G. A. *Hydrogen Compounds of Group IV Elements*; Prentice Hall, Inc., Englewood Cliffs, NJ, 1962.

(33) Macklen, E. D. *J. Chem. Soc.* **1959**, 1984.

(34) Galus, Z. *Stand. Potentials Aqueous Solution* **1985**, 189.

(35) Murray, C. B.; Kagan, C. R.; Bawendi, M. G. *Annu. Rev. Mater. Sci.* **2000**, *30*, 545.

(36) Burda, C.; Chen, X. B.; Narayanan, R.; El-Sayed, M. A. *Chem. Rev.* **2005**, *105*, 1025.

(37) Yu, W. W.; Falkner, J. C.; Shih, B. S.; Colvin, V. L. *Chem. Mater.* **2004**, *16*, 3318.

(38) Swift, D. L.; Friedlander, S. K. *J. Coll. Sci.* **1964**, *19*, 621.

(39) Friedlander, S. K.; Wang, C. S. *J. Colloid Inter. Sci.* **1966**, *22*, 126.

(40) Shah, P. S.; Husain, S.; Johnston, K. P.; Korgel, B. A. *J. Phys. Chem. B* **2001**, *105*, 9433.

(41) Watzky, M. A.; Finke, R. G. *J. Am. Chem. Soc.* **1997**, *119*, 10382.

Chapter 6: High Yield Solution-Liquid-Solid Synthesis of Germanium Nanowires*

6.1 INTRODUCTION

Research in semiconductor nanowires has been fueled by their unique optical, electronic, and mechanical properties and their potential use in optoelectronic devices, chemical and biological sensors, computing devices, and photovoltaics[1]. Semiconductor nanowires have been synthesized under a wide range of conditions, from high temperature (<1100°C) gas-phase reactions[1,2] to relatively low temperature (>250°C) solution-phase conditions[1,3-5]. Solution-phase routes to semiconductor nanowires are particularly interesting due to their potential for good size and shape control, chemical surface passivation, colloidal dispersibility, and high throughput continuous processes.

Nanocrystals and nanowires of Group IV materials, such as C, Si and Ge, have been extremely challenging to synthesize in solution due to their

* Portions of this chapter have been previously published as Lu, Xianmao; Fanfair, Dayne D.; Johnston, Keith P.; Korgel, Brian A., *J. Am. Chem. Soc.*, **2005**, *127*, 15718-15719. Copyright 2005 American Chemical Society.

high crystallization energy barrier, and the propensity of those elements to form stable oligomeric species with hydrocarbons. In the past, our approach to crystalline Si[6] and Ge nanowires[7] and multiwall carbon nanotubes[8] has been to use supercritical solvents that are heated well above their boiling points to temperatures between 350°C and 650°C by pressurization. These temperatures exceed the decomposition temperatures of organosilane and organogermane precursors and the Au:Si and Au:Ge eutectic temperatures (~360°C), making it possible to promote Au nanocrystal-seeded nanowire growth.[9] Although very high quality nanowires are obtained, it would be more desirable to synthesize crystalline nanowires under milder conditions to alleviate solvent decomposition and safety concerns.

In this chapter, solution-liquid-solid synthesis of crystalline Ge nanowires with high yield is reported. Bi nanocrystals are used as seeds to promote nanowire growth in trioctylphosphine (TOP) from decomposing GeI_2 at ~350°C. This is the first example of a Group IV nanowire synthesis in a conventional solvent under atmospheric pressure.

The low melting metal Bi, forms a eutectic with Ge at 271.4°C (Figure 6.1)[10], which is well within the temperature window for conventional solvents. Buhro[4] first showed that Bi nanocrystals could seed SLS growth of CdSe

nanowires, which Fanfair and Korgel[5] later extended to Group III-V nanowire synthesis. Based on the Bi:Ge phase diagram, Bi is also a good candidate for Ge nanowire synthesis. Ge nanowire synthesis in a conventional solvent also requires a precursor that is sufficiently reactive at ~350°C. We recently identified GeI_2 as an effective precursor for Ge nanocrystal synthesis at 300°C in TOP, with high yields and minimal organic contamination.[11]

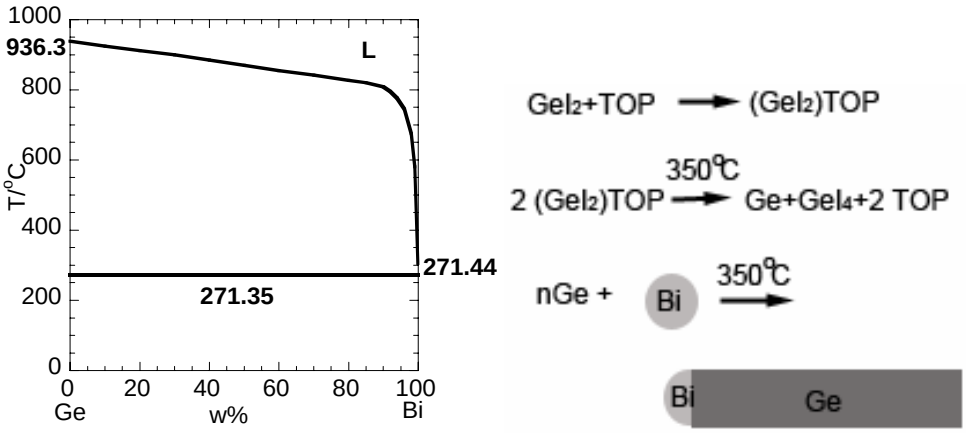

Figure 6.1 Binary phase diagram of Ge-Bi and Ge nanowire growth mechanism.

6.2 EXPERIMENTAL

6.2.1 Ge nanowire synthesis

Ge nanowires were synthesized under nitrogen in a three-neck flask on a Schlenk line. GeI_2 (Strem Chemicals, packed under argon) were stored in a nitrogen-filled glovebox upon purchase. Tri-n-octylphosphine (Tech. grade, Aldrich) was degassed through a freeze-pump-thaw technique and distilled at 200°C and 0.3 Torr. All other solvents were used as received from Fisher Scientific without further purification. A precursor solution of 0.3 M GeI_2 in TOP was prepared by adding 0.2 g GeI_2 into 2 ml TOP in the glovebox. A clear yellow solution was formed after stirring for 1 hr. Bi nanocrystals were prepared following the procedure described in ref #15. 0.6 mg Bi nanoparticles were mixed with 0.5 ml TOP and sonicated for 2 hrs to form a grey dispersion. 0.5ml Bi nanoparticle dispersion and desired volume of GeI_2 solution in TOP (0.8 ml for GeI_2 to Bi mole ratio of 80:1, 0.5 ml for a ratio of 50:1) were loaded into a 3 ml plastic syringe. 4 ml TOP was loaded into a 3-neck flask and heated to 365°C under N_2, followed by the injection of the GeI_2 and Bi nanocrystal solution through a rubber septum with stirring. The introduction of the precursor and growth seeds immediately produced a gray solution. The temperature dropped down to 350°C and the reaction was

allowed to proceed at 350°C for 10 min before taking the reaction flask off the heating mantle and allowing it to cool to room temperature. The nanowire dispersions were diluted with 10 mL toluene and centrifuged at 8,000 rpm for 5 min. The nanowires in the black precipitate were redispersed in 2.5 ml $CHCl_3$ and precipitated with 2.5 ml ethanol and centrifuged again to obtain a purified nanowire product. Nanowires were dried with a rotary evaporator and stored under nitrogen prior to characterization.

6.2.2 Materials characterization

The nanocrystals were characterized by scanning electron microscopy (SEM), transmission electron microscopy (TEM), energy-dispersive X-ray spectroscopy (EDS) and powder X-ray diffraction (XRD). SEM samples were prepared by drop casting chloroform-dispersed nanowires onto Si substrates. SEM was performed on a LEO 1530 field emission gun SEM, operating at 10 kV accelerating voltage, and digital SEM images were acquired using an inlens detector and LEO 32 software system. TEM specimens were prepared by drop casting dilute dispersions of nanowires after washing with 5% HCl acid for 5 min onto 200-mesh copper grids coated with lacy carbon film (Ladd Research Co.). High resolution TEM (HRTEM) was performed on a JEOL 2010F TEM; images were obtained digitally with a

GATAN digital photography system. EDS was performed on the JEOL 2010F HRTEM equipped with an Oxford spectrometer. X-ray diffraction (XRD) was obtained from ~2 mg nanowires deposited by drop casting on quartz slides (Gem Dugout, State College, PA) with continuous scan for 3 hours at a rate of 12°/min and 0.02° per step using a Bruker-Nonius D8 Advance powder diffractometer with Cu K_α radiation (λ=1.54 Å) and a rotary sample stage (30rpm).

6.3 RESULTS

Figure 6.2 shows Ge nanowires produced by injecting GeI_2 along with sterically-stabilized 20 nm diameter Bi nanocrystals into TOP at 365°C on a Schlenk line. The Bi nanocrystals were synthesized by room temperature reduction of bismuth ethylhexanoate ($Bi[OOCCH\text{-}(C_2H_5)C_4H_9]_3$) in dioctylether in the presence of TOP as described in Ref. 5. TOP serves as a capping ligand that prevents significant nanocrystal aggregation but does not interfere with nanowire growth. After injecting the precursor/nanocrystal mixture swiftly into pre-heated TOP at 365°C, the reaction vessel was stirred for 10 min at 350°C. The resulting black precipitate of nanowires was washed with toluene, chloroform and ethanol. The best Ge nanowire product was obtained using a GeI_2:Bi mole ratio of 80:1. SEM of the reaction

product synthesized from GeI_2 and Bi nanoparticles in TOP at 350°C showed a large amount of nanowires (Figure 6.2). The wires were long and generally straight, ranging in diameter from 20 to 150 nm with an average of ~50 nm, with aspect ratios exceeding 100. The average length of the nanowires is greater than 5 μm and many are longer than 10 μm. The relatively broad diameter distribution is primarily the result of the Bi nanocrystals used to seed the reaction—although the Bi nanocrystals were relatively size-monodisperse to begin with, Bi nanocrystals are notoriously difficult to stabilize and aggregate quickly during the nanowire synthesis, leading to a broad nanowire diameter distribution. The product was nearly free of contaminants and the Ge nanowire reaction yield is very high: 7.5 mg of pure Ge nanowires were obtained in a typical reaction with 0.6 mg Bi nanoparticles and 75 mg GeI_2 in 5 ml TOP, corresponding to a yield of ~40%. Bi particles could be observed at the ends of some Ge nanowires, as shown in Figure 6.2C. Energy-dispersive X-ray spectroscopy (EDS) mapping of the observed confirmed that the particles are composed of Bi (SI-2). At a lower GeI_2:Bi ratio (GeI_2:Bi=50:1), both straight and tortuous wires were observed (Figure 6.1D)—the tortuous wires have a similar average diameter but shorter length (<1μm).

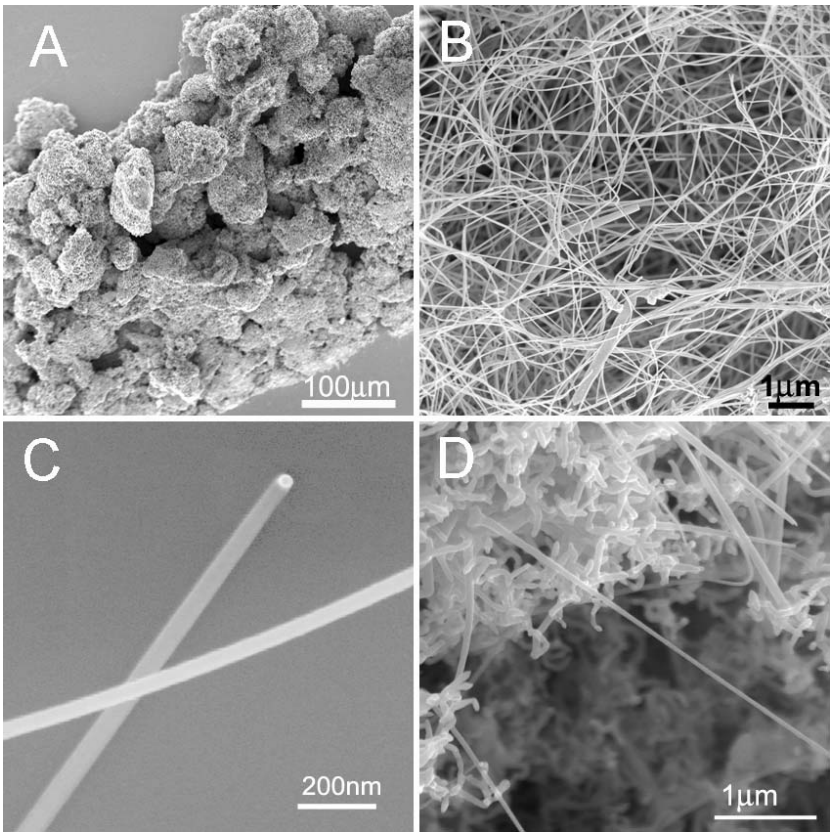

Figure 6.2 (A,B,C) SEM images of Ge nanowires made from GeI_2 in TOP at 350°C with Bi nanocrystals as growth seeds (GeI_2:Bi=80:1 n:n). SEM reveals a high yield of high quality Ge nanowires with an average diameter of 50 nm. (C) A representative Ge nanowire shows a Bi nanoparticle at its tip. (D) Ge nanowires synthesized at a lower mole ratio of GeI_2 to Bi of 50:1 (n:n) were of lower quality.

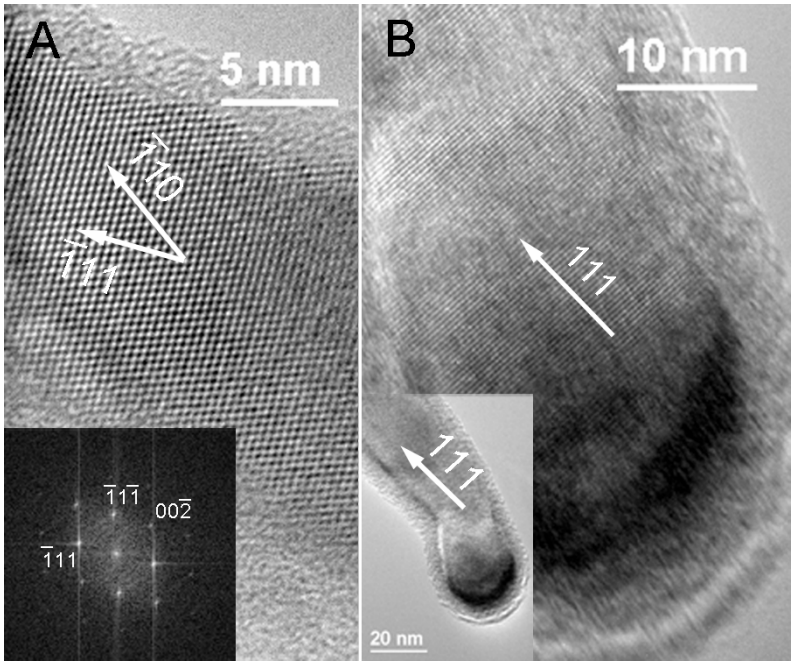

Figure 6.3 High resolution TEM images of the Ge nanowires. (A) A 15 nm nanowire with <111> growth direction. (Inset) FFT indicates the nanowire was imaged down the [110] zone axis. The forbidden spot of $[\,00\bar{2}\,]$ is from double diffraction of $[\,\bar{1}\,1\,\bar{1}\,]$ and $[\,1\,\bar{1}\,1\,]$. (B) Ge nanowire with a tip showing presence of Bi by EDS analysis. (Inset) A lower magnification TEM image of the wire with <111> growth direction.

High resolution transmission electron microscopy (HRTEM) (Figure 6.3) and X-ray diffraction (XRD) (Figure 6.4) both confirmed that the nanowires were crystalline diamond cubic Ge. Figure 6.3 shows two nanowires imaged by TEM: the nanowire growth direction was predominantly <111>, as seen here. A small number of nanowires (~10% of the sample) exhibited <110> growth direction (SI-1). A mixture of <111> and <110> growth direction is similar to what has been observed for Ge nanowires synthesized in supercritical solvents.[7,12] The straight Ge nanowires are single crystals, nearly free of extended defects. The XRD pattern in Figure 6.4 exhibits diffraction peaks corresponding to the {111}, {220}, {311} reflections of diamond cubic Ge. A small amount of GeO_2 can also be observed in the XRD pattern, which is consistent with TEM images that showed the nanowire surfaces to be oxidized.

6.4 DISCUSSIONS

Figure 6.1 outlines the nanowire growth mechanism. Two key aspects of the chemistry enable the production of crystalline Ge nanowires in TOP: (1) the low temperature Bi:Ge eutectic at ~270°C and (2) the highly reactive organic-free Ge precursor, GeI_2. GeI_2 disproportionates to Ge and GeI_4 with relatively high chemical yield at temperatures greater than

~330°C—far below its boiling point at 550°C and the boiling point of many widely used solvents, *e.g.* Tri-n-octylphosphine (TOP). GeI_2 also forms a very soluble complex of

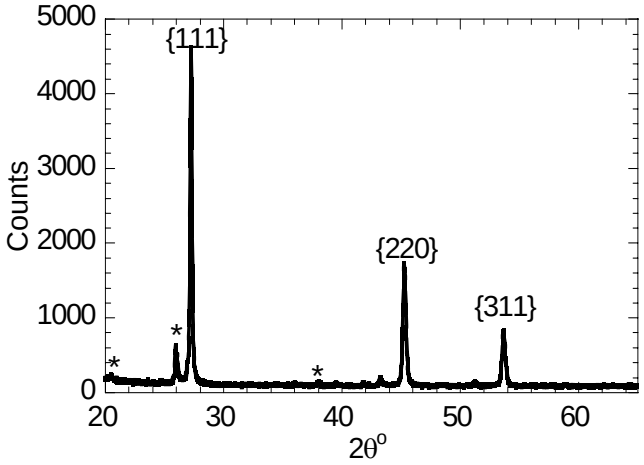

Figure 6.4 XRD of Ge nanowire shows diamond cubic crystal structure of Ge with {111}, {220} and {311} peaks. The peaks labeled with * are from hexagonal GeO_2.

(GeI_2)•R_3P,[13] when mixed with TOP, which dissociates at 120°C, making it an ideal precursor for SLS Ge nanowire synthesis. Control experiments where GeI_2 was injected without Bi nanocrystals into TOP at 365°C showed Ge nanoparticle formation in just 5 min, indicating rapid homogeneous GeI_2 decomposition. With Bi present in the concentrations used for nanowire synthesis, Ge nanoparticles were not observed. Although small Ge clusters may nucleate homogeneously, their interfacial free energy is greatly lowered by incorporation into the much larger 20 nm Bi particles. Heterogeneous GeI_2 decomposition on the Bi seed particle surface could also occur.

It should be possible to extend the approach to Si, as Bi:Si also have a eutectic temperature at ~270°C. The key to Si nanowire synthesis will be the identification of a suitable reaction pathway to produce a high yield of Si from molecular precursors at temperatures below 350°C. In addition to Bi, other low melting metals, such as In (156°C)[3] and Sn (231°C)[14], form liquid alloys with Ge/Si at mild temperatures, making them promising candidates for group IV nanowire growth seeds as well.

6.6 REFERENCES

(1) Law, M.; Goldberger, J.; Yang, P. D. *Ann. Rev. Mater. Res.* **2004**, *34*, 83.

(2) Hu, J. T.; Odom, T.W.; Lieber, C. M. *Accts. Chem. Res.* **1999**, *32*, 435.

(3) Trentler, T. J.; Hickman, K.M.; Goel, S.C.; Viano, A.M.; Gibbons, P.C.; Buhro, W.E. *Science* **1995**, *270*, 1791.

(4) Yu, H.; Li, J. B.; Loomis, R. A.; Gibbons, P. C.; Wang, L. W.; Buhro, W. E. *J. Am. Chem. Soc*. **2003**, *125*, 16168.

(5) Fanfair, D. D.; Korgel, B. A. *Crystal Growth & Design* **2005**, *5*, 1971.

(6) Holmes, J. D.; Johnston, K. P.; Doty, R. C.; Korgel, B. A. *Science* **2000**, *287*, 1471.

(7) Hanrath, T.; Korgel, B. A. *J. Am. Chem. Soc*. **2002**, *124*, 1424.

(8) Lee, D. C.; Mikulec, F. V.; Korgel, B. A. *J. Am. Chem. Soc.* **2004**, *126*, 4951.

(9) Shah, P. S.; Hanrath, T.; Johnston, K. P.; Korgel, B. A. *J. Phys. Chem. B* **2004**, *108*, 9574.

(10) Olesinski, R. W.; Abbaschian, G. J. *Metal Progress* **1985**, *128*, 55.

(11) Lu, X.; Korgel, B. A.; Johnston, K. P. *Chem. Mater.* **2005**, 17, 6479.

(12) Hanrath, T.; Korgel, B.A. *Small* **2005**, *1*, 717.

(13) King, R. B. *Inorg. Chem*. **1963**, *2*, 199.

(14) Gao, P. X.; Ding, Y.; Wang, Z. L. *Nano Lett*. **2003**, *3*, 1315.

Chapter 7: Conclusions and Recommendations

7.1 CONCLUSIONS

7.1.1 Synthesis of Si nanowires on substrate

7 nm Au nanocrystals were used to grow single crystal Si nanowires on a substrate in supercritical cyclohexane. By degrading diphenylsilane (DPS) at a temperature and pressure above the critical point of cyclohexane[1], Si dissolves in the Au nanocrystals and subsequently crystallizes in the form of wires. The nanowire diameter reflects the gold nanocrystal diameter, ranging from 5 to 30 nm, with lengths of several micrometers. Both batch and flow reactors were used. The flow reactor minimized the undesirable deposition of Si particulates formed in the bulk solution. A kinetic analysis of the process explains the dependence of the nanowire morphology on the reaction conditions qualitatively. The ability to manipulate the precursor concentration, the seed particle concentration and size provides great flexibility in controlling the nanowire morphology.

7.1.2 Synthesis of Ge nanocrystals in SCFs

Ge nanocrystals with various sizes of 2-70 nm in diameter were synthesized in supercritical hexane at 400~550^{o}C and 20.7 MPa in a flow reactor by thermolysis of DPG or TEG in the presence of octanol. The nanocrystals were characterized by HRTEM, EDS, FTIR spectroscopy and XRD. Relatively size-monodisperse nanocrystals could be produced, with standard deviations about the mean diameter as low as ~10%. Blue-shifted UV-visible absorbance and PL spectra of Ge nanocrystals in the 3 to 4 nm diameter size range were observed, with a PL quantum yield of up to 6.6%.

7.1.3 Synthesis of Ge nanocrystals in sc-CO_2

By using the same Ge precursors, DPG or TEG, Ge nanocrystals were also synthesized in supercritical (sc) CO_2 at 500^{o}C and 27.6 MPa with octanol as the capping ligand. On the basis of TEM, the mean diameters of the nanocrystals made from DPG and TEG were 10.1 and 5.6nm, respectively. Much less organic contamination was observed for the nanoparticles synthesized in sc-CO_2 than those made in organic supercritical fluids. Bulk Ge crystals instead of nanocrystals were formed when the same reaction of DPG with octanol was performed in the gas phase without CO_2 present, indicating that the solvation of the hydrocarbon ligands by CO_2 was sufficient

to provide steric stabilization. The presence of steric stabilization in CO_2 may be attributed to a reduction in the differences between ligand-ligand interactions and ligand-CO_2 interactions relative to thermal energy.

7.1.4 Synthesis of Ge nanocrystals with GeI_2

To increase the yield of nanoparticles, a new Ge precursor, GeI_2 was utilized to synthesize Ge nanocrystals in conventional solvents, TOP or TBP, with the reducing agent $LiAlH_4$. High chemical yields, up to 73%, and moderate size polydispersity were achieved for the reaction in TOP at 300°C. High chemical yields are enabled by the high reactivity of GeI_2, high GeI_2 solubility in alkyl phosphines and relatively mild reaction temperature, which minimizes byproduct formation and solvent degradation. FTIR spectra revealed the presence of alkyl groups in the Ge nanocrystals. The small and controllable particle diameters and lack of significant Ge oxidation revealed by XPS indicate that the nanocrystals were chemically passivated with an organic layer.

7.1.5 Synthesis of Ge nanowires with GeI_2

To further take advantage of the chemistry of GeI_2, Ge nanowires were synthesized with GeI_2 and Bi nanocrystals in TOP at 350°C and atmospheric

pressure. This is the first example of group IV semiconductor nanowires synthesized in a conventional solvent. Two key aspects of the chemistry enable the production of crystalline Ge nanowires in TOP: (1) the low temperature Bi:Ge eutectic at ~270°C[2] and (2) the highly reactive organic-free Ge precursor, GeI_2. GeI_2 disproportionates to Ge and GeI_4 with relatively high chemical yield at temperatures greater than ~330°C, which is far below its boiling point at 550°C and the boiling point of many widely used solvents, e.g. TOP. GeI_2 also forms a very soluble complex of $(GeI_2)\bullet R_3P$[3], when mixed with TOP, which dissociates at 120°C, making it an ideal precursor for SLS Ge nanowire and nanocrystal synthesis. The morphology of the Ge nanowires was investigated with SEM, TEM and XRD. The wires are highly crystalline and the mole ratio of GeI_2 to Bi affects the shape of the nanowires significantly – straight wires were obtained at high ratio while tortuous nanowires were observed at low ratio of GeI_2:Bi.

7.2 RECOMMENDATIONS

7.2.1 Patterned growth of Si/Ge nanowires on substrate

Nanowires are attractive as they can be used as building blocks to make functional nanoscale devices that could overcome limitations of

conventional fabrication for microelectronics. However, it has been challenging to assemble nanowires into well-ordered array. Huang et al. reported that nanowires can be parallel aligned on a substrate to form networks by combining fluidic alignment with surface-patterning techniques[4]. It would be desirable to synthesize nanowires into ordered array on a substrate during synthesis.

A recent study of Hong et al. showed that carbon nanotubes can be grown aligned on a substrate with chemical vapor deposition methods by using a laminar flow reactor[5]. This reactor can be adapted to make Si or Ge nanowires on a substrate with supercritical fluid method or solution phase synthesis approach at atmospheric pressure. Figure 7.1 shows the schematic design of the reactor which can achieve laminar flow. The stability of the flow in the reactor can be determined by the Reynolds number $\mathrm{Re} = \rho dv / \gamma$, which can be obtained with the density of the flow ρ, the velocity of flow v, the diameter of the reactor d, and the viscosity coefficient γ.

By reducing the diameter of the reactor d, the Re can be lowered into the laminar flow range (<2000), which would favor aligned growth as proved by Hong et al. Instead of using a round tube in Hong's design, an inner reactor with rectangular opening which fits the substrate would further lower

the Reynolds number. A substrate with attached growth seeds, such as Au[6] or Ni[7] nanocrystals, can be placed into the inner reactor. Similar reaction can be carried out as described in Chapter 3 by flowing through the Si or Ge precursor solution. The flow type in the reactor will be controlled by the flow rate and the cross section area of the inner reactor opening. A lower Reynolds number flow would produce aligned nanowires arrays (Figure 7.2).

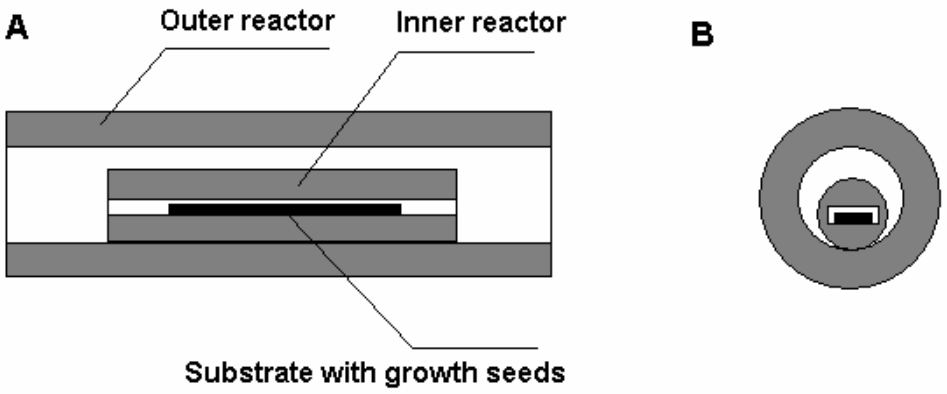

Figure 7.1 Schematic of the reactor to achieve laminar flow to grow nanowires into ordered array. (A) An inner reactor is used to lower the Reynolds number of the flow. (B) Cross section of the reactor showing a rectangular opening of the inner reactor which fits the substrate.

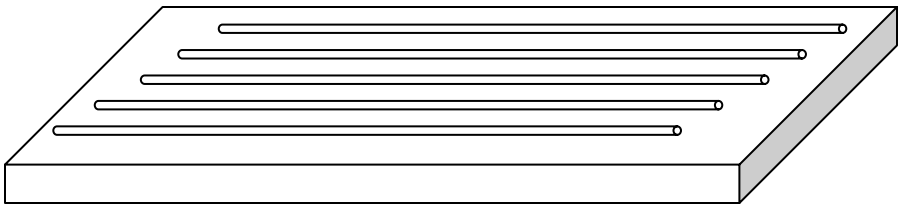

Figure 7.2 Schematic for ordered growth of nanowires on a substrate.

7.2.2 Size-dependent optical properties of Ge nanocrystals

Previous work shows that Ge nanocrystals exhibit size-dependent UV-visible absorption and photoluminescence spectra as discussed in Chapter 3. However, a comprehensive study of the size-dependent optical properties of Ge nanocrystals is far from complete. It would be desirable to obtain a serious of optical spectra for different size of nanocrystals and the relationship between the size of the particles and their absorption edge and photoluminescence maximum. The high yield of Ge nanocrystals synthesized with GeI_2 in TOP combining size-selective separation of the nanoparticles into fractions with narrow size distributions enables the investigation of the quantum confinement effect on optical properties for Ge nanocrystals with various sizes. Size-selective separation of the Ge nanocrystals can be done with solvent-antisolvent precipitation method. To

do the anti-solvent precipitation, the Ge nanocrystals must be well passivated with organic capping ligand. This has been achieved by heating the Ge nanocrystals in dodecanethiol as described in Appendix C.

7.3 REFERENCES

(1) Yaws, C. L. *Handbook of Thermodynamic Diagrams*; Gulf Publishing Company: Houston, TX, **1996**; Vol. 2.

(2) Olesinski, R. W.; Abbaschian, G. *J. Metal Progress* **1985**, 128, 55.

(3) King, R. B. *Inorg. Chem.* 1963, 2, 199.

(4) Huang, Y.; Duan, X. F.; Wei, Q. Q.; Lieber, C. M. *Science* **2001**, 291, 630-633.

(5) Hong, B. H.; Lee, J. Y.; Beetz, T.; Zhu, Y.; Kim, P.; Kim, K. S. *J. Am. Chem. Soc.*, **2005**, ACS ASAP.

(6) Lu, X.; Hanrath, T.; Johnston, K. P.; Korgel, B. A. *Nano Lett.* **2003**, 3, 93.

(7) Tuan, H. Y.; Lee, D. C.; Hanrath, T.; Korgel, B. A. *Nano Lett.* **2005**, 5, 681.

Appendix A: Electrogenerated Chemiluminescence of Ge Nanocrystals*

This paper was written primarily by Noseung Myung based on collaboration where my primary role was the particle synthesis. Organic layer capped Ge nanocrystals were synthesized by an arrested-growth method within supercritical octanol. Electrogenerated chemiluminescence (ECL) from the Ge nanocrystals dispersed in DMF containing 0.1 M TBAP was observed during potential scans or pulses through the annihilation of electrogenerated oxidized and reduced species. The light emission intensity was higher during the oxidation scans and pulses, suggesting that the reduced forms were more stable than the oxidized ones. The ECL spectrum was obtained by potential stepping between the potentials for oxidation and reduction. The ECL spectrum was red-shifted from the photoluminescence spectrum by ~ 200 nm, which implied, in agreement with previous studies, ECL emission predominantly via surface states and the importance of the surface passivation on ECL.

* Portions of this appendix have been previously published as Myung, Noseung; Lu, Xianmao; Johnston, Keith P.; and Bard, Allen J.; *Nano Lett.*, **2004**, 4, 183-185.

A.1 INTRODUCTION

Semiconductor nanocrystals or quantum dots, have been extensively studied due to their quantum confinement effects that exhibit unique size dependent electronic and optical properties[1,2] The II-VI semiconductor nanocrystals, such as CdSe and CdTe, have attracted particular attention, following reports of successful methods to grow highly crystalline monodisperse nanocrystals using TOPO (trioctylphosphine oxide) as a capping agent.[3]

There has also been interest in nanocrystals of indirect band gap, elemental semiconductors, such as Si and Ge, especially since these show useful levels of photoluminescence (PL) in the visible region and suggest possible applications in optoelectronics and microelectronics.[4-8] Compared to Si, Ge nanocrystals are of particular interest, since the Bohr radius is lager in Ge than Si, which consequently should lead to more prominent quantum confinement effect. In addition, while Si nanocrystals remained an indirect band gap semiconductor even at sizes near 1.5 nm,[9] Ge nanocrystal is more likely to undergo a transition to a direct band gap semiconductor since Ge is nearly a direct bad gap semiconductor in the bulk[10,11] and the lowest direct band gap for Ge is 0.8 eV, which is only about 0.1 eV above the indirect band

gap, making it an interesting material for the photonic applications in the IR region.

Recently, a new synthetic method using a supercritical solvent to produce highly crystalline and monodisperse Si quantum dots passivated with a capping agent was described.[9,12] The Si quantum dots clearly revealed quantum size effects, such as a substantial blue shift in the UV absorbance and PL spectrum from the bulk band gap energy. Interesting features were observed from the electrochemical experiments. For example, the differential pulse voltammetry (DPV) and electrogenerated chemiluminescence (ECL) of Si NCs revealed a quantized charging effect and a significant red-shift (~220 nm) from the PL maximum, respectively[12]. A similar red shift was observed from the ECL of CdSe nanocrystals.[13]

In this article, we describe the ECL of Ge nanocrystals in *N*,*N'*-dimethylformamide (DMF) containing 0.1 M tetra-*n*-butylammonium perchlorate (TBAP). The nanocrystals were synthesized for the first time in a supercritical fluid by an arrested-growth method in hexane with octanol as capping ligand.

A.2 EXPERIMENTAL SECTION

The Ge nanocrystals were synthesized by decomposing 62.5 mM Ge precursor, tetraethylgermane, in supercritical mixture of hexane:octanol (v:v=3:1) at 450ºC in a batch reactor.[14] They were polydisperse in nature with an average size of 4.0 nm and capped with an organic layer of C_8 hydrocarbon chains bound through an alkoxide layer(Figure A.1). ECL of Ge nanocrystals in DMF containing 0.1 M TBAP was measured using a Pt working, Pt counter and Ag reference electrodes placed in a cylindrical Pyrex vial. Experimental methods are described in detail elsewhere.[12,13]

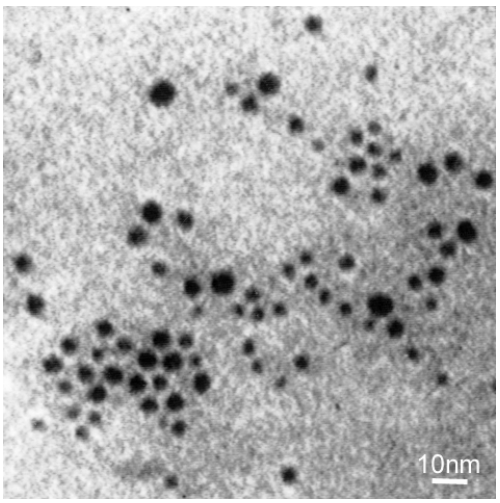

Figure A.1 TEM image of the Ge nanocrystals made from tetraethylgermane in hexane:octanol at 450ºC.

A.3 RESULTS AND DISCUSSION

Nanocrystals can be oxidized and reduced by charge injection during electrode potential cycling or potential steps between the potentials for oxidation and reduction. Light emission occurs through an annihilation (electron transfer) process when electrochemically oxidized species collide with reduced species. Therefore, to observe ECL, electrogenerated charged nanocrystals must be stable enough to show electron transfer upon colliding with an oppositely charged species.[12,13,15]

Figure A.2 shows light emission from the Ge nanocrystals in a DMF solution containing 0.1 M TBAP. ECL was observed through the annihilation mechanism when the electrode potential was cycled between +1.5 V and –2.3 V at a scan rate of 1.0 V/s. As shown in the Figure, ECL light was not observed within the potential gap that corresponded to the threshold voltage (~2.1 V). Several important features were observed. First, the electrogenerated reduced species are more stable than oxidized ones, as indicated by the relative ECL light intensities at positive and negative potentials. In other words, electrogenerated reduced forms produced in the negative potential region are stable enough to maintain their states until the electrode potential is sufficiently positive to generate oxidized species. This results in the light

emission through an annihilation mechanism. On the other hand, the light emission upon reduction is lower and broader in intensity, suggesting some decay of the oxidized forms during the time the potential moves to the reduction region. Unlike the Si quantum dots, poor electrochemical behavior was observed from the Ge nanocrystals with cyclic voltammetry and differential pulse voltammetry, so that well-defined peaks were not observed. This behavior is similar to the case of CdSe nanocrystals.[13]

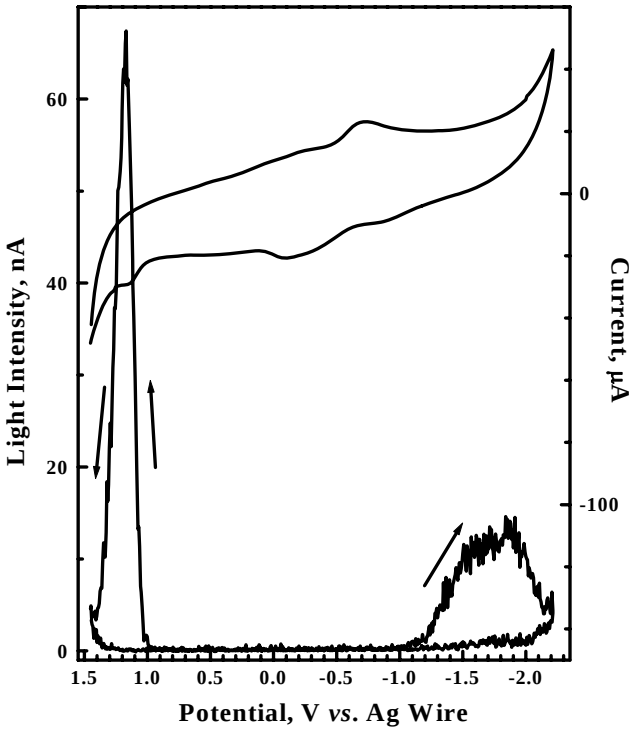

Figure A.2 Cyclic voltammogram and ECL emission as a function of electrode potential curve of Ge nanocrystals in DMF containing 0.1 M TBAP (scan rate: 1.0 V/s).

ECL transients for annihilation of the oxidized and reduced forms were obtained by switching the electrode potential between oxidation and reduction of Ge nanocrystals. The potential was stepped from 0.0 V to –2.5 V, and then pulsed between –2.5 V and +1.5 V in 0.5 s steps. As seen in Figure A.3, an initial step from 0.0 V to –2.5 V generated weak and broad ECL light, although only reduced species was generated during this potential step. Similar behavior, a so-called preannihilation process, was observed and discussed before. The next step to 1.5 V generated substantially sharp and intense light emission through the annihilation mechanism. The ECL light intensity was higher when the potential was stepped to the oxidation potential, suggesting again that the reduced forms of Ge NC are more stable. However, ECL light generated upon oxidation decayed faster than the light generated upon reduction and this may be related to the similar peak shape in Figure A.2.

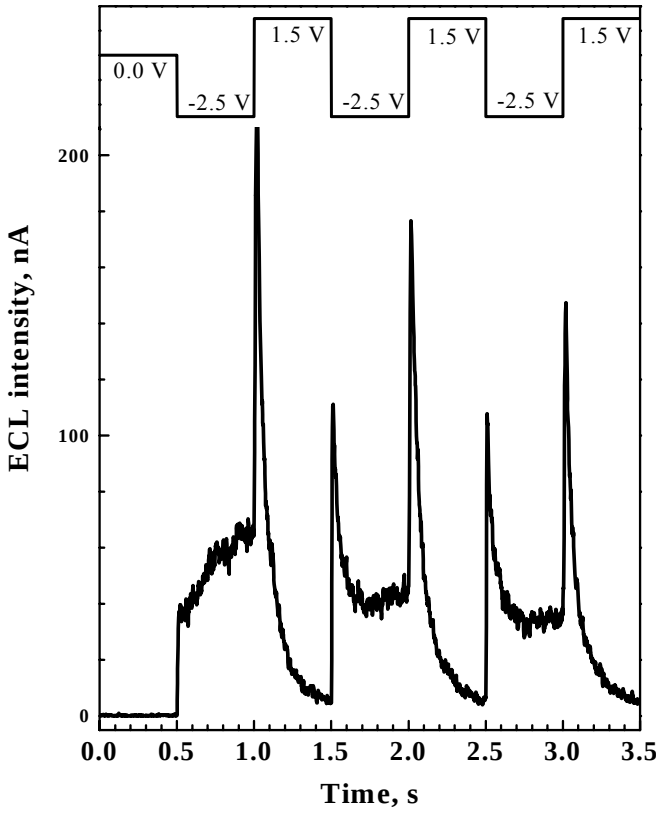

Figure A.3 ECL transients in DMF containing 0.1 M TBAP obtained by potential steps between +1.5 V and –2. 5 V.

Figure A.4 shows the ECL spectrum obtained from the Ge nanocrystals dispersed in a DMF solution containing 0.1 M TBAP using alternating potential steps between +1.5 V and –2.5 V at a 10 Hz rate for 30 min. The ECL spectrum shows a maximum wavelength, which is ~ 200 nm red-shifted compared with the PL spectrum (inset). This substantial red shift was also observed in the previous experiments with Si and CdSe nanocrystals

and it was attributed to the strong role surface states on the nanocrystals in electrochemical and ECL processes.[12,13]

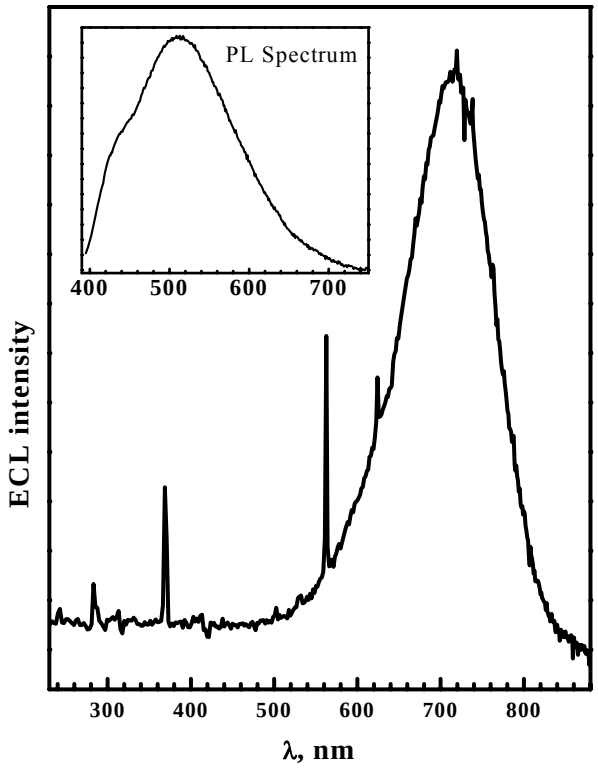

Figure A.4 ECL spectrum of Ge nanocrystals in 0.1 M TBAP DMF electrolyte by stepping electrode potential between +1.5 V and – 2. 5 V at 10 Hz rate for 30 min. Inset: PL spectrum obtained from the Ge nanocrystals dispersed in $CHCl_3$. Excitation wavelength: 380 nm. The large spikes represent the effect of cosmic ray events on the CCD.

Charge injection into the nanocrystals generally occurs via surface states, so ECL should be more sensitive to the surface state energetics than

PL, which occurs mainly from the interior of the NC. Thus completely passivated nanocrystals should show an ECL spectrum that is very similar to the PL spectrum. In fact, such an ECL spectrum is seen with CdSe nanocrystals passivated with the wider band gap ZnSe in a core/shell structure, suggesting an important advantage of ECL to probe surface states.[16] In addition, an ECL spectrum from the Si nanocrystals, which were size selected by a column chromatography, showed a similar red-shift. Therefore, we believe that the red-shift is not attributed to the size distribution or polydispersity of the nanocrystals, although the broad PL spectrum in inset reflects the size distribution of the Ge nanocrystals. Based on the above explanations, the red shift implies ECL emission from surface states of the Ge nanocrystals. Finally, a new synthetic method using a supercritical solvent revealed quantum confinement effects from the organic layer capped Ge nanocrystals. Size-controlled and band gap engineered semiconductor nanocrystals have a potential wide range of applications, so light emission through PL or ECL in the visible region may find possible applications in optoelectronics and microelectronics.

A.4 REFERENCES

(1) Alivisatos, A. P. *Science* **1996**, *271*, 933-937.

(2) Alivisatos, A. P. *J. Phys. Chem.* **1996**, *100*, 13226-13239.

(3) Murray, C. B.; Norris, D. J.; Bawendi, M. G. *J. Am. Chem. Soc.* **1993**, *115*, 8706-8715.

(4) English, D. S.; Pell, L. E.; Yu, Z. H.; Barbara, P. F.; Korgel, B. A. *Nano Lett.* **2002**, *2*, 681-685.

(5) Lin, C.-W.; Lin, S.-Y.; Lee, S.-C.; Chia, C.-T. *J. App. Phys.* **2002**, *91*, 1525-1528.

(6) Wu, Y. Y.; Yang, P. D. *Adv. Mater.* **2001**, *13*, 520.

(7) Wilcoxon, J. P.; Provencio, P. P.; Samara, G. A. *Phys. Rev. B* **2001**, *64*, 035417.

(8) Niquet, Y. M.; Allan, G.; Delerue, C.; Lannoo, M. *App. Phys. Lett.* **2000**, *77*, 1182-1184.

(9) Holmes, J. D.; Ziegler, K. J.; Doty, R. C.; Pell, L. E.; Johnston, K. P.; Korgel, B. A. *J. Am. Chem. Soc.* **2001**, *123*, 3743-3748.

(10) Peng, C. S.; Huang, Q.; Cheng, W. Q.; Zhou, J. M.; Zhang, Y. H.; Sheng, T. T.; Tung, C. H. *Phys. Rev. B* **1998**, *57*, 8805-8808.

(11) Okamoto, S.; Kanemitsu, Y. *Phys. Rev. B* **1996**, *54*, 16421-16424.

(12) Ding, Z. F.; Quinn, B. M.; Haram, S. K.; Pell, L. E.; Korgel, B. A.; Bard, A. J. *Science* **2002**, *296*, 1293-1297.

(13) Myung, N.; Ding, Z. F.; Bard, A. J. *Nano Lett.* **2002**, *2*, 1315-1319.

(14) Lu, X. M.; Ziegler, K. J.; Ghezelbash, A.; Johnston, K. P.; Korgel, B. A. *Nano Lett.* **2004**, *4*, 969-974.

(15) Bard, A. J. *Electroanalytical Chemistry*; Marcel Dekker: New York, 1977; Vol. 10.

(16) Myung, N.; Bae, Y.; Bard, A. J. *Nano Lett.* **2003**, *3*, 1053-1055.

Appendix B: Additional Images

B.1 Additional images for Si nanowires

Figure B.1-3 are SEM images for the Si nanowires synthesized on Si substrate in supercritical cyclohexane in a flow reactor showing different morphologies as discussed in Chapter 2. Figure B.4 is a TEM image for the Si nanowires synthesized in a batch reactor.

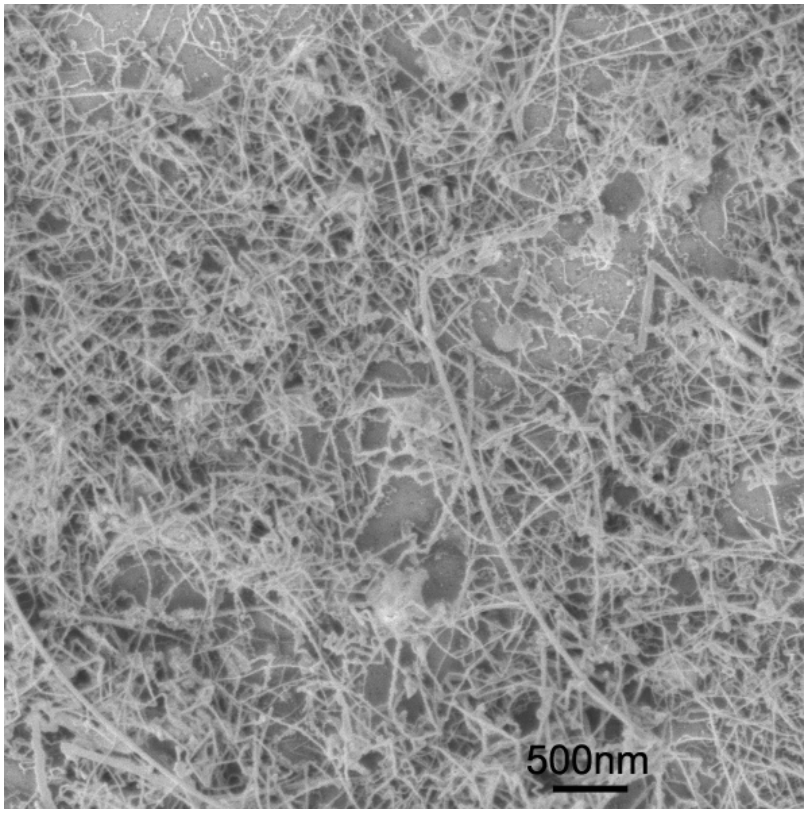

Figure B.1 HRSEM images of Si nanowires synthesized in the flow reactor with [DPS]=0.25 M. The nanowires were grown at 450ºC with DPS feedstock flow rates of 1 ml/min.

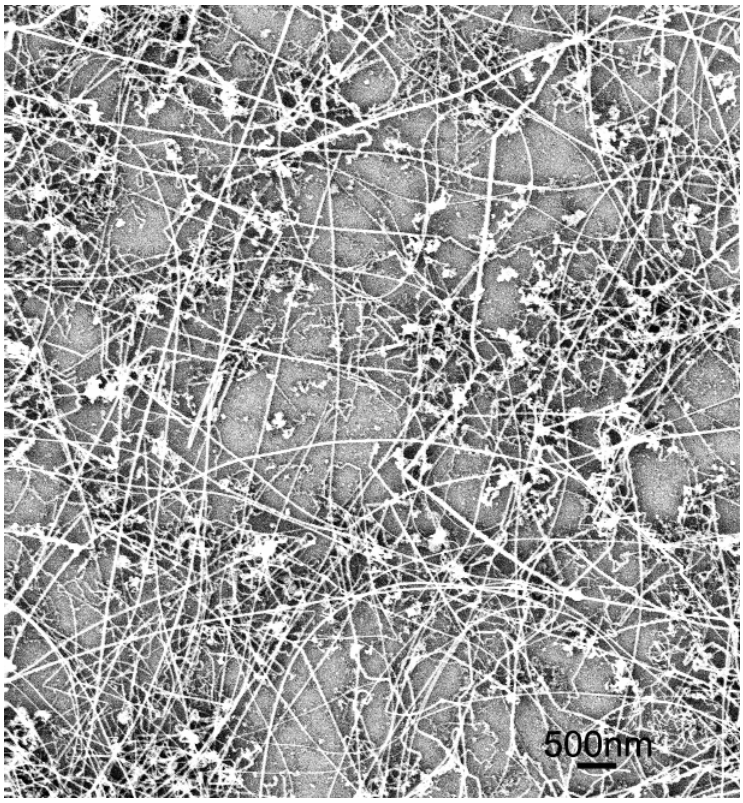

Figure B.2 HRSEM images of Si nanowires synthesized in the flow reactor with [DPS]=0.25 M. The nanowires were grown at 500ºC with DPS feedstock flow rates of 1 ml/min.

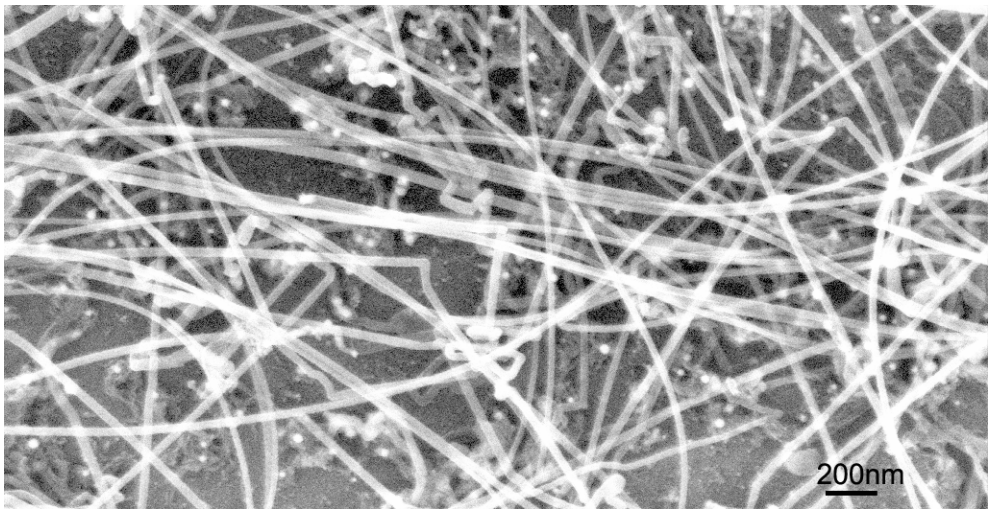

Figure B.3 HRSEM images of Si nanowires synthesized in the flow reactor with [DPS]=0.25 M. The nanowires were grown at 500ºC with DPS feedstock flow rates of 0.5 ml/min.

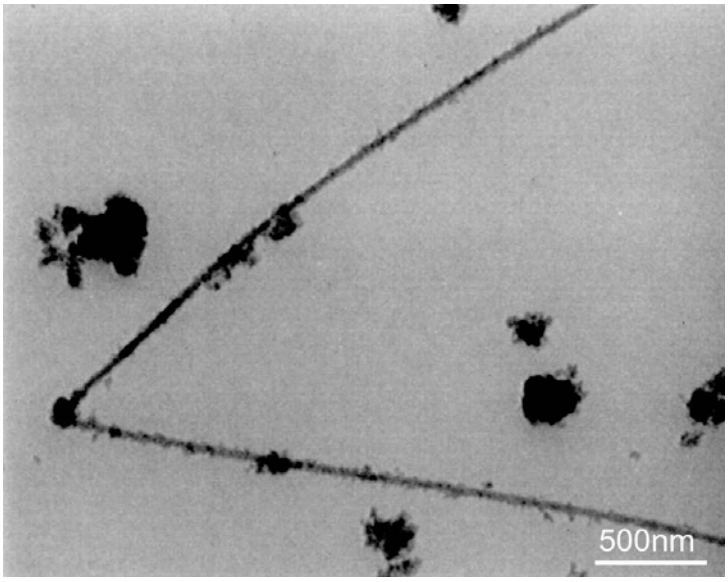

Figure B.4 LRTEM image of Si nanowires grown from Au nanocrystals on a Si substrate in the batch reactor. The Si nanowires were obtained at 500ºC with 0.9 M DPS in a 1 ml Ti high pressure reactor. The rough surface of the nanowires was due to the surrounded by-product contaminants.

B.2 ADDITIONAL IMAGES FOR GE NANOCRYSTALS

Figure B.5-6 show the reaction setup for synthesis of Ge nanocrystals in sc-CO_2. Figure B.7 shows TEM images of the Ge nanoparticles made in sc-CO_2 with broad size distribution discussed in Chapter 4. Figure B.8 consists of additional TEM images of Ge nanoparticles made from GeI_2 reduced with $LiAlH_4$ in TOP showing that an interim state of the particles, which is probably in the form of Ge_xH_{2x+2}, might exist.

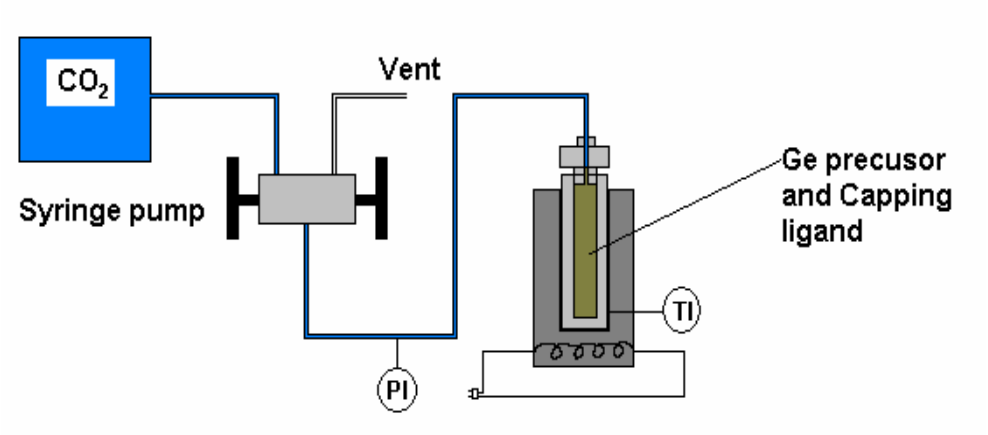

Figure B.5 Schematic reaction setup for synthesis of Ge nanocrystal in sc-CO_2. The Ti high pressure reaction cell is heated with a brass block heater and pressurized with CO_2 using a syringe pump.

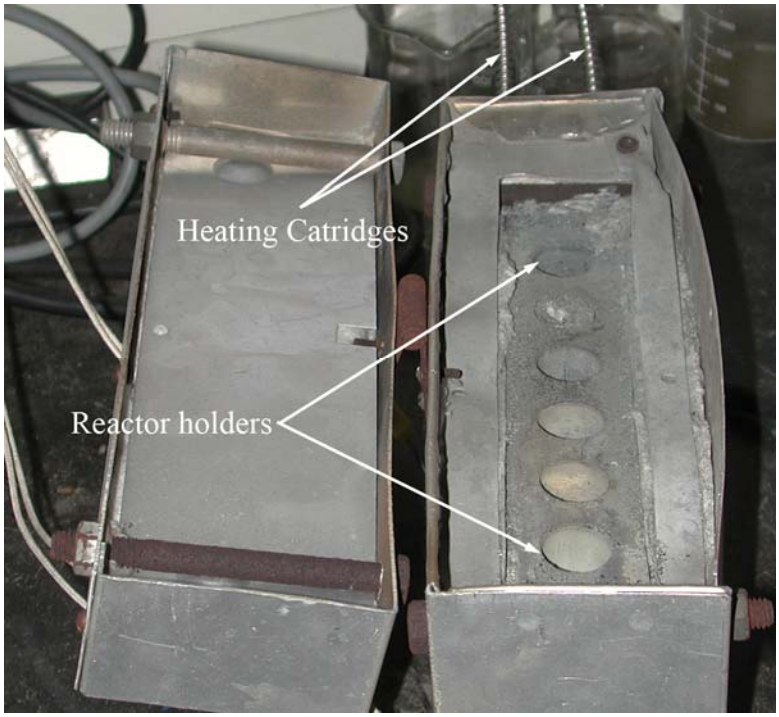

Figure B.6 Digital image for the block heater used to hold high pressure 1 ml reaction cells.

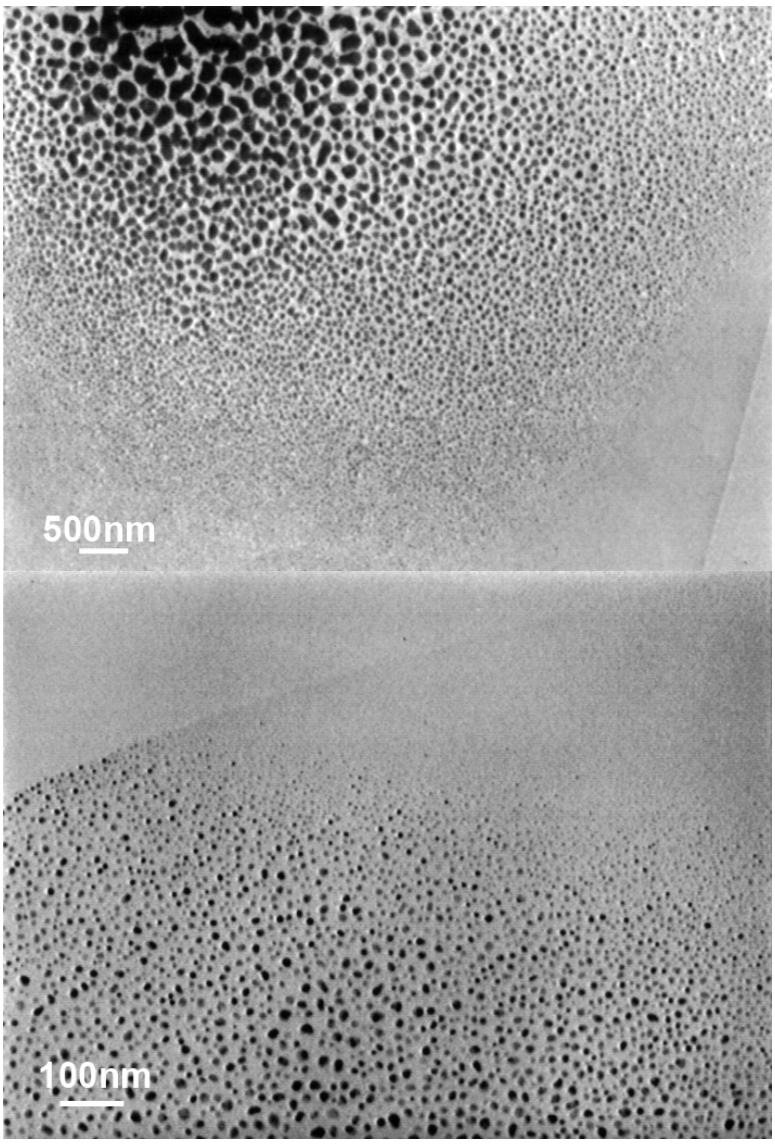

Figure B.7 Ge nanocrystals synthesized from 50μL TEG and 10μL octanol in sc-CO_2 at 500°C and 4000 psi in a 1 ml reactor showing broad size distribution.

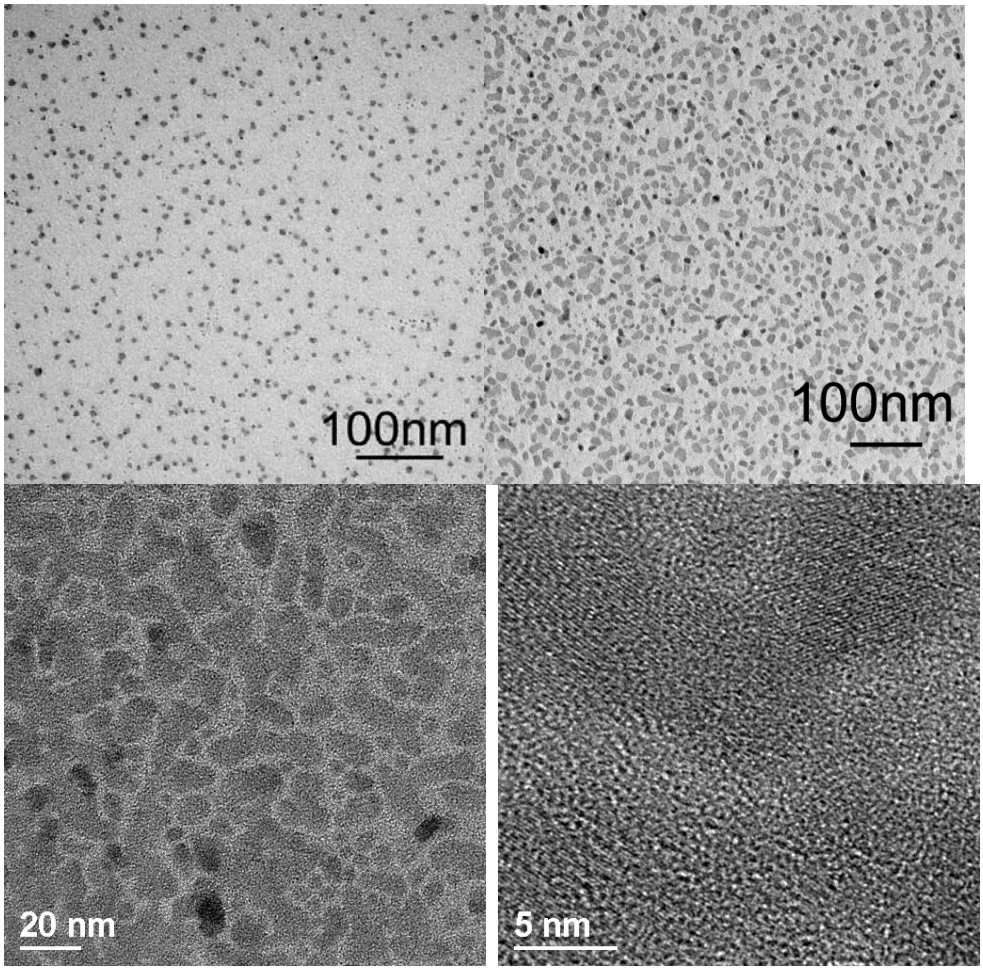

Figure B.8 (A) Ge nanoparticles synthesized from 150 mM GeI_2 reduced with $LiAlH_4$ at 150°C in TOP. (B) The nanoparticles were annealed at 180°C in vacuum oven for 12 hrs showing shape transition of the particles. (C), (D) HRTEM images revealed that the annealed particles are crystalline.

B.3 ADDITIONAL IMAGES FOR GE NANOWIRES

Figure B.9 shows a TEM for the Bi nanocrystal growth seeds for Ge nanowires. Figure B.10 and B.11 are the TEM and SEM images for the Ge nanowires synthesized from different ratio of GeI_2:Bi as discussed in Chapter 6.

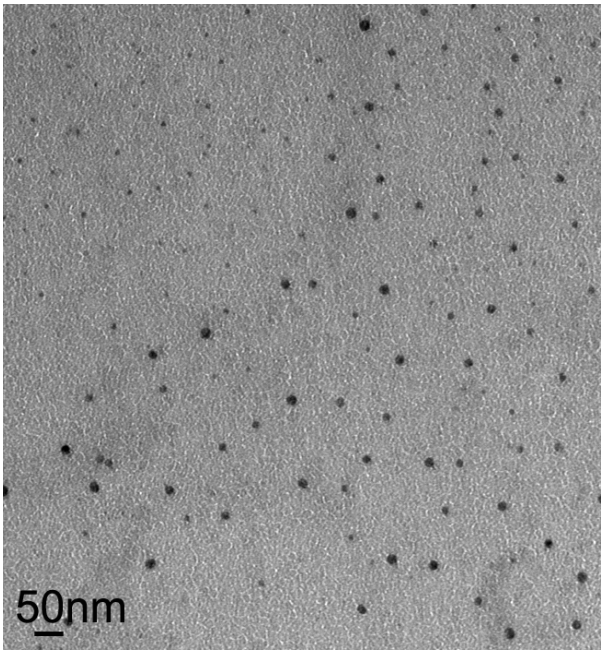

Figure B.9 Bismuth nanoparticles used as growth seeds to synthesize Ge nanowires. The average diameter of the nanocrystals is 20 nm.

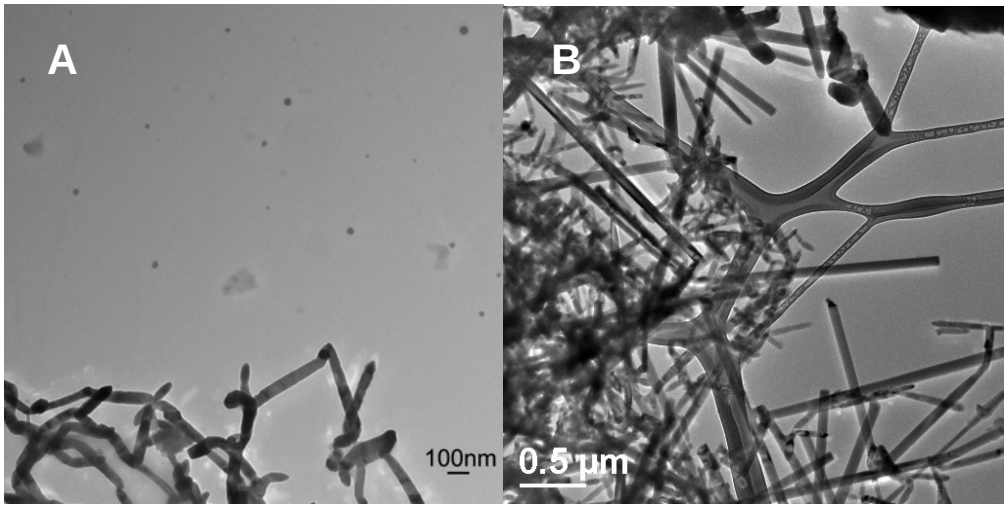

Figure B.10 TEM images for the Ge nanowires made from GeI_2 with Bi nanocrystal growth seeds in TOP at 350°C. (A) The ratio of GeI_2:Bi was 50:1. Bi nanocrystals were seen on the TEM grid and the size of the nanocrystals was comparable to the diameter of the Ge nanowires. (B) Increase of the GeI_2:Bi ratio to 80:1 produced high quality Ge nanowires.

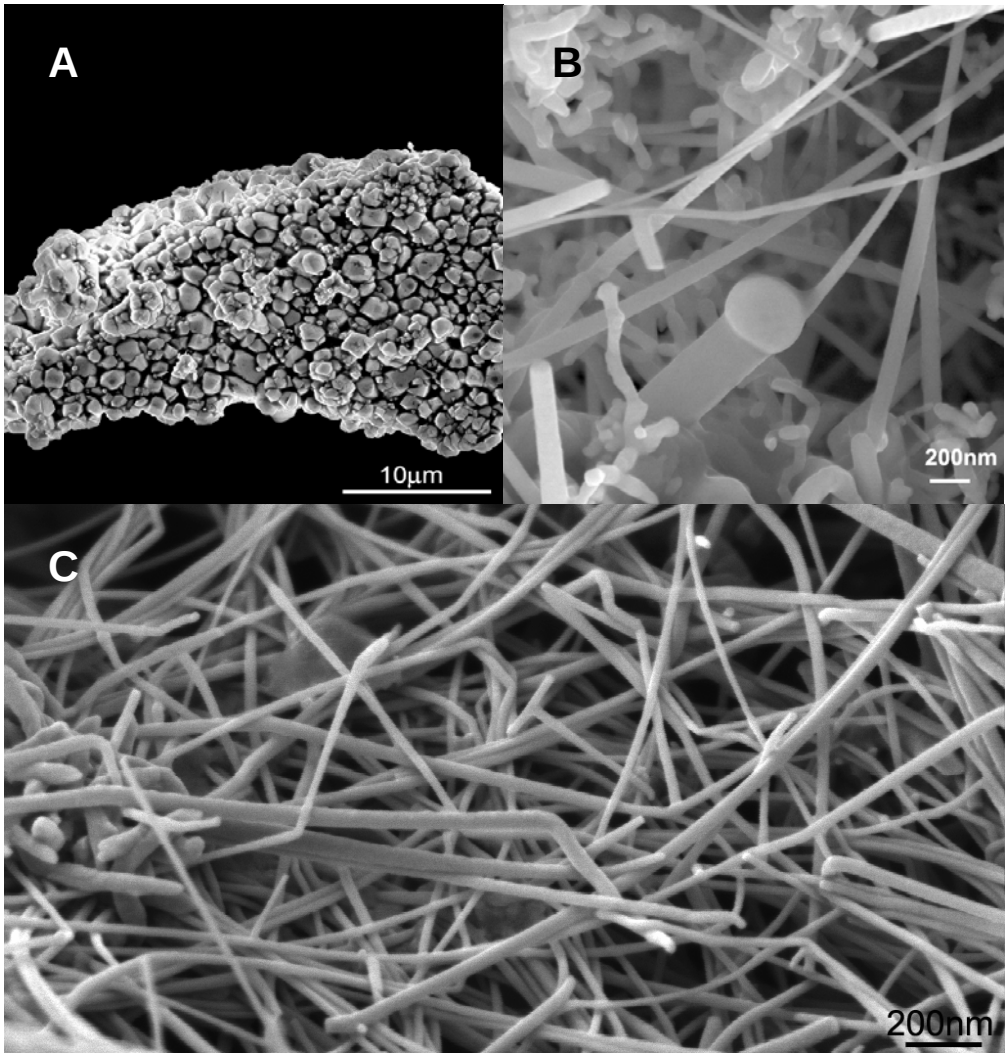

Figure B.11 (A) Ge particles made from GeI_2 with Bi nanocrystals at a ratio of GeI_2:Bi=200:1. (B) Short, tortuous Ge nanowires made at a ratio of GeI_2:Bi=50:1. (C) Long, straight Ge nanowires made at a ratio of GeI_2:Bi=80:1. All the reactions were carried out at 350°C in TOP with standard Schlenk line technique.

Bibliography

Alivisatos, A. P. *J. Phys. Chem.* **1996**, *100*, 13226-13239.

Alivisatos, A. P. *Science* **1996**, *271*, 933.

Bard, A. J. *Electroanalytical Chemistry*; Marcel Dekker: New York, 1977; Vol. 10.

Blackburn, J. M.; Long, D. P.; Cabanas, A.; Watkins, J. J. *Science* **2001**, *294*, 141.

Bley, R. A.; Kauzlarich, S. M. *J. Am. Chem. Soc.* **1996**, *118*, 12461.

Bley, R. A.; Kauzlarich, S. M.; Davis, J. E.; Lee, H. W. *Chem. Mater.* **1996**, *8*, 1881.

Bruchez, M.; Moronne, M.; Gin, P.; Weiss, S.; Alivisatos, A. P. *Science* **1998**, *281*, 2013-2016.

Brust, M.; Walker, M.; Bethell, D.; Schiffrin, D. J.; Whyman, R. *J. Che. Soc. Chem. Commun.* **1994**, *801*, 1994.

Burda, C.; Chen, X. B.; Narayanan, R.; El-Sayed, M. A. *Chem. Rev.* **2005**, *105*, 1025.

Choi, K.; Buriak, J. M. *Langmuir* **2000**, *16*, 7737.

Coleman, N. R.; Morris, M. A.; Spalding, T. R.; Holmes, J. D. *J. Am. Chem. Soc.* **2001**, *123*, 187.

Condo, P. D.; Sumpter, S. R.; Lee, M. L.; Johnston, K. P. *Ind. Eng. Chem. Res.* **1996**, *35*, 1115.

Coutant, R. W.; Levy, A. A Kinetic Study of the Thermal Decomposition of Selected Cyclohexyl and Phenylsilanes; 1969.

Cowley, J. M. Electron Diffraction Techniques; Oxford Science University Press: New York, 1992; Vol. 1.

Cui, Y.; Lauhon, L. J.; Gudiksen, M. S.; Wang, J.; Lieber, C. M. *Appl. Phys. Lett.* **2001**, *78*, 2214.

Cui, Y.; Lieber, C. M. *Science* **2001**, *291*, 851.

Cullity, B. D. Elements of X-Ray Diffraction; Addison-Wesley Publishing Company, Inc.: Reading, MA, 1956.

Dailey, J. W.; Taraci, J.; Clement, T.; Smith, D. J.; Drucker, J.; Picraux, S. T. *J. Appl. Phys.* **2004**, *96*, 7556.

Davidson, F. M.; Schricker, A. D.; Wiacek, R. J.; Korgel, B. A. *Adv. Mater.* **2004**, *16*, 646.

Derycke, V.; Martel, R.; Appenzeller, J. *Nano Letters* **2001**, *1*, 453.

Ding, Z. F.; Quinn, B. M.; Haram, S. K.; Pell, L. E.; Korgel, B. A.; Bard, A. J. *Science* **2002**, *296*, 1293-1297.

Duan, X.; Lieber, C. M. *Adv. Mater.* **2000**, *10*, 298.

Dutta, A. K. Appl. Phys. Lett. **1996**, 68, 1189.

English, D. S.; Pell, L. E.; Yu, Z. H.; Barbara, P. F.; Korgel, B. A. *Nano Lett.* **2002**, *2*, 681-685.

Fanfair, D. D.; Korgel, B. A. *Crystal Growth & Design* **2005**, *5*, 1971.

Fok, E.; Shih, M.; Meldrum, A.; Veinot, J. G. C. *Chem. Commun.* **2004**, 386.

Friedlander, S. K.; Wang, C. S. *J. Colloid Inter. Sci.* **1966**, *22*, 126.

Galus, Z. *Stand. Potentials Aqueous Solution* **1985**, 189.

Gao, P. X.; Ding, Y.; Wang, Z. L. *Nano Lett*. **2003**, *3*, 1315.

Gerion, D.; Zaitseva, N.; Saw, C.; Casula, M. F.; Fakra, S.; Van Buuren, T.; Galli, G. *Nano Lett.* **2004**, *4*, 597.

Gerung, H.; Bunge, S. D.; Boyle, T. J.; Brinker, C. J.; Han, S. M. *Chem. Commun.* **2005**, 1914.

Gromov, D. G.; de Pablo, J. J.; Luna-Barcenas, G.; Sanchez, I. C.; Johnston, K. P. *J. Chem. Phys.* **1998**, *108*, 4647.

Gudiksen, M. S.; Lieber, C. M. *J. Am. Chem. Soc.* **2000**, *122*, 8801.

Hanrath, T.; Korgel, B. A. *Adv. Mater.* **2003**, *15*, 437.

Hanrath, T.; Korgel, B. A. *J. Am. Chem. Soc.* **2002**, *124*, 1424.

Hanrath, T.; Korgel, B. A. *J. Am. Chem. Soc.* **2004**, *126*, 15466.

Hanrath, T.; Korgel, B.A. *Small* **2005**, *1*, 717.

Heath, J. R. *Chem. Soc. Rev.* **1998**, *27*, 65.

Heath, J. R. *Science* **1992**, *258*, 1131.

Heath, J. R.; LeGoues, F. K. *Chem. Phys. Lett.* **1993**, *208*, 263.

Heath, J. R.; Shiang, J. J.; Alivisatos, A. P. *J. Chem. Phys.* **1994**, *101*, 1607.

Hines, M. A.; Guyot-Sionnest, P. *J. Phys. Chem. B* **1998**, *102*, 3655-3657.

Holmes, J. D.; Johnston, K. P.; Doty, R. C.; Korgel, B. A. *Science* **2000**, *287*, 1471.

Holmes, J. D.; Ziegler, K. J.; Doty, R. C.; Pell, L. E.; Johnston, K. P.; Korgel, B. A. *J. Am. Chem. Soc.* **2001**, *123*, 3743.

Hong, B. H.; Lee, J. Y.; Beetz, T.; Zhu, Y.; Kim, P.; Kim, K. S. *J. Am. Chem. Soc.*, **2005**, ACS ASAP.

Hu, J. T.; Odom, T.W.; Lieber, C. M. *Accts. Chem. Res.* **1999**, *32*, 435.

Huang, Y.; Duan, X. F.; Wei, Q. Q.; Lieber, C. M. *Science* **2001**, 291, 630-633.

Huynh, W. U.; Dittmer, J. J.; Alivisatos, A. P. *Science* **2002**, *295*, 2425-2427.

Inagaki, N.; Mitsuuchi, M. *J. Poly. Sci*. **1983**, 21, 2887.

Israelachvili, J. N. *Intermolecular and Surface Forces: With Applications to Colloidal and Biological Systems*, 1985.

Jiang, J.; Chen, K.; Huang, X.; Li, Z.; Feng, D. *Appl. Phys. Lett.* **1994**, *65*, 1799.

Johnston, D. R.; Cole, R. H. *J. Chem. Phys.* **1962**, *36*, 318.

Kanemitsu, Y.; Uto, H.; Masumoto, Y.; Maeda, Y. *Appl. Phys. Lett*. **1992**, 61, 2187.

King, R. B. *Inorg. Chem.* **1963**, *2*, 199.

Klabunde, K. J.; Editor *Nanoscale Materials in Chemistry*; John Wiley & Sons, Inc.: New York, 2001.

Klimov, V. I., Ed. *Semiconductor and Metal Nanocrystals: Synthesis, Electronic and Optical Properties*; Marcel Dekker: New York, 2003.

Klimov, V. I.; Mikhailovsky, A. A.; Xu, S.; Malko, A.; Hollingsworth, J. A.; Leatherdale, C. A.; Eisler, H. J.; Bawendi, M. G. *Science* **2000**, *290*, 314-317.

Kluth, G. J.; Sung, M. M.; Maboudian, R. *Langmuir* **1997**, *13*, 3775.

Korgel, B. A.; Fitzmaurice, D. *Phys. Rev. Lett.* **1998**, *80*, 3531.

Kornowski, A.; Giersig, M.; Vogel, R.; Chemseddine, A.; Weller, H. *Adv. Mater.* **1993**, *5*, 634.

Launay, J. C.; Debegnac, H.; Zappoli, B.; Mignon, C. *J. Cryst. Growth* **1988**, *92*, 323.

Law, M.; Goldberger, J.; Yang, P. D. *Ann. Rev. Mater. Res.* **2004**, *34*, 83.

Lee, C. T.; Johnston, K. P.; Dai, H. J.; Cochran, H. D.; Melnichenko, Y. B.; Wignall, G. D. *J. Phys. Chem. B* **2001**, *105*, 3540-3548.

Lee, D. C.; Mikulec, F. V.; Korgel, B. A. *J. Am. Chem. Soc.* **2004**, *126*, 4951.

Lin, C.-W.; Lin, S.-Y.; Lee, S.-C.; Chia, C.-T. *J. App. Phys.* **2002**, *91*, 1525-1528.

Littau, K. A.; Szajowski, P. J.; Muller, A. J.; Kortan, A. R.; Brus, L. E. *J. Phys. Chem.* **1993**, *97*,1224.

Lu, X.; Hanrath, T.; Johnston, K. P.; Korgel, B. A. *Nano Lett.* **2003**, 3, 93.

Lu, X.; Korgel, B. A.; Johnston, K. P. *Chem. Mater.* **2005**, 17, 6479.

Lu, X.; Korgel, B. A.; Johnston, K. P. *Nanotechnology* **2005**, *16*, S389.

Lu, X.; Ziegler, K. J.; Ghezelbash, A.; Johnston, K. P.; Korgel, B. A. *Nano Lett.* **2004**, *4*, 969.

Luna-Barcenas, G.; Meredith, J. C.; Sanchez, I. C.; Johnston, K. P.; Gromov, D. G.; de Pablo, J. J. *J. Chem. Phys.* **1997**, *107*, 10782.

Macklen, E. D. *J. Chem. Soc.* **1959**, 1984.

Maeda, Y.; Tsukamoto, N.; Yazawa, Y.; Kanemitsu, Y.; Masumoto, Y. *Appl. Phys. Lett.* **1991**, *59*, 3168.

Melnikov, D. V.; Chelikowsky, J. R. *Solid State Commun*. **2003**, 127, 361.

Meredith, J. C.; Johnston, K. P. *Langmuir* **1999**, *15*, 8037-8044.

Meredith, J. C.; Johnston, K. P. *Macromolecules* **1998**, *31*, 5507.

Meredith, J. C.; Johnston, K. P. *Macromolecules* **1998**, *31*, 5518-5528.

Meredith, J. C.; Sanchez, I. C.; Johnston, K. P.; de Pablo, J. J. *J. Chem. Phys.* **1998**, *109*, 6424.

Morales, A. M.; Lieber, C. M. *Science* **1998**, *279*, 208.

Morales, A. M.; Lieber, C. M. *Science* **1998**, *279*, 208.

Murray, C. B.; Kagan, C. R.; Bawendi, M. G. *Annu. Rev. Mater. Sci.* **2000**, *30*, 545-610.

Murray, C. B.; Norris, D. J.; Bawendi, M. G. *J. Am. Chem. Soc.* **1993**, *115*, 8706.

Myung, N.; Bae, Y.; Bard, A. J. *Nano Lett.* **2003**, *3*, 1053-1055.

Myung, N.; Ding, Z. F.; Bard, A. J. *Nano Lett.* **2002**, *2*, 1315-1319.

Myung, N.; Lu, X.; Johnston, K. P.; Bard, A. J. *Nano Lett.* **2004**, *4*, 183.

Newman, R. C.; Wake-field, J. *Solid State Phys. Electron. Telecomm., Proc.* **1960**, *1*, 160.

Niquet, Y. M.; Allan, G.; Delerue, C.; Lannoo, M. *App. Phys. Lett.* **2000**, *77*, 1182-1184.

Norris, D. J.; Sacra, A.; Murray, C. B.; Bawendi, M. G. *Physical Review Letters* **1994**, *72*, 2612-2615.

Odom, T. W.; Huang, J.-L.; Kim, P.; Lieber, C. M. *Nature* **1998**, *391*, 62.

Oh, J.; Campbell, J. C. *J. Electron. Mater.* **2004**, *33*, 364.

Okamoto, H.; Massalski, T. B. *J. Metals* **1984**, *36*, 57.

Okamoto, S.; Kanemitsu, Y. Phys. Rev. B. **1996**, 54, 16421.

Olesinski, R. W.; Abbaschian, G. J. *Metal Progress* **1985**, *128*, 55.

Omi, H.; Ogino, T. *Appl. Phys. Lett.* **1997**, *71*, 2163.

ONeill, M. L.; Yates, M. Z.; Harrison, K. L.; Johnston, K. P.; Canelas, D. A.; Betts, D. E.; DeSimone, J. M.; Wilkinson, S. P. *Macromolecules* **1997**, *30*, 5050-5059.

Pai, R. A.; Humayun, R.; Schulberg, M. T.; Sengupta, A.; Sun, J.-N.; Watkins, J. J. *Science* **2004**, *303*, 507.

Pan, L.; Lew, K.-K.; Redwing, J. M.; Dickey, E. C. *Nano Lett.* **2005**, *5*, 1081.

Peck, D. G.; Johnston, K. P. *Macromolecules* **1993**, *26*, 1537-1545.

Pell, L. E.; Schricker, A. D.; Mikulec, F. V.; Korgel, B. A. *Langmuir* **2004**, *20*, 6546.

Peng, C. S.; Huang, Q.; Cheng, W. Q.; Zhou, J. M.; Zhang, Y. H.; Sheng, T. T.; Tung, C. H. *Phys. Rev. B* **1998**, *57*, 8805-8808.

Peng, X. G.; Wickham, J.; Alivisatos, A. P. *J. Am. Chem. Soc.* **1998**, *120*, 5343-5344.

Peng, Z. A.; Peng, X. G. *J. Am. Chem. Soc.* **2001**, *123*, 183-184.

Pouchert, C. J. *The Aldrich Library of FT-IR spectra*; 2nd ed. Milwaukee, Wis., 1997.

Pretsch, E.; Clerc, T.; Seibl, J.; Simon, W. Tables of Spectral Data for Structure Determination of Organic Compounds; Springer-Verlag: Berlin, 1983.

Ragan, R.; Chen, Y.; Ohlberg, D. A. A.; Medeiros-Ribeiro, G.; Williams, R. S. *J. Crystal Growth* **2003**, *251*, 657-661.

Rappoport, Z., Ed. The Chemistry of Organic Germanium, Tin and Lead Compounds, Volume 2 (Part 1); John Wiley & Sons:Chichester, England, 2002; Vol. 2.

Reboredo, F. A.; Zunger, A. *Phys. Rev. B*. **2000**, 62, R2275.

Reboredo, F. A.; Zunger, A. *Phys. Rev. B*. **2001**, 63, 235314.

Ryan, K. M.; Erts, D.; Olin, H.; Morris, M. A.; Holmes, J. D. *J. Am. Chem. Soc.* **2003**, *125*, 6284.

Sato, T.; Ahmed, H.; Brown, D.; Johnson, B. F. G. *J. Appl. Phys.* **1997**, *82*, 696-701.

Saunders, A. E.; Korgel, B. A. *J. Phys. Chem. B* **2004**, *108*, 16732.

Saunders, A. E.; Shah, P. S.; Park, E. J.; Lim, K. T.; Johnston, K. P.; Korgel, B. A. *J. Phys. Chem. B* **2004**, *108*, 15969.

Saunders, A. E.; Sigman, M. B., Jr.; Korgel, B. A. *J. Phys. Chem. B* **2004**, *108*, 193.

Schmeisser, D.; Schnell, R. D.; Bogen, A.; Himpsel, F. J.; Rieger, D.; Landgren, G.; Morar, J. F. *Surf. Sci.* **1986**, *172*, 455-465.

Shah, P. S.; Hanrath, T.; Johnston, K. P.; Korgel, B. A. *J. Phys. Chem. B* **2004**, *108*, 9574.

Shah, P. S.; Holmes, J. D.; Doty, R. C.; Johnston, K. P.; Korgel, B. A. *J. Am. Chem. Soc.* **2000**, *122*, 4245-4246.

Shah, P. S.; Holmes, J. D.; Johnston, K. P.; Korgel, B. A. *J. Phys. Chem. B* **2002**, *106*, 2545.

Shah, P. S.; Husain, S.; Johnston, K. P.; Korgel, B. A. *J. Phys. Chem. B* **2001**, *105*, 9433.

Shah, P. S.; Husain, S.; Johnston, K. P.; Korgel, B. A. *J. Phys. Chem. B* **2002**, *106*, 12178.

Shevchenko, E. V.; Talapin, D. V.; Rogach, A. L.; Kornowski, A.; Haase, M.; Weller, H. *J. Am. Chem. Soc.* **2002**, *124*, 11480-11485.

Shi, W.; Zhang, Y.; Lee, C. S.; Lee, S. T. *Adv. Mater.* **2001**, *13*, 591.

Shim, M.; Guyot-Sionnest, P. *J. Am. Chem. Soc.* **2001**, *123*, 11651-11654.

Sigman, M. B., Jr.; Saunders, A. E.; Korgel, B. A. *Langmuir* **2004**, *20*, 978.

Sirard, S. M.; Gupta, R. R.; Russell, T. P.; Watkins, J. J.; Green, P. F.; Johnston, K. P. *Macromolecules* **2003**, *36*, 3365.

Socrates, G. Infrared Characteristic Group Frequencies: Tables and Charts; 2nd ed.; John Wiley & Sons: New York, 1994.

Son, S. U.; Jang, Y.; Yoon, K. Y.; Kang, E.; Hyeon, T. *Nano Lett.* **2004**, *4*, 1147.

Steckel, J. S.; Coe-Sullivan, S.; Bulovic, V.; Bawendi, M. G. *Adv. Mater.* **2003**, *15*, 1862-1866.

Stone, F. G. A. *Hydrogen Compounds of Ground IV Elements*; Prentice Hall, Inc., Englewood Cliffs, NJ, 1962.

Stowell, C. A.; Wiacek, R. J.; Saunders, A. E.; Korgel, B. A. *Nano Lett.* **2003**, *3*, 1441.

Sun, S. H.; Anders, S.; Thomson, T.; Baglin, J. E. E.; Toney, M. F.; Hamann, H. F.; Murray, C. B.; Terris, B. D. *J. Phys. Chem. B* **2003**, *107*, 5419-5425.

Sun, S. H.; Murray, C. B.; Weller, D.; Folks, L.; Moser, A. *Science* **2000**, *287*, 1989-1992.

Swift, D. L.; Friedlander, S. K. *J. Coll. Sci.* **1964**, *19*, 621.

Takagahara, T.; Takeda, K. *Phys. Rev. B*. **1996**, 53, R4205.

Talapin, D. V.; Rogach, A. L.; Mekis, I.; Haubold, S.; Kornowski, A.; Haase, M.; Weller, H. *Colloids Surf., A* **2002**, *202*, 145-154.

Tanke, R. S.; Kauzlarich, S. M.; Patten, T. E.; Pettigrew, K. A.; Murphy, D. L.; Thompson, M. E.; Lee, H. W. H. *Chem. Mater.* **2003**, *15*, 1682.

Taylor, B. R.; Fox, G. A.; Hope-Weeks, L. J.; Maxwell, R. S.; Kauzlarich, S. M.; Lee, H. W. H. *Mater. Sci. Eng. B-Solid State Mater. Adv. Technol.* **2002**, *96*, 90-93.

Taylor, B. R.; Kauzlarich, S. M.; Delgado, G. R.; Lee, H. W. *Chem. Mater.* **1999**, 11, 2493.

Taylor, B. R.; Kauzlarich, S. M.; Lee, H. W. H.; Delgado, G. R. *Chem. Mater.* **1998**, *10*, 22-24.

Trentler, T. J.; Hickman, K. M.; Goel, S. C.; Viano, A. M.; Gibbons, P. C.; Buhro, W. E. *Science* **1995**, *270*, 1979.

Tuan, H. Y.; Lee, D. C.; Hanrath, T.; Korgel, B. A. *Nano Lett.* **2005**, *5*, 681.

Wagner, R. S.; Ellis, W. C. *App. Phys. Lett.* **1964**, *4*, 89.

Wagner, R. S.; Ellis, W. C.; Jackson, K. A.; Arnold, S. M. *J. Appl. Phys.* **1964**, *35*, 2993.

Wang, D.; Dai, H. Angew. Chem. Int. Ed. **2002**, 41, 4783.

Wang, D.; Tu, R.; Zhang, L.; Dai, H. *Angew. Chem.-Int. Edit.* **2005**, *44*, 2925.

Wang, W. Z.; Huang, J. Y.; Ren, Z. F. *Langmuir* **2005**, *21*, 751-754.

Watkins, J. J.; Blackburn, J. M.; McCarthy, T. J. *Chem. Mater.* **1999**, *11*, 213.

Watkins, J. J.; McCarthy, T. J. *Chem. Mater.* **1995**, *7*, 1991.

Watzky, M. A.; Finke, R. G. *J. Am. Chem. Soc.* **1997**, *119*, 10382.

Wehrenberg, B. L.; Wang, C. J.; Guyot-Sionnest, P. *J. Phys. Chem. B* **2002**, *106*, 10634-10640.

Wilcoxon, J. P.; Provencio, P. P.; Samara, G. A. *Phys. Rev. B* **2001**, *64*, 035417.

Wu, Y. Y.; Yang, P. D. *Adv. Mater.* **2001**, *13*, 520.

Wu, Y.; Yang, P. *Chem. Mater.* **2000**, *12*, 605.

Wu, Y.; Yang, P. *J. Am. Chem. Soc.* **2001**, *123*, 3165.

Yates, M. Z.; ONeill, M. L.; Johnston, K. P.; Webber, S.; Canelas, D. A.; Betts, D. E.; DeSimone, J. M. *Macromolecules* **1997**, *30*, 5060

Yaws, C. L. *Handbook of Thermodynamics Diagrams*; Gulf Publishing Company: Houston, Texas,1996.

Yoffe, A. D. *Adv. Phys.* **2001**, *50*, 1-208.

Yu, H.; Buhro, W. E. *Adv. Mater.* **2003**, *15*, 416.

Yu, H.; Li, J. B.; Loomis, R. A.; Gibbons, P. C.; Wang, L. W.; Buhro, W. E. *J. Am. Chem. Soc*. **2003**, *125*, 16168.

Yu, H.; Li, J. B.; Loomis, R. A.; Wang, L. W.; Buhro, W. E. *Nat. Mater.* **2003**, *2*, 517.

Yu, W. W.; Falkner, J. C.; Shih, B. S.; Colvin, V. L. *Chem. Mater.* **2004**, *16*, 3318.

Yun, M. H.; Myung, N. V.; Vasquez, R. P.; Lee, C. S.; Menke, E.; Penner, R. M. *Nano Lett.* **2004**, *4*, 419-422.

Zach, M. P.; Ng, K. H.; Penner, R. M. *Science* **2000**, *290*, 2120-2123.

Zaitseva, N.; Harper, J.; Gerion, D.; Saw, C. *Appl. Phys. Lett.* **2005**, *86*, 053105.

Zhang, Y. F.; Tang, Y. H.; Wang, N.; Lee, C. S.; Bello, I.; Lee, S. T. *Phys. Rev. B* **2000**, *61*, 4518.

Ziegler, K. J.; Doty, R. C.; Johnston, K. P.; Korgel, B. A. *J. Am. Chem. Soc*. **2001**, 123, 7797-7803.

Vita

Xianmao Lu was born in Shandong, China on November 18, 1974 to Zhishu Lu and Jianmei Liu. Upon graduating from Laiwu No. 4 High School, Laiwu, Shandong, China in 1992, he enrolled at Tsinghua University in Beijing, China. While at Tsinghua University, he conducted undergraduate research and received his B.E. in Chemical Engineering with an option in Dynamic Simulation of Distillation Columns in June of 1997. He enrolled at the graduate school of Tsinghua University in September 1997 conducting research in real-time prediction of product qualities for crude oil distillation columns under the direction of Professor Xiaorong He and received a M.E. degree in Chemical Engineering in June 2000. In September 2000, he enrolled at the University of Texas at Austin where he conducted research under the supervision of Dr. Keith P. Johnston and Dr. Brian A. Korgel. He will receive his Ph.D. in Chemical Engineering in December 2005.

Permanent Address: Shitouwan, Lixin, Laiwu,
Shandong Province, China 271105

This dissertation was typed by the author.